



UNIVERSITÀ
DEGLI STUDI
FIRENZE

UNIVERSITÀ DEGLI STUDI DI FIRENZE
DIPARTIMENTO DI INGEGNERIA DELL'INFORMAZIONE (DINFO)
CORSO DI DOTTORATO IN INGEGNERIA DELL'INFORMAZIONE
CURRICULUM: TELECOMUNICAZIONI E SISTEMI TELEMATICI

ADVANCED SOLUTIONS OF VISIBLE
LIGHT COMMUNICATION FOR
INFOMOBILITY APPLICATIONS

Candidate

Stefano Caputo

Supervisors

Prof. Lorenzo Mucchi

Dr. Luca Simone Ronga

Prof. Francesco Saverio Cataliotti

Prof. Marco Pierini

PhD Coordinator

Prof. Fabio Schoen

CICLO XXXII, 2016-2019

Università degli Studi di Firenze, Dipartimento di Ingegneria
dell'Informazione (DINFO).

Thesis submitted in partial fulfillment of the requirements for the degree of
Doctor of Philosophy in Information Engineering. Copyright © 2020 by
Stefano Caputo.

Acknowledgments

I would like to acknowledge the efforts and input of my supervisor, in particular professor Lorenzo Mucchi and professor Francesco Saverio Cataliotti. I would like to thank also all my colleagues of the Visible Light Communications Research Lab (VisiCoRe) who were of great help during my research. My thanks go to professor Carla Balocco, professor Elisabetta Baldanzi and professor Alessandro Farini who collaborated on a parts of my research work. I would like to thanks Dr. Jacopo Catani of National Institute of Optics (INO CNR) who collaborated on the electronics parts of prototype and on the main parts of measurements campaign. Lastly, I would like to thanks all students that they have done a their thesis in VisiCoRe Lab for their contribute of my research work.

Abstract

The replacement of conventional light sources with Light Emitting Diodes (LEDs) has recently increased scientific and industrial activity in Visible Light Communications (VLC). In the VLC, the same optical radiation in the visible light spectrum used to standard illumination is also used for data communication through a fast modulation of the light source. VLC systems have a great potential for different applications, in particular for infomobility, due to their efficiency and low latency. The VLC for infomobility can be used for applications in offices, in museums and in Intelligent Transportation Systems (ITS). The main aim of this PhD dissertation is a characterization of communication channel between a traffic light and a vehicle for ITS applications. This is a typical example of communication Infrastructure to Vehicular (I2V). After creating a low-cost prototype IEEE 802.15.7 compliant, the communication channel has been analyzed through some tests. Each test was necessary in order to characterize every singular components of the system. The propagation channel has been deeply investigated to characterize the irregular optical path of transmission of the regulatory traffic light and to study the optical lens used for receiving a signal. Finally, the performance of this system was evaluated in terms of Packet Error Rate (PER). The created system has been used also in 5G experiments in Prato, and the latency of a joint 5G-VLC communication has been measured. In addition, two other aspects of VLC are present in this PhD dissertation: a comparative study between lighting design standards for illumination system and the lighting design for optimization signal of VLC system and a study of human perceptions of objects illuminated by a lamp with VLC system integrated.

Contents

Contents	vii
1 Introduction	1
1.1 Motivations and Objectives	1
1.2 Contributions	3
2 Visible Light Communication	5
2.1 Introduction to VLC	7
2.1.1 Comparison of VLC with other technologies	9
2.2 IEEE Standard for VLC	9
2.2.1 IEEE 802.15.7	10
2.3 Generic System Model	12
2.3.1 Preliminary study and experiment on VLC	13
3 Infrastructure-to-Vehicle VLC link characterization	27
3.1 System Model	29
3.2 Equipment	31
3.2.1 VLC Transmitter	33
3.2.2 VLC Receiver	33
3.2.3 Transfer function of equipment	34
3.3 Traffic light emission pattern and wireless channel	37
3.3.1 Measurement Campaign	38
3.3.2 Propagation Model	42
3.4 Receiver optical lens	59
3.4.1 Comparison between model and experimental data	62
3.5 Implementation and experimental test of a relay-based VLC:	
I2V2V	64
3.5.1 I2V2V ADR system	68

3.5.2	Measurement Campaign	74
3.5.3	PER Analysis	75
3.5.4	Ultra-low ADR latency performances	77
3.5.5	Application to road safety	85
3.6	Implementation and experimentation of VLC in 5G network	88
3.6.1	The 5G Prato project	92
3.6.2	Latency of combined 5G and VLC Systems	93
4	Other research projects	95
4.1	VLC lamp for indoor application	96
4.2	Human perception of modulated light	101
4.2.1	Optometric Equipment	103
4.2.2	Ishihara	107
4.2.3	Reading performance	110
4.2.4	Variation of colour perception	113
4.2.5	Conclusion	115
4.3	Light design and Visible Light Communication	115
4.3.1	Techniques and tools for office light characterization	116
4.3.2	Compliance with lighting regulations	121
4.3.3	Conclusion	125
5	Conclusion	127
5.1	Summary of contribution	127
5.2	Directions for future work	128
	Publications	129
	Bibliography	131

Chapter 1

Introduction

1.1 Motivations and Objectives

The exigency to research an additional wireless communication technology is the outcome of exponential increase in demand for high speed wireless connectivity. The radio frequencies (RF) results a easier solution to satisfy this necessity for connectivity, but, in some application, an optical wireless communication (OWC) system could result more efficient. For this reason, the research community begins to deepen the use of OWC system. The scope, initially, are the optimization of technology that carried information by modulation in Infra-Red (IR) spectrum. The growth of high power light emitted diode (LEDs) for illumination system shifting focus of the research community to the visible spectrum (400-700 nm).

VLC consist to fast switching a light source. The LED, unlike the old light bulbs, can be modulated at the frequencies, that the human eye cannot perceive. However, the pulse sequence may produce imperceptible glare and flicker, which disturb to people's work after a prolonged exposure to modulated light. This constitutes a subject for deep investigation on which the scientific community is focusing before the commercial release of the first VLC lamp (see a section 4.2).

An OWC has a great potential for many application, in particular for infomobility solutions due to their low latency communication, and high density of people. The term infomobility refers to use of information technology to support the movement of people through a fast and interactive access to resources that enhance the perception of reality. Infomobility can

be used anywhere, in the office with real-time information on the progress of some activities, inside a museum through the use of interactive and personalized guides. But surely the greatest use of infomobility is in the field of intelligent transport systems (ITS).

The automotive industry is facing a technological revolution and new vehicles are equipped with many sensor to reduce the accidents. The next step to further reduce damage to people or vehicles is the creation of a communication network. As the manufacturing industry is going towards the fourth industrial revolution (Industry 4.0), the transport system needs a communication network to be more efficient. Actual ITS are based on radio technology, e.g. the Audi company has development a system to know the times of traffic light, to optimize the consumption of vehicles and to avoid pass with the red light. This service requires a paid subscription due to cost of using RF licenses. One of the main advantages of VLC technology is that used unlicensed frequencies to carry information, and therefore this same infomobility application could be release without a paid subscription. Furthermore, the LEDs are present in road infrastructure and on vehicle, and therefore, the use of VLC for vehicular communication is cheap solution. Finally, it is important to note that the majority of research has aimed demonstrating higher data rates capable to OWC in comparison to existent RF communication systems. The outdoor communication in realistic scenario, represents a field which the state-of-the art lacks of a deep investigation.

The main objective of PhD dissertation is a creation and study of VLC communication system to carry information from a traffic light to vehicle in realistic scenario (see a chapter 3). Experimental tests began in physics laboratories, with the study of the first modulation system and the characterization of the propagation of a singular LED in controlled conditions. Subsequently, a study on the electronics of high-power LEDs was necessary to transfer the prototype in real conditions. Once the prototype was obtained, the communication channel was characterized and its performance analysed, through some measurement campaigns. The first research topic was focused to characterized the transmission pattern and the propagation channel. Subsequently, it was necessary an investigation of the optical lens of receiver. Finally, the study was focused on the performance analysis in terms of latency and packet error rate (PER). The prototype obtained has been used also in Prato 5G experimentation due to low latency characteristic. Moreover in this PhD dissertation there are two other objectives. A

experimental test for demonstrate the effect of modulated light source to human perception of object. And a comparative study between lighting design standards for illumination system and for optimization signal of VLC.

1.2 Contributions

The main contributions of this thesis are the following:

- In Chapter 3, a main objective of PhD dissertation, a description of VLC system used to carry information from traffic light and the vehicle. The main contribution of this chapter are the following:
 - In section 3.3, the transmission pattern and wireless channel characterization in real urban scenario.
 - In section 3.4, the optical lens of receiver characterization
 - In section 3.5, the Packet Error Rate (PER) analysis for a automotive application with low latency (sub-millisecond) communication system.
 - In section 3.6, the application of previous prototype system in Prato 5G experimentation.
- In Chapter 4, the parallel activities with other research groups for a characterization of VLC from the different point of view:
 - In Section 4.2, an investigation of a critical condition of flicker compromise the ability to read and perception colour.
 - In Section 4.3, through the use of software typically used in the design of lighting systems, the characteristics of a correct design for the purposes of the standards that characterize the lighting of an office were compared to the areas that require a high availability of signal.

The collaborations with other department of the University of Florence and research center are necessary to organize the measurement campaign and to become an element of an interdisciplinary research.

More in details, the institutions and the people who collaborated in the research, in addition to tutors, are:

- European Laboratory for Non-Linear Spectroscopy (LENS) and National Institute of Optics (INO-CNR) with Dr. Jacopo Catani, Tas-sadaq Nawaz and Marco Seminara for the traffic light measurement campaign.
- Department of construction engineering of University of Florence, with the Prof. Carla Balocco and the student Alessio Scacchi for the standards of lighting design.
- National Institute of Optics (INO-CNR) and Institute for Research and Studies in Optics and Optometry (IRSOO), with the Prof. Elisabetta Baldanzi, Prof. Alessandro Farini and the students Valentina Orsi and Vittoria D'Antoni for the human perception of the light.

Chapter 2

Visible Light Communication

This chapter gives an overview of Visible Light Communication (VLC). Advantages of this communication technology and the innovation compared to radio-frequency (RF) and Infra-Red (IR) solution can be understood with a analysis of literature review. IEEE standard for this technology is constantly changing, due to arise a innovative application. Along the chapter a mathematical approach to generic system model of Visible Light Communication through a measurement campaign carried out in laboratory.

1

From ancient times to the 19th century, all communication system in visible light spectrum relied on the human eye as the receiver. The invention of the photo-phone by Alexander Graham Bell is the first revolution of visible light communication concept [18]. Thanks to the utilisation of the selenium resistance and its property of convert the light intensity in electrical current, it was possible send a signal audio through a light communication.

Until the 1950s, the research of materials with a higher sensitivity to detection light radiation has taken to materials infra-red frequency sensitive, precluding visible light to be using as a transmission medium. The introduction of light-emitting diodes (LED) reawakened the interest for visible light radiation used to communication systems.

¹A preliminary of work presented in this chapter has been published as “Experimental-based propagation model for VLC” in *Networks and Communications (EuCNC),2017 European Conference*.

Technological developments have taken to dissemination of solid-state lights due to high energy efficiency, longer lifespan and best colour rendering. LEDs have replaced the old incandescent and fluorescent lamps for every indoor and outdoor illumination. People use these lights in their homes, the new street lamps and the road signs use this technology and Automotive companies have started to invest in LEDs lamps [87].

One additional benefit of solid-state light is the capacity to fast switching between different light intensity. Actually, this property is used to make light intensity as constant as possible or to control the colour in multi-colour LEDs lamps (RGB LEDs) [51]. The switching of luminous intensity is very fast that the human eye cannot perceive [91]. This functionality has given rise to a new communication technology (known as Visible Light Communication, VLC).

It is often possible to find the term Li-Fi, "Light Fidelity", instead of VLC. Dr. Harald Haas of the University of Edinburgh coined this term during his appearance at TED Talk Global 2011 [93] where he was able to transmit high volumes of data at high-speed capacity with a LEDs lamps, even if the first high-speed communication in visible light were performed in Japan in 2004 [63].

One of the first standardization to work on a VLC standard was the Visible Light Communications Consortium (VLCC) of Japan. In 2008, they broadened the infrared Data Association (IrDA) standard to the visible light spectrum [66].

Recently, VLC research has a growth of interest in academic and industrial fields. The important activity developed in a last few years are [94]:

- Basic6 is a American start-up company, that it develop an indoor positioning system, GeoLiFi. This technology uses a store's lights to delivery proximity messaging about products, promotions and visual shopping lists for customers. At the same times, the retailer can see an analysis of store and department dwell times. The company cooperates with OLEDCOMM, a French spin-off of the University of Versailles Saint-Quentin-en-Yvelines.
- The Li-Fi Hotspot developed at Fraunhofer Heinrich Hertz Institute (HHI) allows the installation of a private high-speed network. The performance of this system is up to 1Gbps data rates, over a distance of up to 30 meter and "full duplex" communication. There is also a version of the product that allows a 3Gbps data rate using RGB LEDs.

- Lucibel is a French Company and it have developed the first industrialized Li-Fi system in Europe. Lucibel Li-Fi solution offers high speed mobile connectivity (bidirectional line rate up to 42Mbit/s) and the VLC network supports multiple access and the "handover". Sogeprom was the first company to test this solution of LiFi. Now, the Microsoft innovation centre in Issy-les-Moulineaux is implementing this Li-Fi system. Lucibel cooperates with pureLiFi, a start-up founded by Harald Haas.
- LVX system is an American company, and they have recently signed a Space Act Agreement with NASA.
- Velmenni is an Estonian start-up company and are presently doing numerous pilot projects to VLC. The system offers a bidirectional line rate up to 1Gbps, but the distance of communication is several tens of centimetre. The prototype is development in collaboration with Airbus to use this technology on the air-planes.

Also company, as Samsung, Apple, LG and other, are deposing many patents on this technology, because VLC has become a potential candidate technology for fifth generation (5G) networks [72].

2.1 Introduction to VLC

Visible light communication (VLC) combines all OWC system that carried information by modulating light in visible spectrum, used principally for illumination. A significant energy saving can be obtained by exploiting the same lights using for illumination to carry information, and a considerable installation saving to using the existing infrastructure of lighting system. For these reasons the VLC result a "green" technology.

The visible light spectrum includes electromagnetic waves with frequency approximately between 428 to 750 THz (Fig. 2.1). The bandwidth is over 1000 times wider than radio frequencies which allows high capacity for communication.

The light cannot penetrate objects and walls, which make it highly locale and directed communication media. The coverage range is reduced but this permit to create a small cell of communication without intercell interference, cost for licensed and secure.

The most important advantages of VLC are:

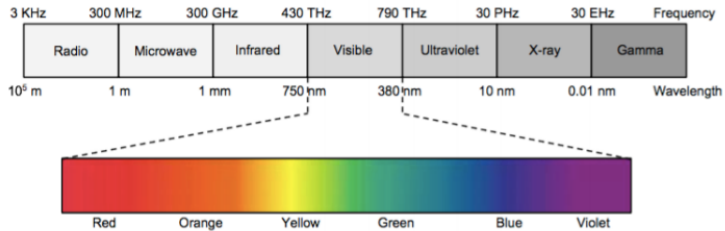


Figure 2.1: Visible light spectrum.

- energy efficiency of LEDs
- easy implementation into existing infrastructure
- spectrum crunch alleviation
- interference absence
- low cost devices
- security enhance
- spatial reuse possible
- safety of VLC transmission for human

Possible services benefiting from VLC can be classified in three groups:

- Image sensor communication (ISC)
- Low rate photodiode receiver communication (LR-PC)
- High rate photodiode receiver communication (HR-PC)

1 Mbit/s of data rate is considered a threshold between low and high rate.

ISC use light source as transmitted and a image sensor as receiver, often found under the name of Optical Camera Communication (OCC). LR-PC use the same transmitter to ISC, but the receivers is a low speed photodiodes. The main application are similar to those for ISC. Instead HR-PC use the high-rate photodiode as receiver. Continuous data streaming for all applications should be supported with bidirectional functionality as well as short packet transmissions where low latency is required.

2.1.1 Comparison of VLC with other technologies

VLC communication has some advantages compared to traditional radio frequencies (RF) and infra-red (IR) communication. The major advantage is definitely the bandwidth similar to that IR but wider to RF. The RF band is only 300GHz, strictly limited and regulated. The major disadvantage is certainly the low coverage range.

Another advantage is low power consumption and low implementation costs through the use of existed infrastructure for illumination. IR and RF require own base station. Hence the biggest difference is propagation through obstacles.

When comparing the health risks of technologies, the RF may have more potential risks. There are some studies to the effect of radio frequencies to human but it have not been conclusively proved. Moreover, the IR absorbed to the human skin and eye, with a damage for cornea and visual loss. For this reason, the maximum power to emission in IR frequencies is very low. The VLC technology has only a problem of a high intensity blue light emitted from sources caused a health risk known as blue light hazard (BLH), but this is a problem of illumination technology. The use of RGB LEDs probably is a solution of BLH, but this technology increases the production cost. With this change in technology, the VLC would have a significant advantage, i.e. the possibility of using three channel (red, green and blue) separately with an increase in performance. RF and IR communications have a longer research history and standardization.

A comparison summary between a RF and VLC systems is reported in Table 2.1:

VLC technology is fully compatible with RF and IR communications. The performance of these technologies improves in hybrid or heterogeneous networks, i.e. RFs guarantee better signal coverage while VLCs reduce radio bandwidth usage.

2.2 IEEE Standard for VLC

The first standard for Visible light communication, IEEE Std. 802.15.7-2011 on "Short-Range Wireless Optical Communication Using Visible Light" was completed in 2011 by the IEEE 802.15 Working Group. A project to revise was authorized in 2014 with the name "Optical Wireless Communication (OWC)" which includes LED-ID (or LR-PC), Optical Camera Communica-

Table 2.1: Comparison between VLC, RF and IR communications.

	VLC	RF	IR
Bandwidth	Unlicensed ≈ 400 THz	Regulated ≤ 300 GHz	≈ 400 THz
EM Interference	No	Yes	No
Power Consumption	Low	Medium	Low
Mobility	Limited	Yes	Limited
Standard	802.15.7	several, matured	802.11
Coverage	Narrow	Wide	Narrow
Health risks	BLH	Several	Thermal
Implementation cost	Low	Low-medium	medium

tion (OCC) and LiFi (or HR-PC), and is currently active. It intend to crate a standard for light wavelengths from Infrared to Ultraviolet (10000 nm - 190 nm).

The group is divided in March 2017:

- 802.15.7m will continue work on Optical Camera Communication
- 802.15.13 Task Group established for multi-Gigabit per Second Optical Wireless Communication

In addition, IEEE 802.15 Vehicular Assistant Technology (VAT) interest group is considering VLC as a communication option. In late 2016, also the IEEE 802.11 Working Group initiated a Topic Interest Group (TIG) on Light Communication. The target of this TIG is to determine the economic and technical opportunities due to use light for wireless communication. IEEE 802.11bb work for the development of the standard document since 2018. Also ITU-T Study Group 15 develop standard for VLC which is entitled "High speed indoor visible light communication transceiver - System architecture physical layer and data link layer specification".

2.2.1 IEEE 802.15.7

A first release of IEEE 802.15.7 standard defines a rules for the implementation of VLC systems. In particular, a physical (PHY) and media access

Table 2.2: PHY operating modes.

PHY I Operating modes

Modulation	RLL code	Optical clock rate	FEC		Data rate
			Outer code (RS)	Inner code (CC)	
OOK	Manchester	200 kHz	(15,7)	1/4	11.67 kb/s
			(15,11)	1/3	24.44 kb/s
			(15,11)	2/3	48.89 kb/s
			(15,11)	none	73.3 kb/s
			none	none	100 kb/s
VPPM	4B6B	400 kHz	(15,2)	none	35.56 kb/s
			(15,4)	none	71.11 kb/s
			(15,7)	none	124.4 kb/s
			none	none	266.6 kb/s
			none	none	266.6 kb/s

PHY II Operating modes

Modulation	RLL code	Optical clock rate	FEC	Data rate
VPPM	4B6B	3.75 MHz	RS(64,32)	1.25 Mb/s
			RS(160,128)	2 Mb/s
		7.5 MHz	RS(64,32)	2.5 Mb/s
			RS(160,128)	4 Mb/s
OOK	8B10B	15 MHz	none	5 Mb/s
			RS(64,32)	6 Mb/s
		30 MHz	RS(160,128)	9.6 Mb/s
			RS(64,32)	12 Mb/s
		60 MHz	RS(160,128)	19.2 Mb/s
			RS(64,32)	24 Mb/s
		120 MHz	RS(160,128)	38.4 Mb/s
			RS(64,32)	48 Mb/s
RS(160,128)	76.8 Mb/s			
none	96Mb/s			

control (MAC) layers for short-range optical wireless communication for indoor and outdoor applications are been considered. The main contribution of PhD dissertation is focused on a physical layer.

The IEEE 802.15.7-2011 standard defines three physical layer types. PHY I and PHY II use only one wavelength of light, instead the PHY III combines multiple optical sources with a modulation format called color shift keying (CSK). In this PhD dissertation are not present solutions with multiple optical sources, and so only the first two are summarized in the table 2.2.1.

In particular, the PHY I was indicated for outdoor communications due to it is optimized for low rate but high coverage. There are two modulation techniques in PHY I: OOK and VPPM. OOK consists of transmitting a rectangular pulse in a fixed time slot if the coded bit is '1', while the absence of a pulse during a time slot represent a coded bit '0'. Whereas, Variable Pulse Position Modulation (VPPM) is a PPM technique, i.e. to transmit the coded bit '0', the pulse is at the beginning of time slot, where if the pulse is at the end, it was represent the coded bit '1'. The adjective 'Variable' allows to control the perceived intensity of light. OOK with a Manchester RLL code is the equivalent of the VPPM with pulse width set at 50%.

The 4B6B RLL coding, as 8B10B, is more efficient of Manchester, but it is more prone to flickering effect. For this reason, it is used with elevate optical clock rate. Different forward error correction (FEC) schemes are suggested in this standard to the transmission reliability, but in this thesis dissertation the work focused on a transmission without FEC (100 kb/s), due to the low computational level of hardware used.

2.3 Generic System Model

The simplest VLC system is composed by a transmitter (TX, i.e. a LED), a propagation channel and a receiver (RX, i.e. a photodiode).

LEDs emit incoherent light, so the communication is based on intensity modulation. The polarization of the light is not considerable, due to the main function of the lamp is illumination and the use of filter reduce the efficient of the lamp. The carrier wave is the colour of light, but in IEEE 802.15.7 standard for PHI I and II is not defined a particular colour, due to the transmission coverage is very limited. A propagation channel is a wireless connection link and it is possible to characterize the Line-Of-Sight

(LOS) link and a Non-Line-Of-Sight (NLOS). In the LOS, LED is in Field-Of-View (FOV) of the receiver. While for a characterization of NLOS, it is necessary to analyse a reflection of the light. A photodiode receives light, and it converts the incident optical intensity into a current signal.

In more complex system, there are an optical lens after a transmitter and before the receiver (See the Chapter 3).

In this section, a characterization of a simple VLC system is proposed with a experimental measurements. This work was exposed to the Networks and Communication Conference (EuCNC) in 2017 [79].

The scope is to come up with a fine tuned propagation model which also accounts for reflection from the optical bench. The experiments were conducted in the European Laboratory of Non Linear Spectroscopy (LENS). The proposed propagation model can be used to evaluate the performance of visible light communications. In the current literature, channel models developed for infrared (IR) frequencies in the past [45,60,86] are used for performance evaluation of VLC systems without a solid justification [30,64,81]. However, it is known that visible light and IR bands exhibit different characteristics [69] due to the absorption and reflection of surface are different and it is necessary the development of a proper VLC channel model.

Ray-tracing technique is a tool often used for modelling reflection in VLC system [77], with illumination simulation software (e.g. Zemax) [76]. A few papers characterized the VLC propagation channel with real measurement [35], and a mathematical model is not present. A typical approach on VLC channel model is summarize in [89].

2.3.1 Preliminary study and experiment on VLC

A measurement campaign was performed in indoor scenario with a absence of ambient light. A transmitter source is a 3W LED green light EPISTAR WX-PAXG851A3, a low power LED can be controlled with a function generator. It has been modulated with a sine signal with centre frequency of 5 kHz. The voltage to alimentation was in a range of amplitude from 2.3 to 4 V, which corresponds to a light power variation from 0 to 120mW.

Whereas, a Vishay BP34W photodiode was used as a receiver. it connected to a circuit composed by:

- a alimentation circuit (Hobbs): a low noise alimentation circuit for photodiodes due to it increase a response time.

- a transimpedance stage: a first stage of amplification, it was set to receive a frequency of transmission signal.
- an amplification stage: it was set for used all range of oscilloscope.

This circuit was been connected to Oscilloscope for recorder a received signal.

A LED fixed in a corner of optical bench with a dimension of 1200 x 900 mm, whereas a receiver moved in measurement grid with an 80 positions. Each measurement position was far 100 mm from another in both directions (x-axis and y-axis). The optical bench was closed with black walls for eliminate a contribution of ambient light. The surface of receiver has a fixed orientation angle, it always was parallel to a short side of the bench (see Fig. 2.2)

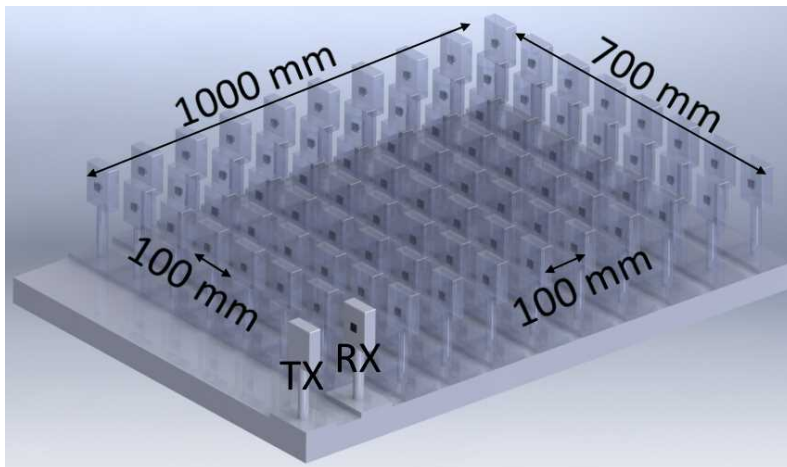


Figure 2.2: Optical bench used for the measurement campaign.

The amplitude of this signal is proportional to the irradiance at the detector since:

$$E = \frac{P_i}{S} = \frac{i_g}{S \cdot R(\lambda)} = \frac{V_t}{r_t} \frac{1}{S \cdot R(\lambda)} = \frac{V_o}{G_a} \frac{1}{r_t} \frac{1}{SR(\lambda)} \quad (2.1)$$

where:

- E : irradiance at the photodetector;
- P_i : incident optical power;

- S : photodetector sensible area;
- i_g : photodetector generated current;
- $R(\lambda)$: photodetector responsivity;
- V_t : transimpedance output voltage;
- r_t : transimpedance feedback resistance;
- V_o : amplifier output voltage;
- G_a : total amplifier gain.

Since the radiation propagation can be assumed symmetric with respect to XZ plane, we have obtained the irradiance pattern depicted in Fig. 2.3.

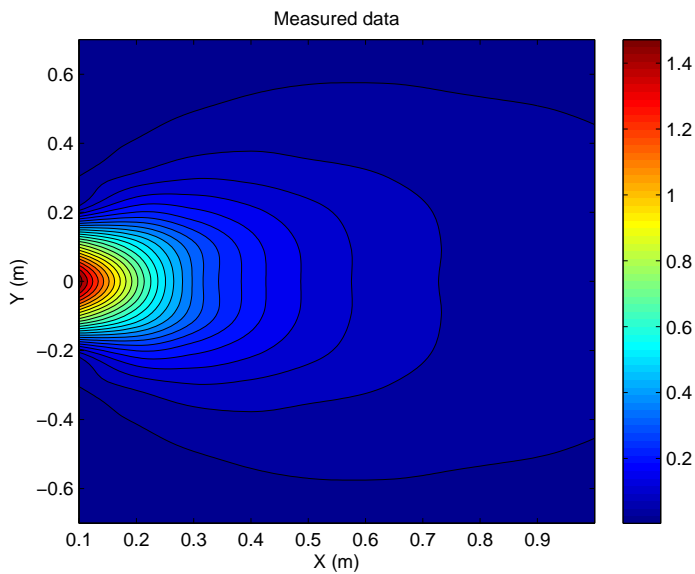


Figure 2.3: Irradiance as a function of detector position. The legend is expressed in Volts (V).

Mathematical approach

The mathematical model that best fits the experimental data, depends to a emission pattern of source, a reflection of the optical bench and the receiver angle.

The dimension of LED is very small compared to a distance, and so the transmitter can be considered a point source. The emission pattern can be homogenous for every irradiance angle, in this case it is known as spherical emission. The irradiance angle is the angle between the perpendicular axis to the LED surface and the line that combines TX and RX. In literature, Lambertian model is typical used to characterize a LED pattern, i.e. the emission is proportional to the cosine of irradiance angle.

The receiver angle is define with a solid angle $d\Omega$ as:

$$d\Omega = \frac{dS \cos \psi}{r^2} \quad (2.2)$$

where dS is a photo-receiver surface, ψ is a receiver angle, i.e. the angle between a perpendicular to the photodiode surface and the the line that combines TX and RX, and r is a distance between the source and receiver. This is a geometrical definition of solid angle. Using 2.2 and the radiation flux Φ definition can be define as:

$$d\Phi = I(\alpha)d\Omega = I(\alpha)\frac{dS \cos \psi}{r^2} \quad (2.3)$$

where $I(\alpha)$ is a LED emission pattern in function of irradiation angle. With the definition of irradiance (E), it is possible to support that:

$$E = \frac{d\Phi}{dS} = \frac{I(\alpha) \cos \psi}{r^2} \quad (2.4)$$

In this case, the receiver angle ψ is the same of irradiance angle α due to LED and receiver surface are parallel for every position of photodiode ($\psi = \alpha$). The irradiance E of 2.4 can be define as a function of the distance and the irradiance angle.

Point source with spherical emission

In a case of spherical emission the intensity $I(\alpha)$ can be considered constant (I_0) and the equation 2.4 becomes:

$$E = \frac{I_0 \cos \alpha}{r^2} \quad (2.5)$$

In figure 2.4(a) it is represent the mathematical model of irradiance (E) that it follows the equation 2.5, and in figure 2.4(b) the error percent between the propagation model and the experimental data. Average error is about 40%, it is high in particular for high value of irradiance angle (α).

The figure 2.5 represent the irradiance (E) scaled to the diffusion contribution (r^2) in function of the irradiance angle. If it were not present the contribution of reflection and, in the case of align the receiver in every position, this figure represent the emission pattern of the LED. The "noise" of red line depends to the contribution of reflections.

The curve shape of red line is more closed compared to model (blue line), for this reason, probably the emission pattern is more similar to a Lambertian model.

Point source with Lambertian emission

The Lambertian emission model is a typical model used in literature, it is characterized to a emission, in function of irradiance angle, similar a cosine.

$$I(\alpha) = I_0 \cos \alpha \quad (2.6)$$

The equation of irradiance E (equation 2.4) with a Lambertian emission model (equation 2.6) becomes:

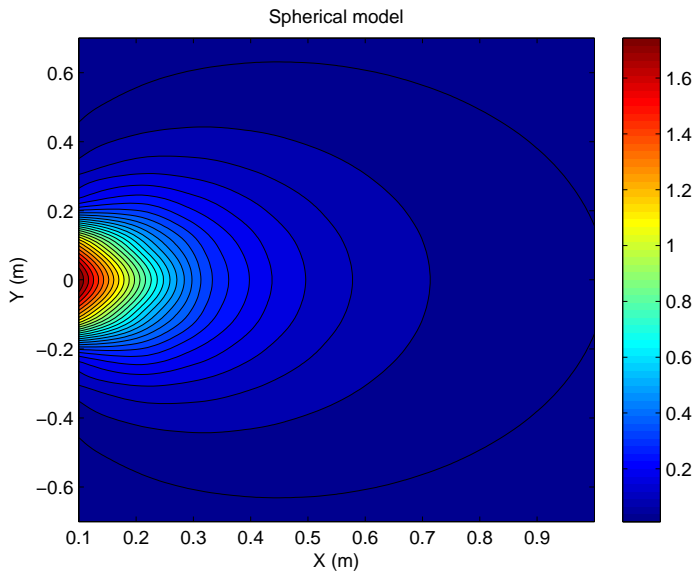
$$E = \frac{I_0(\cos \alpha)^2}{r^2} \quad (2.7)$$

The obtained irradiance is reported in figure 2.6(a), it is similar to a irradiance obtained with a spherical emission model (Fig. 2.4(a)). it is important to note that now the shape in this more similar to oval, while in the previous case it is more circular. With the spherical model, the main contribution of error can be detected for high irradiance angle value. While, in this case, the error is more uniform as can be seen from a figure 2.6(b).

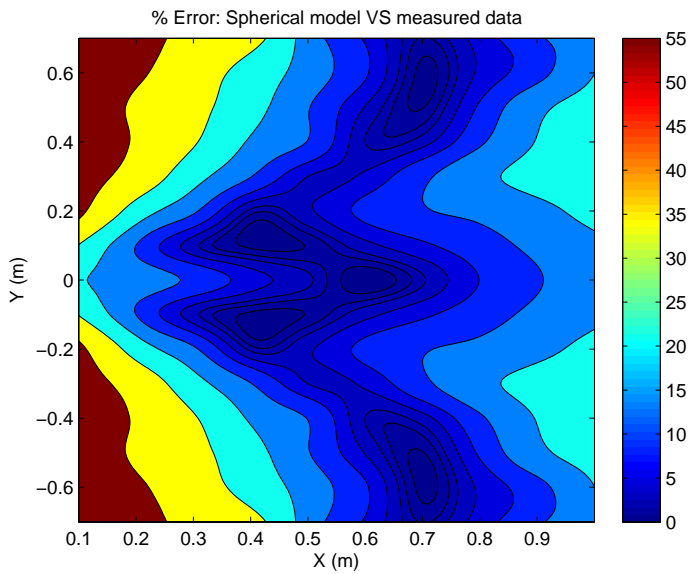
Moreover in figure 2.7, it is important to note how the model (blue line) better fit than the previous model. The contribution of NLOS affects the irradiance estimate by 30%, the average error of this model.

Non-Line-Of-Sight Contribution

The path loss of the reflected light is important and it generally increases the signal amplitude. When light hits an obstacle, as all electro-magnetic



(a) Data results from the propagation model. The legend is expressed in Volts (V).



(b) Error (%) between the propagation model and the experimental data.

Figure 2.4: Data from the point-source-constant-spherical-intensity propagation model VS experimental data.

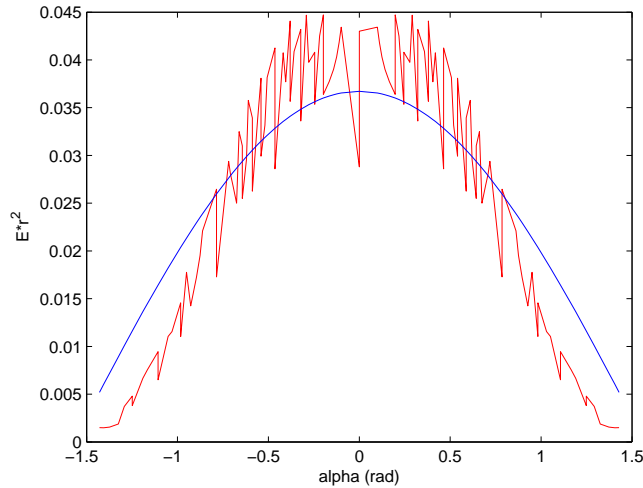
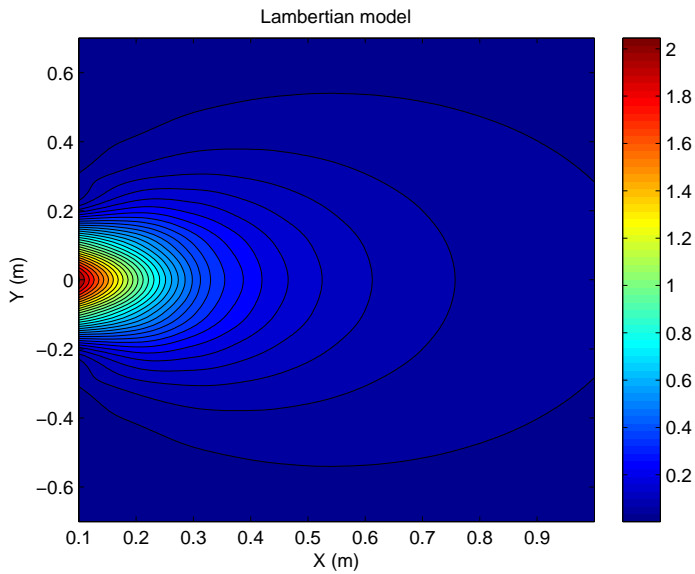


Figure 2.5: Experimental data (red line) and propagation model (blue line).

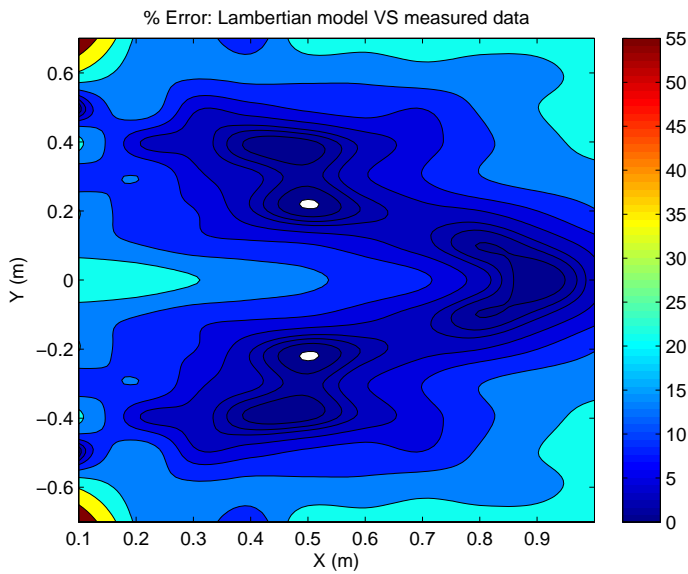
waves, parts of the intensity is absorbed, parts is reflected and parts is let through an object. Materials often show some mix of these behaviours, the portion reflected depends to the proprieties of the materials, the wavelength of light and the angle of incidence. Reflected light can be divided into two categories: specular and diffuse reflection (See fig.2.8)

The specular reflection is typical for glossy surfaces, e.g. polish metal. It is characterized by a single reflection direction, i.e. the reflection angle is the same of incident angle. The diffuse reflection is typical for matte surfaces, e.g. walls, i.e. the intensity of reflection, in function of the angle perpendicular to surface, has a cosine development. The Phong reflection is an example of empirical mathematical model that it combines the two categories of reflection.

In the experimental case, the surface of optical bench is composed by a metal sheet. The contribution of reflection is mainly specular. The mathematical model of irradiance with point source and spherical intensity be-



(a) Irradiance as a function of detector position using a Lambertian emission model. The legend is expressed in Volts (V).



(b) Error (%) between the propagation model and the experimental data.

Figure 2.6: Data from Lambertian propagation model VS experimental data.

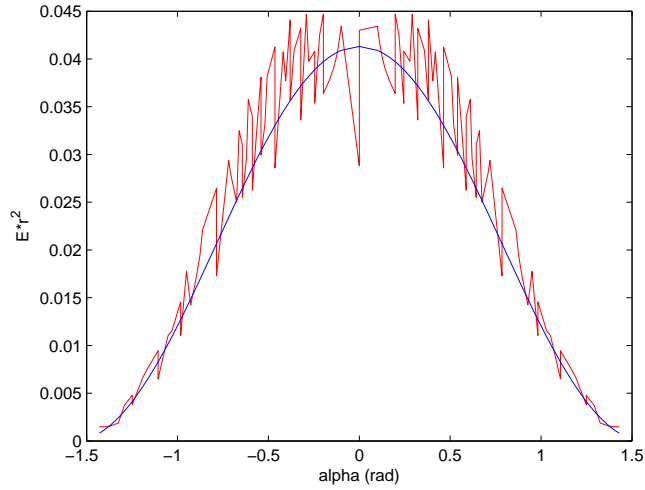


Figure 2.7: Experimental data (red line) and propagation model (blue line).

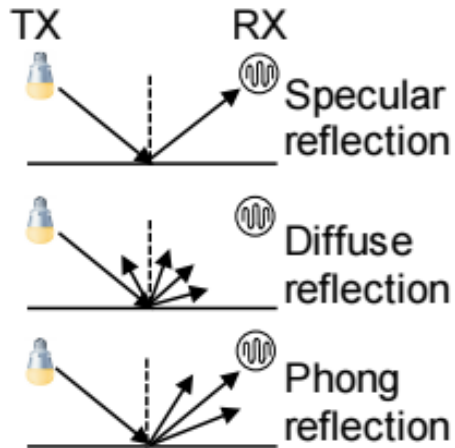


Figure 2.8: Types of reflection.

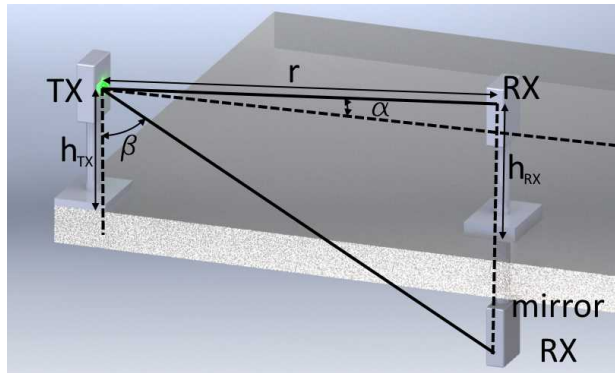


Figure 2.9: Angle and height parameters between source (LED) and receiver (photodiode).

comes:

$$E = \underbrace{\frac{I_0 \cos \alpha}{r^2}}_{\text{Direct path}} + \rho \underbrace{\frac{I_0 \cos \alpha \cos \beta}{(h_{tx} + h_{rx})^2 + r^2}}_{\text{Reflected path}} \quad (2.8)$$

where $\rho \in [0, 1]$ is the reflectivity of bench surface and β is the incident angle (See Fig. 2.9), it can be geometrically obtain from

$$\sin \beta = \sqrt{\frac{r^2}{(h_{tx} + h_{rx})^2 + r^2}} \quad (2.9)$$

For mathematical characterization of specular contribute, it is possible to consider a receiver signal as intensity received to a mirror image of photodiode, as depicted in a figure 2.9.

In figure 2.10 it is possible to note as the model (blue line) better fit the experimental data than the previous model that they not evaluate the contribution of NLOS. The error mean is decrease from about 30% to 12%.

The error is high for elevate irradiance angle value (See Fig. 2.11(b)) due to the emission pattern of LED is wrong.

The Lambertian emission pattern with a contribute of reflection is the last mathematical model proposed in this work. With the same assumption

made in previous model the irradiance (E) becomes

$$E = \frac{I_0(\cos \alpha)^2}{r^2} [1 + \rho(\sin \beta)^4] \quad (2.10)$$

The error mean is decrease to 8%. The percentage error is almost everywhere below 10% except the point with large Y value (See Fig.2.13(b)). However, the measured irradiance for these point is extremely low, making them the least significant. In figure 2.12 it is easy to evaluate how the fitting of the experimental data with this last model is very accurate.

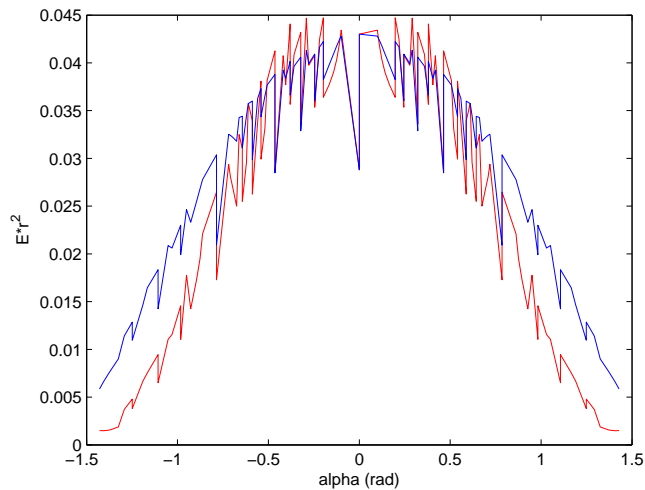
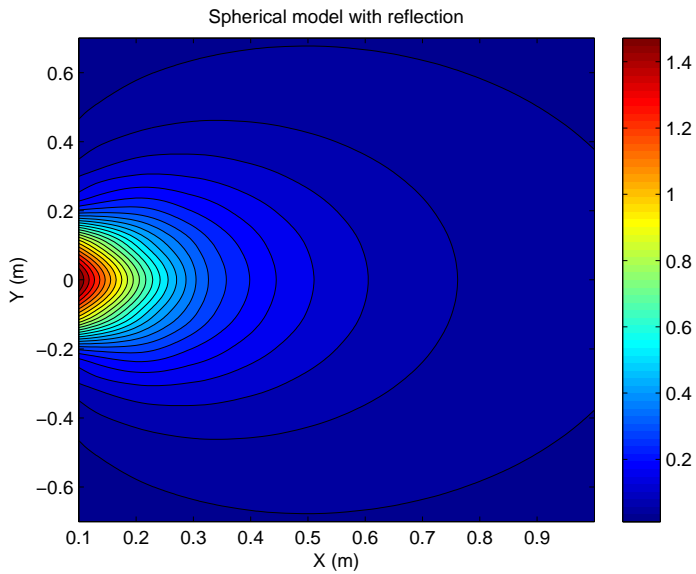
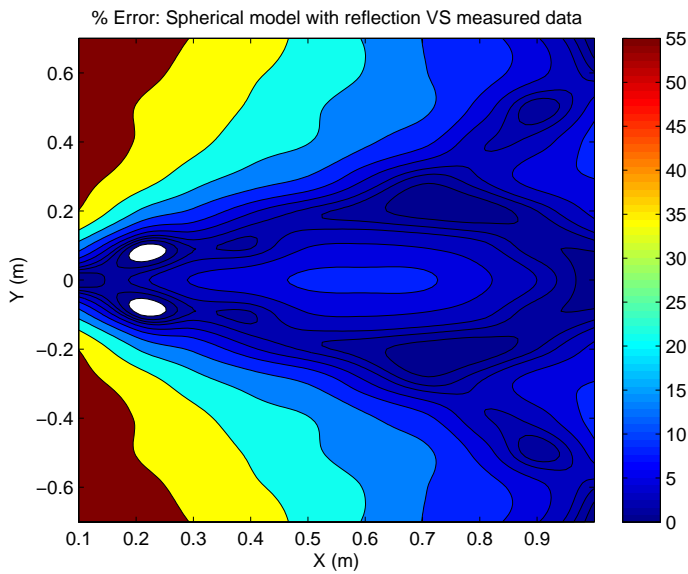


Figure 2.10: Experimental data (red line) and propagation model (blue line).



(a) Irradiance as a function of detector position using a spherical emission model with reflection. The legend is expressed in Volts (V).



(b) Error (%) between the propagation model and the experimental data.

Figure 2.11: Experimental data VS spherical propagation model with reflection.

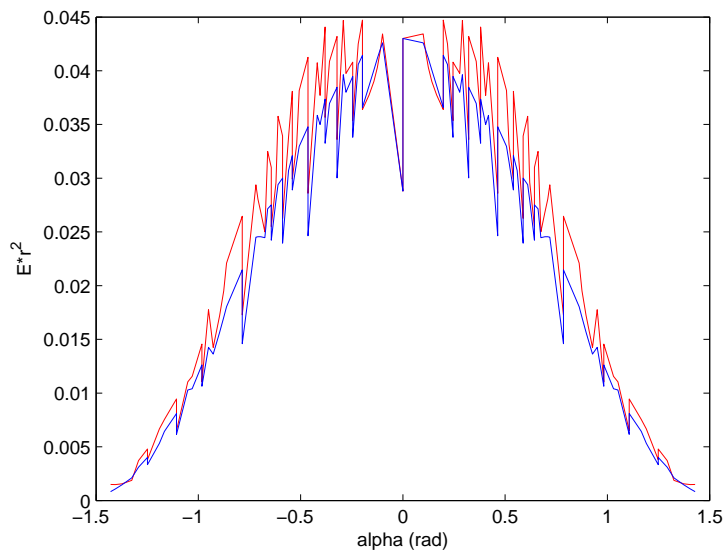
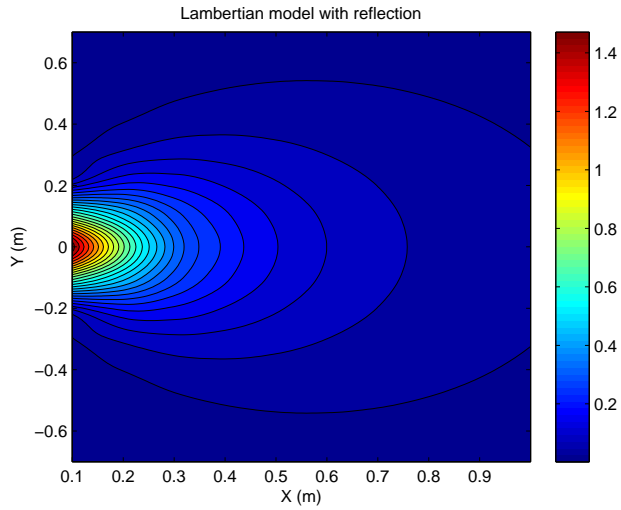
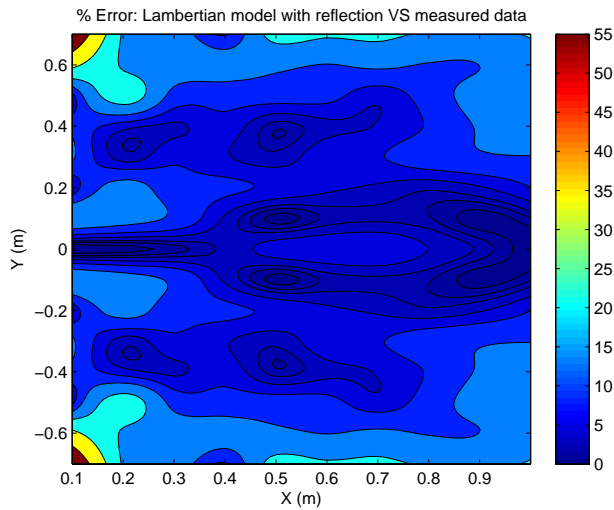


Figure 2.12: Experimental data (red line) and propagation model (blue line).



(a) Irradiance as a function of detector position using a Lambertian emission model with reflection. The legend is expressed in Volts (V).



(b) Error (%) between the propagation model and the experimental data.

Figure 2.13: Experimental data VS Lambertian propagation model with reflection.

Chapter 3

Infrastructure-to-Vehicle VLC link characterization

Visible light communication (VLC) is nowadays envisaged as a promising technology to enable new classes of services in intelligent transportation systems ranging e.g. from assisted driving to autonomous vehicles. In this chapter a measurement campaigns have been carried out by using a real traffic-light as source and a photo-receiver positioned at different distances, heights and azimuth angles along the road. The scopes of this investigation are a characterization of the every communication components and a performance evaluation of the prototype created. In the final part of the chapter, a integration of VLC into a 5G network.^{1 2 3}

¹Part of this work was conducted while the author was a correlator of student Andrea Cioncolini

²Part of this work was conducted while the author working with Prof. Francesco Saverio Cataliotti (European Laboratory Non-Linear Spectroscopy,LENS), Dr. Jacopo Catani (National Institute of Optic, INO-CNR), Dr. Tassadaq Nawaz, Dr. Patrizio Marcocci and PhD student Dr. Marco Seminara.

³A part of work presented in this chapter has been submitted as “Measurement-based VLC channel characterization for I2V communications in a real urban scenario” in *IEEE Transaction on Vehicular Technology*. A part has been published as “IEEE 802.15.7-Compliant Ultra-low Latency Relaying VLC System for Safety-Critical ITS” in *IEEE Transaction on Vehicular Technology*. A part has been published as “Data dissemination to vehicles using 5G and VLC for Smart Cities” in *AET, 2019* and this part of work is the 5G experimentation led by OpenFiber and WindTre in the cities of Prato and L’Aquila, promoted by the Italian Ministry of Economic Development (MiSE).

The ongoing substitution in vehicular and traffic infrastructures of conventional light with LEDs lamp has recently fuelled scientific and industrial activity in VLC technology [14, 29, 62] also in this application field. In the context of vehicular networks [61, 73] where the important communication proprieties are a low latency and reliability, VLC offer significant advantages [28, 101]. In addition, VLC is an energy efficient technology since the power consumption is needed to illuminate the road or for signalling (e.g., traffic lights) [13]. VLC could therefore be significant for V2V or I2V communications, both issues of decisive importance step toward road safety, in particular in the context of assisted- or unmanned-driving [21, 32], due to the sensor technology is unable to further reduce road traffic accidents, only a communication system is able to do an additional step toward road safety.

In recent times, integration of intelligent communication devices in vehicles is significantly increased, aiming at reduction of fatality rates and injuries in urban scenarios. However, according to the World Health Organization report [83], despite sizeable efforts in introducing active or assisted reaction capabilities to sudden events in last generation of vehicles, more than 1.2 million people annually died and 20 to 50 million injured in road accidents. This report further predicts that the traffic-related fatality rates would further increase and become the sixth largest cause of death in world by 2020 whereas it was the ninth largest in 1990 [83, 84]. Increasing the efficiency and safety of entire transportation system clearly poses the need for more advanced pervasive, low-latency vehicular interconnection technologies, aimed at boosting the vehicle's active safety protocols capabilities in response to critical events.

In particular, the emergence of IEEE 802.11p standard for short to medium range inter-vehicle communication, which amends the popular 802.11 protocol suite and the allocation of dedicated frequency band for ITS in Europe have provided the potential solution for future implementations of communication-based ITS safety applications [11, 12]. ITS connects vehicles, humans and roads through state-of-the-art information and communications technologies to increase the safety and efficiency of the transportation system and also to reduce the environmental pollution. The safety and efficiency of the road traffic can be substantially improved by enabling the wireless communications between I2V, V2V and V2I to share the information regarding their dynamical state (e.g position, speed, acceleration etc.) or information about real traffic situations (e.g traffic jams, accidents, critical events

etc.) [12, 40, 59].

A reliable assessment of suitability of VLC technology for V2V or I2V communications [22, 50] requires an accurate characterization of the VLC channel. In literature, the approaches to this problem has been theoretical or empirical. The theoretical approach aims at a mathematical reduction of the problem with approximations, such as Lambertian emission and reflection pattern [13] and ray tracing, allowing for a software physical simulation [70]. These kind of approaches are characterized by simplified scenario to reduce the computational complexity. On the other hand, the empirical approach typically involves a measurement campaign followed by the extraction of a mathematical model of the channel as in [34].

The first works present in this chapter are focused to a characterization of the communication system. After, there are other works to demonstrate that the VLC guarantees new generation communication (5G) requirements, in terms of massive Machine Type Communications (mMTC) and Ultra Reliable Low Latency Communications (URLLC).

3.1 System Model

The VLC channel can be decomposed in three elements: two corresponding to the electronic circuits, i.e., the transmitter and the receiver, and an optical channel. The optical channel can again be decomposed in three elements: two corresponding to the optics installed on the transmitter and on the receiver, respectively, and one corresponding to propagation in free space. Typical model for the VLC channel is shown in Fig. 3.1.

Every single element of the scheme can be represented mathematically by its transfer function $H(f)$, corresponding to the Fourier Transform of the impulse response $h(t)$.

The received signal is the convolution of the transmitted signal with four impulse responses

$$r(t) = s(t) * h_{\text{TX}}^{\text{el}}(t) * h_{\text{TX}}^{\text{op}} * h_{\text{P}}(t) * h_{\text{RX}}^{\text{op}} * h_{\text{RX}}^{\text{el}}(t) \quad (3.1)$$

where

- $h_{\text{TX}}^{\text{el}}(t)$ takes into account the electronic at the transmitter,
- $h_{\text{TX}}^{\text{op}}$ the effects of the optics at the transmitter,

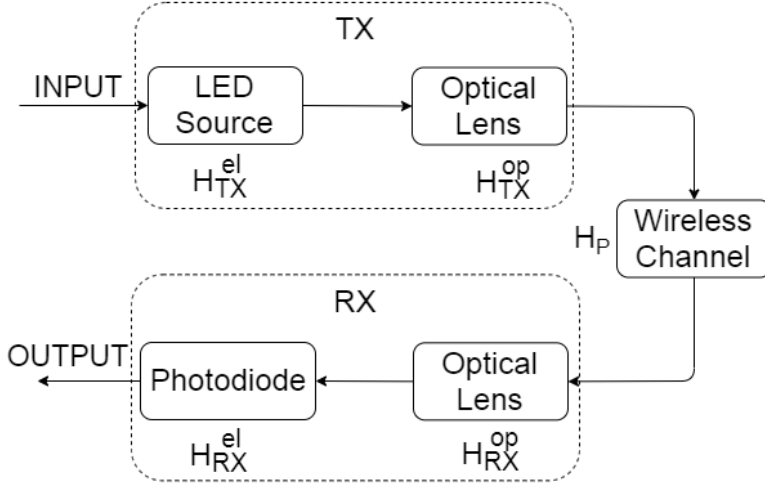


Figure 3.1: VLC system model.

- $h_P(t)$ the light propagation,
- h_{RX}^{op} the optics at the receiver, and
- $h_{RX}^{el}(t)$ the electronic conversion at the receiver.

In the frequency domain, Eq. (3.1) becomes

$$R(f) = S(f) \underbrace{H_{TX}^{el}(f)H_{TX}^{op}(f)H_P(f)H_{RX}^{op}(f)H_{RX}^{el}(f)}_{H(f)} \quad (3.2)$$

It is important to note that $h_P(t)$ does not depend on time, since during the measurements both TX and RX were static, and no variations in the environment occurred.

The first work (Sec.3.2.3) is focused on characterization of Transfer function (TF) of Electro-optical conversion ($h_{TX}^{el}(t)$) and vice versa ($h_{RX}^{el}(t)$). The components of emission pattern (H_{TX}^{op}) and wireless channel (H_P) is been characterized in the section 3.3 with a mathematical model different from Lambertian model, used usually in literature. Finally, A study of receiver optical lens (H_{RX}^{op}) is a subject of the section 3.4

After the characterization of a system model of a singular point-to-point communication, it is possible to analyse a typical case of real scenario

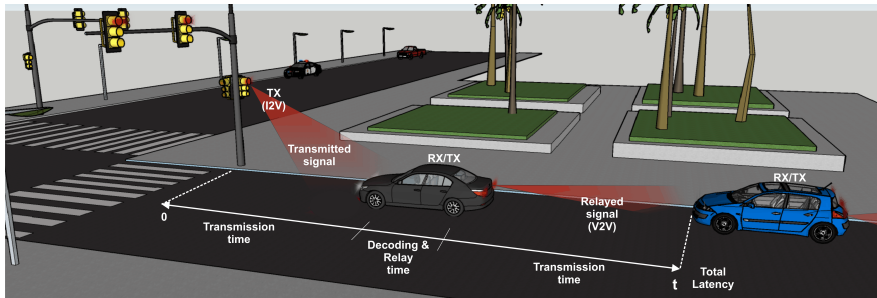


Figure 3.2: Illustration of the proposed I2V2V active decode-and-relay (ADR) scenario: the traffic light sends a message that is received by the first car (I2V) which acts as an active relaying node, decode the message and relay it to the car behind (V2V).

with two vehicles, i.e. an experimental implementation of a combined VLC Infrastructure-to-Vehicle-to-Vehicle (I2V2V) architecture for high-speed transmission of alert messages from a regular traffic light (TX) to an incoming unit (RX) (see a Sec.3.5), which also embeds an ultra-fast active decode-and-relay (ADR) V2V stage towards further incoming units for ultrafast propagation of critical information through the vehicular chain (see Fig. 3.2). IEEE 802.15.7-compliant [91] prototype system is aimed at providing a cost effective solution for a short to medium range VLC to be employed in ITS outdoor safety-critical applications, and is based on a low-cost, open-source microcontroller platform (Arduino DUE) and attains for the first time ultra-low, sub-ms total latencies in the total TX-RX-ADR path through VLC.

This last scenario has been proposed in the 5G experimentation led by OpenFiber and WindTre in the cities of Prato and L'Aquila, promoted by the Italian Ministry of Economic Development (MiSE) (see a Sec.3.6).

3.2 Equipment

The VLC TX and RX stages have been designed in order to feature analogue bandwidths above 150 kHz and to reject low-frequency high-intensity components coming from sunlight or traffic illumination without saturating the first amplification stage.

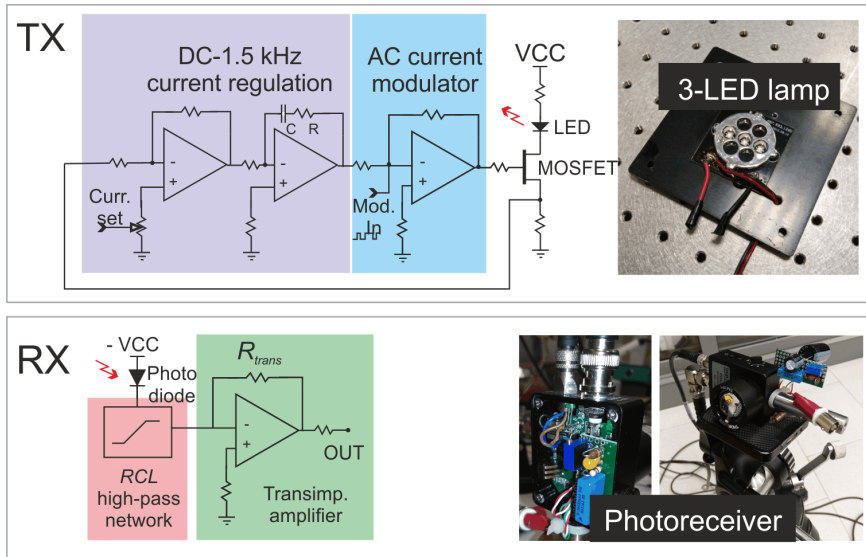


Figure 3.3: Sketch of the TX-RX hardware. RX panel: A PI regulation stage (purple area) stabilized the DC current value in the RC bandwidth for LED to provide the required nominal light intensity, whereas a modulation stage (cyan area) inserts a high-frequency current modulation in the LED source (rightmost panel). RX panel: a Thorlabs PDA36-A is modified through the physical insertion of a high-pass RCL network among the photo-diode and the first stage of transimpedance amplification, to provide for beneficial AC decoupling of photo-current and avoid saturation due to stray ambient lights.

3.2.1 VLC Transmitter

The schematic block diagram of TX hardware is reported in Fig. 3.3. TX hardware is composed by the LED light source, and its current driver. The implementation allows to generate the required current ($\simeq 0.7$ A) for the traffic light LEDs to provide the nominal luminous flux, as well as to insert a current modulation proportional to an external signal, which in turn allows for insertion of data streams into the optical carrier using any kind of protocol based on light intensity modulation. The modulator section (cyan shaded area of Fig. 3.3) is placed after a P - I regulation stage (purple shaded area), stabilizing the supply current, which is sensed by a precision resistor, from DC to $\simeq 1.5$ kHz, given by a proper adjustment of the servo RC constant (see Fig. 3.3). In such configuration, any modulation above the PI servo cut frequency $f_{\text{TX}} = 1/2\pi RC \simeq 1.5$ kHz will not be compensated by the P - I loop, and will be added as a current modulation through the MOSFET transistor. The open loop bandwidth of the op-amp chain can virtually exceed several MHz, whereas, on the other hand, the large parasitic capacitance of the large-area LED module embedded in the traffic light lamp, as well as the presence of non linearity of the actuation chain in the open-loop response, affect the maximum achievable transmission bandwidth. We have limited the relative modulation amplitude to 30% of the average DC value of 700 mA, in order to avoid a possible overburden of the LED sources due to excessive currents in the positive periods of the modulation pattern of the nominal DC value. The transmitted waveform has been chosen to match a OOK Manchester encoding, according to PHY I of standard IEEE 802.15.7 for Outdoor VLC [8].

The (red) LED emitter (Lux Potentia OJ200-R07, 1A 12V) is composed a series of 3 high-power LEDs. In the scheme, the original power supply has been bypassed by MOSFET-based current driver/modulator, while preserving the original case of the LED series, so that the global features of the traffic light illumination pattern are unaltered. A red-coloured Fresnel lens shapes the beam according to the standards [1,3] and increases the visibility at large distances.

3.2.2 VLC Receiver

The receiver hardware is implemented by modifying a Thorlabs PDA36-A active high speed photodiode with a physical AC decoupling of the pho-

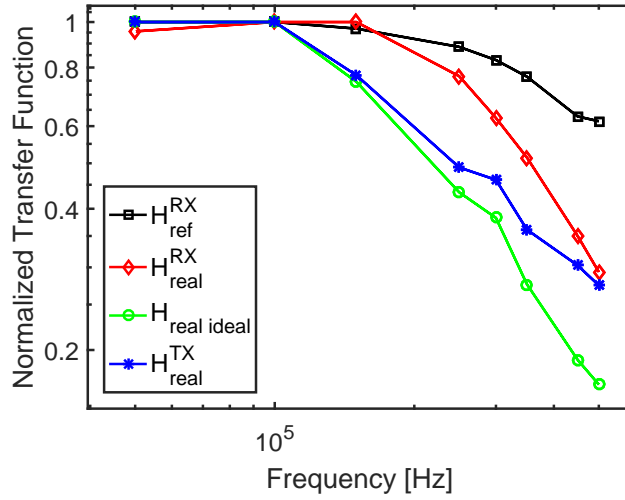
todiode chip from the first transimpedance amplification stage. The time constant $f_{RX} \simeq 5$ kHz of such decoupling is realized through a multi element RLC network, with parameters chosen in such a way to filter out all of the unwanted low-frequency light variations (headlights, sunlight ecc.), still allowing for the modulation signal to pass through the first stage of the receiving electronics. Such configuration allowed for high RX gains without the risk of saturating the amplifier by a large light background (see also Fig. 3.7). The photo receiver gain has been chosen as the highest still preserving a bandwidth > 150 kHz. The concentrator used in this RX setup (rightmost part of RX panel) is the shortest focal, The choice of short-focal, aberration-corrected optical concentrators is crucial in order to keep a good trade-off between reasonably high acceptance angle and global optical gain when the solution to increase the input optics diameter beyond 1" is unaffordable.

Many vehicular applications are leaning towards employing an image sensor for communications, as these devices are found to be on most new vehicles as high-end safety packs. The main concern associated to such devices in realistic high-speed VLC applications is represented by the refresh rate of the sensor and its integration time. When the full frame needs to be employed (e.g. through a wide-angle optics, to avoid necessity of mechanical tracking a specific object, which is instead required if narrow-angle tele-objectives are employed) to catch a 200 kHz modulation, the sensor should virtually run at full refresh rates higher than 100 kHz (compliant with IEEE802.15.7 standard for outdoor applications), which is far from reach (or at least extremely expensive) even in high-end commercial devices.

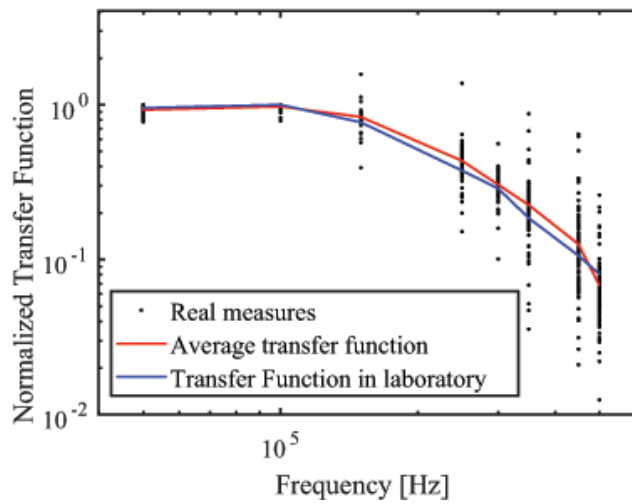
3.2.3 Transfer function of equipment

Laboratory measurements have also been carried out to extract the transfer functions (TFs) of the electronic modules at the transmitter and receiver sides, $H_{TX}^{el}(f)$ and $H_{RX}^{el}(f)$, respectively. Such analysis is fundamental in order to make a realistic estimation, based on the model presented in the end parts of Sec. 3.3.2, on communication performances of a I2V VLC implementation in real urban scenario, quantified through parameters such as bit-error rate (BER) as a function, e.g., of baud rate and of position on the measurement grid (see in the end parts of Sec. 3.3.2) .

In order to retrieve $H_{RX}^{el}(f)$ we replicated the transmission pattern via a 3mm, low-capacitance low-power red LED driven with a fast signal generator, and collected it through the same photodetector used in the on-field



(a) Normalized Transfer function of electronics circuit of transmitter and receiver.



(b) Comparison between global normalized TFs obtained from laboratory (blue line) and real-scenario (dots and red line) measurements.

Figure 3.4: Transfer functions of the overall VLC system.

measurement campaign. This configuration grants a fast TX bandwidth (BW) > 1 MHz, much larger than BW of TX stage used in PHY I of standard IEEE 802.15.7 (See section 2.2.1), and the TX TF is a constant in the desired frequency range. Since the normalized transfer functions of transmission system are given by the product of the normalized transfer functions of RX and TX electronics blocks, for the measured TF in real urban scenario $H_{RX}^{road}(f)$ we can hence write $H_{RX}^{road}(f) = \text{const} \cdot H_{RX}(f)$, allowing for measurement of the frequency-dependent RX block contribution.

An analogous procedure has been performed in order to isolate the frequency-dependent contribution of TX block: a low-gain, fast photo receiver (not used in the on-field campaign where a high-gain configuration was needed due to large distances involved) available in the lab has been used to collect the signal transmitted from the original TX stage (traffic light lamp + modulator). However, since the fast photoreceiver BW was only roughly 3 times larger than the TX bandwidth, its contribution could be represented by a constant term on the whole frequency window. However, this measured TF, $H^{comb}(f)$ can still be employed to determine H_{TX}^{road} : to this scope we perform a final TF characterization using both the fast TX and RX stages, allowing to retrieve a “reference” TF, $H_{RX}^{ref}(f)$. It is easy to argue that the above measurements can now be combined in order to get:

$$H_{TX}^{road} = \text{const} \cdot H_{TX} = \frac{H^{comb}}{H_{RX}^{ref}} \quad (3.3)$$

Normalized TF’s, measured as above, are reported in upper panel of Fig. 3.4, whereas the lower panel shows a comparison between the global TF, obtained on-field data in real urban scenario (dots correspond to each position in the grid, red solid line connects the average for discrete frequency values), and the global TF measured as $H_{TX}^{road} \cdot H_{RX}^{road}$ (blue). The substantial agreement between the two confirms the validity of VLC block diagram description, as well as, the resilience of prototype system against stray effects stemming from the outdoor realistic scenario (sun, headlamps, reflections ecc.), at level of accuracy.

3.3 Traffic light emission pattern and wireless channel

Whilst the optical wireless channel has been characterized in literature for infrared (IR) communication as in [17], and recently a comparison between IR and VLC appeared [69], in order to enable the use of VLC technology for safety-critical / smart driving applications [16, 103], it is mandatory to test and analyse the VLC-based V2V and I2V communication channel in a real urban environment, with regulatory LED sources and infrastructures. As for today, however, a comprehensive characterization of the VLC channel in a realistic scenario is still lacking, due to intrinsic difficulties mainly represented by the influence of non-ideal external factors, such as ambient light and irregularities of the emission pattern of LED-based headlights or traffic lights [55, 78].

In this section we present an outdoor measurement campaign, aimed at the extensive characterization of the VLC transmission channel in a real urban scenario, carried out in the city of Prato (Italy) in collaboration with ILES srl. The measurements have been taken in a real urban road, with regulatory traffic light emitting a VLC signal to the receiver located along the same road. The receiver has been located at three different heights corresponding, respectively, to that of a car headlights, dashboard and internal mirror. Measurements have been performed in the presence of sunlight and of other car headlights interference.

The data has been used to extract a mathematical model of the VLC signal propagation. In addition, the transmitter-receiver transfer function is also modelled, including those of the electronic and optical elements.

The setup demonstrates attainable distances of several tens of meters, mainly limited by the directional emission pattern of the semaphore lamps, optimized for maximum visibility at $\simeq 15$ m for typical dashboard heights.

In particular, this section is focused on a characterization of transmitted lens with irregular emission pattern and the path loss of the wireless channel.

This work presents an extensive measurement campaign aimed at VLC channel characterization for I2V communication, carried out by using a real traffic-light in a typical urban road. The receiver has been located at three different heights corresponding to car headlights, dashboard and internal mirror, respectively. A specific hardware for modulating the LED of the traffic light has been designed and implemented. The data have been then

used to mathematically model the transmission pattern and the propagation channel. Three models have been proposed and compared in terms of complexity and accuracy, together with the conventional Lambertian model. The results show that the Lambertian model is not accurate enough to describe the VLC transmission-propagation from traffic-light to vehicles. The proposed model can be extended to distances wider than those considered during the measurements campaign. The model can be used to evaluate the performance of VLC technology for automotive applications. In addition, the theoretical error probability of the VLC signal has been derived by using the experimental data. The results highlight that an uncoded error probability of 10^{-3} is achievable at 30 m distance, showing that prototype implementation can be safely used for data service in I2V applications.

3.3.1 Measurement Campaign

In this measurement campaign, the signal transmitted by the LED lamp with an Agilent AFG 1062 function generator is represented by a time-dependent rectangular function

$$s(t) = \sum_{j=0}^{\infty} s_j(t - jN_bT) \quad (3.4)$$

where

$$s_j(t) = A \sum_{k=0}^7 s_k \cdot \text{rect} \left(\frac{t - T/2 + kT}{T} \right) \quad (3.5)$$

and A is the amplitude, T is the duration of the single rectangular pulse, s_k is the transmitted symbol and N_b is the number of transmitted symbol sequences. The symbol sequence is $\vec{s} = \{1, -1, 1, -1, 1, 1, -1, -1\}$, chosen in order to encompass all of the possible logic transitions appearing in Manchester encoding, where no more than two consecutive symbols can be of the same sign [36] (see Fig.3.5).

The on-field measurements campaign have been carried out in the city of Prato (Italy) in collaboration with ILES srl, a company producing and installing road signalling infrastructures. The company has installed one traffic light in a real urban scenario consisting of a two-lane road with buildings on both sides (see Fig. 3.6). The traffic light has been positioned on the right side of the rightmost lane, with 0.75 m indentation, at the height of 2.83 m, in accordance to Italian regulations UNI11248 [1] and UNI13201-

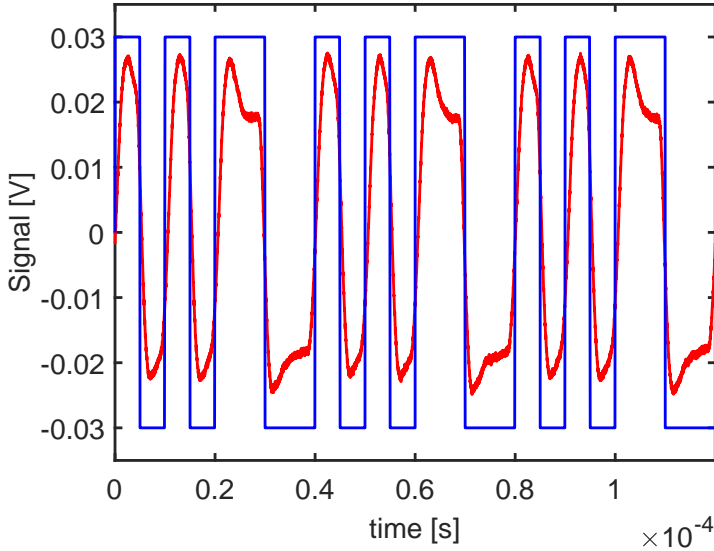


Figure 3.5: The blue curve represents the transmitted signal, modulated with OOK Manchester NRZ scheme, as indicated in standard IEEE 802.15.7 for outdoor VLCs. The red curve represents the signal received at the reference position indicated in Fig. 3.6, averaged over 4 acquisition periods.

2 [3]. The measurements have been carried out during one entire day (sunny conditions).

The red lamp of the traffic light has been modulated with the information signal (see Fig. 3.6). In particular, the red LED lamp has been controlled by prototype driver circuit which, besides controlling and supplying the DC nominal operating current, allows for the insertion of the bit sequence via an external function generator. The LED driver is the only component that has been replaced in the commercial traffic light.

The photodetector has been positioned in a grid on points in front of the emitting traffic light (Fig. 3.6). The grid has been centered at the position of the traffic light, with the x -axis along the road length, the y -axis along the road width and a vertical z -axis. The grid points along the x -axis ranges from 3 to 30 m, with more density in the first 10 m: [3 m, 4 m, 5 m, 7 m, 10 m, 15 m, 20 m, 25 m, 30 m]. Along the y -axis we included an offset of 0.75 m

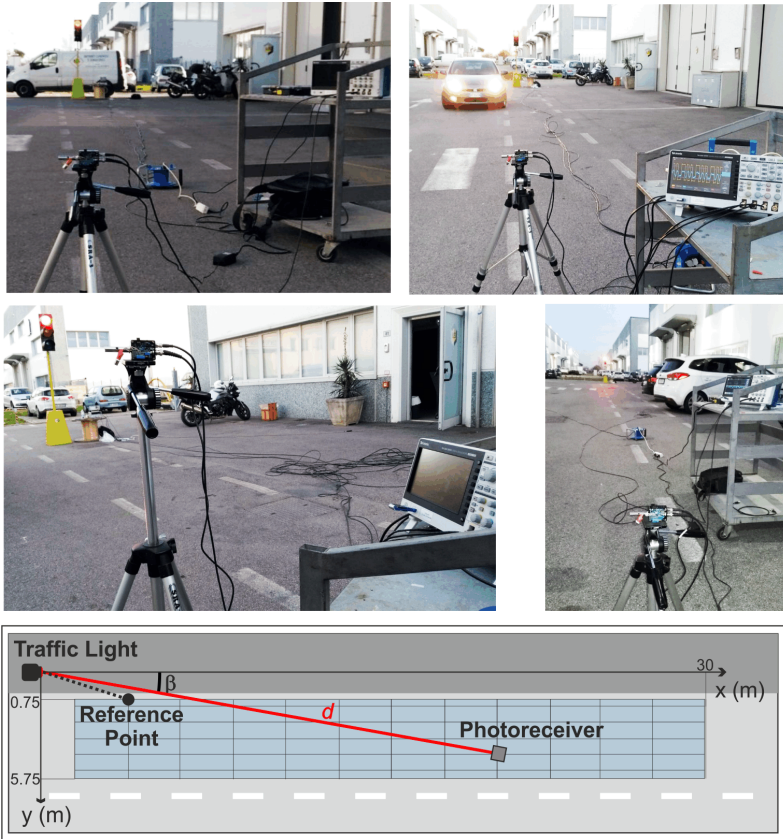


Figure 3.6: Experimental setup for the measurement campaign in a real urban scenario. Several different conditions has been tackled. The AC coupling of the photodetector washes the contribution of ambient and artificial stray lights out during all the day and the evening, even in the case of direct stray sunlight and/or headlight illumination. In the lower panel, a sketch of the measurement grid is reported. Measurements have been repeated in the grid-area for three different receiver heights (see main text). The reference (0 dB) point is located at (4, 0.75) m, for a height of 1.35 m.

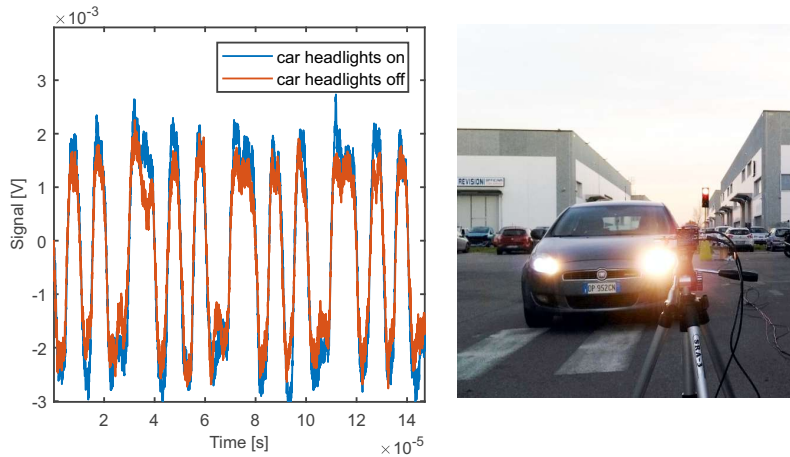


Figure 3.7: Test on the influence of different source of lights (sun and car headlights) on the received VLC signal. Due to physical AC coupling of the photodetector, no influence on the quality of the signal due to external light sources is detected.

since the traffic light has this indentation on the sidewalk. The step between measurement points is fixed to 1 m: [0.75 m, 1.75 m, 2.75 m, 3.75 m, 4.75 m, 5.75 m]. This two-dimensional grid is repeated for three different heights (z-axis) to simulate where the receiver could be placed on the vehicle: car headlights (0.75 m), dashboard (1 m) or rear-view inside mirror (1.35 m).

The photodetector is connected to an oscilloscope to display and record the VLC signal coming from the traffic light . The oscilloscope is triggered by a sync output of the function generator whose period, highlighted in Fig 3.5, corresponds to a full Manchester modulation cycle. The record length is 200 kpts at a sampling rate of 0.5 GHz, encompassing 10 full modulation periods. For each measurement we acquired both a single shot and the average of 4 traces.

In all of the points of the grid we chose to align the optical axis of the receiver towards the centre of traffic light red lamp, de facto maximizing the amplitude of the received signal in each specific point of the grid.

Noticeably, thanks to the specific design of prototype RX hardware, when either strong direct sunlight and/or incoming cars headlamps lights were interfering with measurement process (see Fig. 3.7), we did not observe any

influence on the detected signal, as demonstration of resilience to DC stray light components. The effect of interfering car headlights has been evaluated experimentally for one position of the car and receiver over the measurement field. We did not observe any quality degradation on the received signal with a car headlights positioned at a distance of 3 m from the receiver.

3.3.2 Propagation Model

The experimental (raw) data, recorded in each point of the 3D grid, has been processed to reduce the noise effects and estimate the received amplitude in the frequency domain. The processing steps on the raw data can be summarized as follows:

- Data Binning;
- Fast Fourier Transform, normalized to a reference value chosen as maximum signal obtained in the "reference point" (see Fig. 3.6);
- Reconstruction of the amplitude of the received signal in each position (x, y, z) of the grid.

Each step is detailed in the following.

We have observed that the frequency components of the received signal over 500 kHz show a negligible amplitude, thus we applied a data binning, equivalent to a downsampling procedure, to reduce the frequency observation interval hence filtering out unnecessary high-frequency components, laying above prototype electronic system bandwidth. The binning procedure takes a cluster of consecutive (time) samples and replaces the cluster with the average value of the samples.

The binning value can be defined as

$$N_{\text{bin}} = \frac{f_c}{2f_{\text{max}}} \quad (3.6)$$

where f_c is the initial sampling frequency of the received signal and f_{max} is the highest frequency of the desired observation window. In this experiment, $N_{\text{bin}} = 250$, since the sampling frequency of the oscilloscope is 250 MHz.

The ratio between the transfer function⁴ (TF) of the whole system calculated in each single point of the grid and the TF calculated in the reference

⁴The ratio $\frac{S_{\text{RX}}(f)}{S_{\text{TX}}(f)}$ is usually defined as the transfer function of a generic system (black box) that has $s_{\text{TX}}(t)$ as input and $s_{\text{RX}}(t)$ as output.

position can be used to define the propagation model of the VLC signal from the traffic light to the vehicle

$$\Delta H_i = \frac{H_i(f)}{H_{\text{ref}}(f)} \quad (3.7)$$

with

$$H_i(f) = \frac{S_{\text{RX}_i}(f)}{S_{\text{TX}_i}(f)}; \quad H_{\text{ref}}(f) = \frac{S_{\text{RX}_{\text{ref}}}(f)}{S_{\text{TX}_{\text{ref}}}(f)} \quad (3.8)$$

where $S_{\text{TX}_i}(f)$ and $S_{\text{RX}_i}(f)$ is the Fast Fourier Transform (FFT) of the transmitted and received signal, respectively, at location i , $H_i(f)$ represents the TF between the traffic light and the i th point on the grid and $H_{\text{ref}}(f)$ stands for the TF between the traffic light and the reference point. All measurements have been triggered on the same signal, and thus the FFT of transmitted signal will be the same for each point $S_{\text{TX}_i}(f) = S_{\text{TX}_{\text{ref}}}(f)$. Thus, Eq. (3.7) can be then rewritten as

$$\Delta H_i = \frac{S_{\text{RX}_i}(f)}{S_{\text{RX}_{\text{ref}}}(f)} \quad (3.9)$$

From Eq. (3.9) we can deduce that ΔH_i depends only on the spectrum of the received signal at the i -th location and at the reference point. In addition, we can safely assume that ΔH_i does not depend on the carrier and modulation frequencies, as the large spectral width of the optical carrier emitted by the LED source makes the contribution of absorption lines of air absolutely irrelevant for any channel loss, whilst the large difference between modulation and carrier frequencies avoids any frequency-dependent interference effect in line-of-sight tests.

Fig. 3.8 shows the map of the amplitudes ΔH_i measured in each point of the grid at different height [0.75, 1, 1.35] m. Amplitudes are reported in logarithmic (dB) scale. We have used the point on the grid that shows the maximum amplitude (0 dB) as reference ("reference point" in Fig. 3.8).

It is worth to point out that the ratio in Eq. (3.9) makes us to neglect the effects of the electronic components, $H_{\text{TX}}^{\text{el}}(f)$ and $H_{\text{RX}}^{\text{el}}(f)$, of the i -th received signal. The effects of the optics at the receiver is neglected too, since the TF of the optical part at the receiver is nearly constant for every point of the grid.. Due to the operations described above, ΔH_i in Eq. (3.9) does not depend on the frequency.

With a ratio in formula (3.9), the elettro-optical conversion ($H_{\text{TX}}^{\text{el}}$) and vice versa ($H_{\text{RX}}^{\text{el}}$) reduces due to they are the same in every measurement

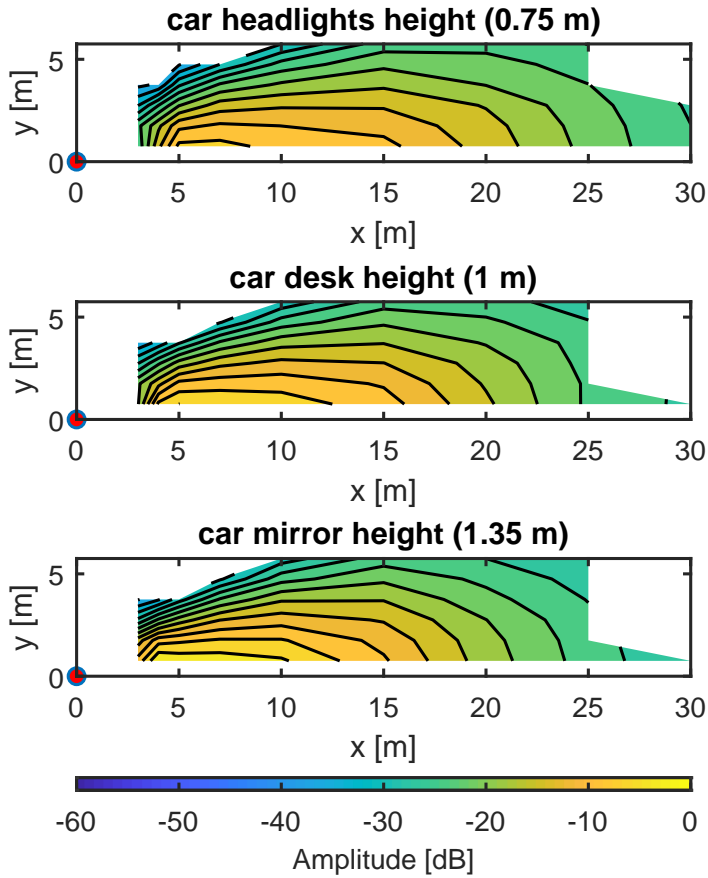


Figure 3.8: Amplitude map (dB) of the VLC signal ΔH_i measured over the grid for three different heights [0.75, 1, 1.35] m corresponding to car headlights, can desk and car internal mirror, respectively. The map reports the measurement data (intensity) over the field test grid shown in Fig. 3.6.

points. Also a term of receiver optical lens (H_{RX}^{op}) is possible to reduce with a receiver tracking of the source.

Lambertian Model

In the Lambertian model [13], the path loss is given by

$$I = \frac{I_0 * \cos^m(\phi)}{d^2} \quad (3.10)$$

where I_0 is the intensity in the axis of irradiance, ϕ is a irradiance angle, m is a parameter for characterized the influence of optical lens in traffic light and d is a distance the transmitter and the receiver.

Proposed propagation model

To mathematically characterize the propagation of the VLC signal, we aim to model the amplitude ΔH_i of the received signal over the grid, which in turn is quantified by its intensity. The intensity of the received signal depends on the position of the receiver in spherical coordinates

$$I(\alpha, \beta, d)$$

where α is the elevation, β is the azimuth and d is the distance between the transmitter and the receiver.

The traffic light lamp produces a light pattern which is symmetric in reflection with respect to a vertical plane containing the optical axis, but it is in general not axially symmetric to a specific axis. For this reason, the application of standard axial-symmetric Lambertian propagation models does not describe accurately the measured emission pattern.

The first model proposed here (3.11) is derived by modifying the well-known Lambertian propagation model [13]. Here the optical intensity is taken as:

$$I_1(\alpha, \beta, d) = \frac{f(\alpha, \beta)}{d^2}, \quad (3.11)$$

scaling as inversely proportional to the square of the distance. Differently by Lambert's law, the numerator has been generalized as a function of α and β .

The Lambert's cosine propagation law assumes that the source of light is a homogeneous diffuser. Whilst remaining a valid approximation in the analysis of emission of many direct sources as LEDs, this hypothesis is highly

inaccurate in case of shaped beam patterns, i.e. in presence of lenses (as in traffic lights). Thus, the second propagation model proposed here only preserves a global $1/d^2$ dependence of radiated optical intensity:

$$I_2(\alpha, \beta, d) = \frac{f(\alpha, \beta, d)}{d^2}. \quad (3.12)$$

The numerator is instead a generic polynomial function of (α, β, d) .

A more general approach can consider the optical intensity as a function

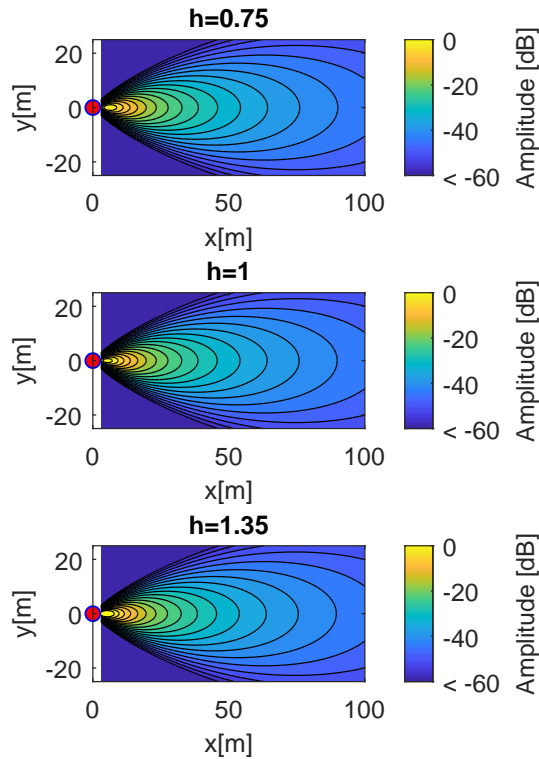


Figure 3.9: Intensity of the Lambertian model in an area 100×50 m. The photodetector heights are $\{0.75, 1, 1.35\}$ m.

of (α, β, d) without the term $1/d^2$ at the denominator, i.e.,

$$I_3 = f(\alpha, \beta, d) \quad (3.13)$$

This is the third, more general approach that we propose to model the measurements. Depending on the specific needs and applications, one can choose a general or a more specific model which in general will feature very different convergence performances as a function of the number of parameters employed in the fitting procedure.

The multiple generalized linear regression (MGLR) method has been used to find the best fitting parameters for the three models I_1 , I_2 and I_3 . Multiple linear regression is a generalization of simple linear regression to the case of more than one independent variable, and a special case of general linear models, restricted to one dependent variable. The generalized linear model (GLM) is typically used to model an irregular emission pattern [31, 39, 74] as it is a flexible generalization of ordinary linear regression that allows for response variables that have error distribution models other than a normal distribution. The GLM generalizes linear regression by allowing the linear model to be related to the response variable via a link function and by allowing the magnitude of the variance of each measurement to be a function of its predicted value. The output of the MGLR method is a set of polynomial coefficients of the function that fits the intensity.

In this procedure, the inputs of the MGLR method are the following parameters: the model under evaluation (I_1 , I_2 , I_3), the maximum order of the polynomial function for each variable (α, β, d) , the statistical distribution of the error (Normal, Poisson, Gamma)⁵

Let y_1, \dots, y_n denote n independent observations on a response. We treat y_i as a realization of a random variable Y_i . In the general linear model we assume that Y_i has a normal distribution with mean μ_i and variance σ . We further assume that the expected value μ_i is a linear function of p

⁵Linear regression models describe a linear relationship between a response and one or more predictive terms. Many times, however, a nonlinear relationship exists. Nonlinear Regression describes general nonlinear models. A special class of nonlinear models, called generalized linear models, uses linear methods. Ordinary linear regression can be used to fit a straight line, or any function that is linear in its parameters, to data with normally distributed errors. This is the most commonly used regression model; however, it is not always a realistic one. Generalized linear models extend the linear model in two ways. First, assumption of linearity in the parameters is relaxed, by introducing the link function. Second, error distributions other than the normal can be modeled [75].

predictors that take values $\mathbf{x}_i = (x_{i1}, x_{i2}, \dots, x_{ip})$ for the i -th case, so that

$$E[Y_i] = \mu_i = \mathbf{x}_i^T \mathbf{b} \quad (3.14)$$

where \mathbf{b} is a vector of unknown parameters. Once found \mathbf{b} from (3.14) we can write

$$\mu_i = b_0 + b_1 x_{i1} + b_2 x_{i2} + \dots + b_p x_{ip} \quad (3.15)$$

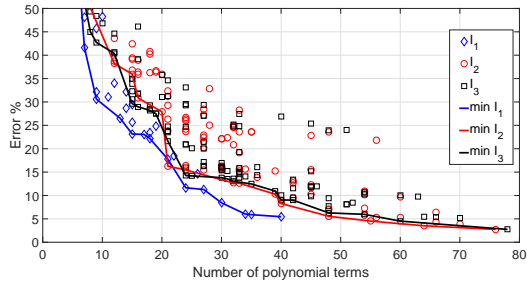
Different (from Normal) statistical distribution of the error can be used by taking into account the generalized linear model. In a generalized linear model, the outcome Y_i of the dependent variables is assumed to be generated from a particular distribution in the exponential family (Normal, Poisson and Gamma). The vector of the mean μ_i of the distribution depends on the independent variables \mathbf{x}_i through

$$\mu_i = g^{-1}(\mathbf{x}_i^T \mathbf{b}) \quad (3.16)$$

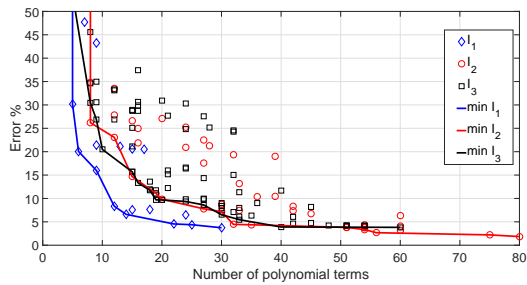
where $g(\cdot)$ is the *link* function.

To find the highest polynomial order for each of the variables (α, β, d) to be inserted into the MGLR method still avoiding the overfitting problem, a k-fold method is used [37, 57, 67]. The k-fold has been applied to every model (I_1, I_2, I_3) for each one of the error distribution (Normal, Poisson, Gamma). Thus, nine models have been evaluated. The polynomial order of α and d ranges from 1 to 9, while the order of β can assume only even values, from 2 to 8, because of azimuthal-symmetric nature of the emitted pattern.

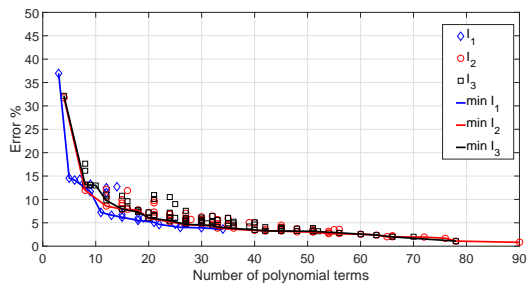
The percentage error for each of the proposed models $I_1(\alpha, \beta, d)$, $I_2(\alpha, \beta, d)$, $I_3(\alpha, \beta, d)$ as a function of the number of polynomial terms with a Normal (Fig. 3.10(a)), Gamma (Fig. 3.10(b)) e Poisson (Fig. 3.10(c)) distribution of the error in the MGLR method. Each point corresponds to a specific parameter configuration. For example, one red square in Fig.3.10(a) represents the error produced by the model $I_3(\alpha, \beta, d)$ with a specific number of polynomial terms for α, β and d coming out from the application of the k-fold and MGLR procedures. The error is calculated as the RMSE between the original measured data and the corresponding values of the polynomial fitting function over the whole grid. Solid lines are a guide to the eye connecting the best parameter configuration minimizing the error for a specific number of terms. Given a specific error threshold, it is possible to reach it with the lowest number of polynomial terms, after which the minimization procedure loses efficiency.



(a) Normal distribution.



(b) Gamma distribution.



(c) Poisson distribution.

Figure 3.10: Percentage error for each of the proposed models $I_1(\alpha, \beta, d)$, $I_2(\alpha, \beta, d)$, $I_3(\alpha, \beta, d)$ as a function of the number of polynomial terms with a different distributions of the error in the MGLR method. Solid lines are a guide to the eye connecting the best parameter configuration minimizing the error for a specific number of terms.

Table 3.1: Number of terms, orders of the variables and error for the solution (3.21) of model $I_1(\alpha, \beta, d)$ with Gamma distribution. Only values of (α, β) that minimize the error are reported (see the curve $\min I_1$ in Fig. 3.10(b)).

No. of terms	Order of α	Order for β	Error (%)	RMSE
30	8	6	3.7307	0.014001
25	6	8	4.3831	0.017496
22	6	6	4.5449	0.018839
14	4	6	6.5972	0.02563
12	4	4	8.3422	0.030691
9	2	6	16.002	0.061841
6	2	4	20.056	0.084346
5	2	2	30.182	0.10461

Table 3.2: Number of terms, orders of the variables and error for the solution (3.22) of model $I_2(\alpha, \beta, d)$ with Poisson distribution. Only values of (α, β, d) that minimize the error are reported (see the curve $\min I_2$ in Fig. 3.10(c)).

No. terms	Order α	Order β	Order d	Error (%)	RMSE
90	8	8	2	0,8221	0,0016
66	7	6	2	1,9923	0,0049
60	6	4	4	2,5728	0,006811
48	5	6	3	3,0709	0,010701
40	6	6	1	3,3717	0,010796
20	5	2	1	5,9458	0,014649
12	3	2	1	8,5654	0,029661
4	1	2	1	31,776	0,056186

As it can be seen in Fig. 3.10(a), the error decreases faster for model $I_1(\alpha, \beta, d)$. The other two models can get more accurate, at the expenses of introducing a high number of polynomial terms. Hence depending on the particular needs one can either choose a more "efficient" or a more "accurate" model for the VLC system.

If a Gamma or Poisson distribution is used in the MGLR method, the error decreases faster than using the Normal distribution. The I_2 model with Poisson distribution reaches the lowest error, but it requires a high number of polynomial terms (80) for the fitting function. If a low number of polynomial terms is desired, the model I_1 with Gamma or Poisson distribution reaches a lower error. A low number of polynomial terms is useful for extending the model to an area larger than the one where the measurements are taken. The k-fold method is used to avoid the overfitting problem in the area of the measurements.

Only two models have been compared to define a propagation model which is valid for distances out of measurement's range. The first one is I_1 with Gamma distribution, while the second is I_2 with Poisson distribution, the model I_3 results similar to I_2 , due to in this work is not considered. The first one has been selected because the error decreases more rapidly, the second one has been selected because it reaches the lowest error.

In case of $I_1(\alpha, \beta, d)$ with Gamma distribution, the vector \vec{y} of the intensity measured over the grid is

$$\vec{y} = (\Delta H_1 d_1^2, \Delta H_2 d_2^2, \dots, \Delta H_n d_n^2) \quad (3.17)$$

where n is the number of points over the grid of the measurements, ΔH_i is the intensity (in dB) in the i -th point of the grid and d_i is the distance of the i -th point of the grid from the source of the VLC signal (the traffic light). The predictor matrix is composed by

$$[X] = [\vec{x}_1 \ \vec{x}_2 \ \dots \ \vec{x}_n]^T \quad (3.18)$$

with

$$\vec{x}_i = [1 \ \vec{\alpha}_i \ \vec{\beta}_i \ \vec{\alpha}_i \otimes \vec{\beta}_i] \quad (3.19)$$

where \otimes stands for the element-by-element product operator, $\vec{\alpha}_i = (\alpha_i, \alpha_i^2, \dots, \alpha_i^p)$ is the vector of the elevation angles and $\vec{\beta}_i = (\beta_i^2, \beta_i^4, \dots, \beta_i^{2q})$ is the vector of the azimuth (squared) angles. The parameters p and $2q$ represent the maximum polynomial order for the elevation parameter α and the azimuth parameter β , respectively.

In case of $I_3(\alpha, \beta, d)$ with Poisson distribution, the vector \vec{y} of the intensity measured over the grid is the same (3.17), while

$$\vec{x}_i = [1 \quad \vec{\alpha}_i \quad \vec{\beta}_i \quad \vec{d}_i \quad \vec{\alpha}_i \otimes \vec{\beta}_i \otimes \vec{d}_i] \quad (3.20)$$

where $\vec{d}_i = (d_i, d_i^2, \dots, d_i^r)$. The parameter r is the maximum polynomial order for the distance parameter d .

The objective is to find the coefficients $\vec{b} = (b_1, \dots, b_m)^T$ (with $m = pq + 1$) so that

$$E[\mathbf{y}]^{-1} = \mathbf{X}\mathbf{b} \quad (3.21)$$

in case of model $I_1(\alpha, \beta, d)$ with Gamma distribution, and

$$\log(E[\mathbf{y}]) = \mathbf{X}\mathbf{b} \quad (3.22)$$

in case of model $I_2(\alpha, \beta, d)$ with Poisson distribution (with $m = pqr + 1$).

Table 3.1 and 3.2 show the different solutions for (3.21) and (3.22), respectively, increasing the order of the polynomial function. The error associated to each model compared with the measurements is reported as average percentage error

$$\epsilon_{\text{perc}} = \frac{1}{n} \sum_{i=1}^n \frac{|y_i - I_{li}|}{y_i} \times 100 \quad (3.23)$$

as well as root mean squared error (RMSE)

$$\epsilon_{\text{RMSE}} = \sqrt{\frac{\sum_{i=1}^n (y_i - I_{li})^2}{n}} \quad (3.24)$$

with $i = 1, \dots, n$ and $l = 1, 2, 3$.

The polynomial function for the model $I_1(\alpha, \beta, d)$ (3.11) with Gamma distribution with 12 terms is

$$\begin{aligned} I_1(\alpha, \beta, d) = & \frac{1}{d^2} (b_1 + b_2\alpha + b_3\beta^2 + b_4\alpha^2 + b_5\alpha\beta^2 + b_6\beta^4 \\ & + b_7\alpha^3 + b_8\alpha^2\beta^2 + b_9\alpha\beta^4 + b_{10}\alpha^4 + b_{11}\alpha^3\beta^2 \\ & + b_{12}\alpha^2\beta^4)^{-1} \end{aligned} \quad (3.25)$$

while for the model $I_2(\alpha, \beta, d)$ (3.12) with Poisson distribution with 12 terms is

$$\begin{aligned} I_2(\alpha, \beta, d) = & \frac{1}{d^2} \exp\{b_1 + b_2\alpha + b_3\beta^2 + b_4d + b_5\alpha^2 \\ & + b_6\alpha\beta^2 + b_7\alpha d + b_8\beta^2 d + b_9\alpha^3 + b_{10}\alpha^2\beta^2 \\ & + b_{11}\alpha^2 d + b_{12}\alpha\beta^2 d\} \end{aligned} \quad (3.26)$$

Table 3.3: Values of the coefficient \mathbf{b} for the models $I_1(\alpha, \beta, d)$ with Gamma distribution and $I_2(\alpha, \beta, d)$ with Poisson distribution.

Coefficient	Value for I_1 model	Value for I_2 model
b_1	0.088395	6,1107
b_2	1.8365	20,436
b_3	0.53823	-9,8384
b_4	14.718	-0,09868
b_5	6.3874	47,629
b_6	0.92338	-12,142
b_7	46.406	-1,0858
b_8	26.178	-0,08044
b_9	-7.8413	52,16
b_{10}	52.665	13,944
b_{11}	39.219	-1,4756
b_{12}	-1.3364	0,90893

and the value of the coefficients is reported in Table 3.3. We selected the 12 terms since this choice provides in both models a fair tradeoff between performance (error below 10%) and complexity.

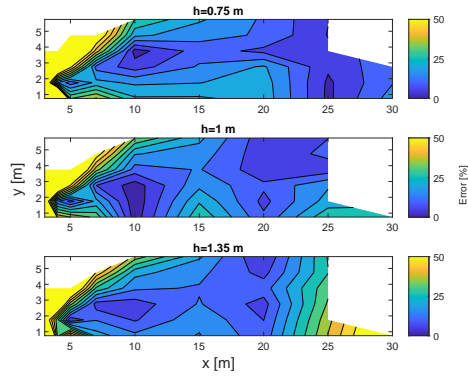
It is important to note that the element b_j of vector \vec{b} is set to zero if the corresponding order of the associated variables (α , β , d) exceeds the maximum between the selected order of α , β or d .

Comparison between proposed and Lambertian model

The proposed models have been compared to the conventional Lambertian model [62], widely used in literature. Fig. 3.11 shows the accuracy of the Lambertian model as well as of the proposed new models, over the experimental measurements grid. It is important to note that the accuracy has been calculated only over the points where we had the value corresponding to a real measurement. We could not measure the intensity on the other side of the traffic-light since there was no lane available, as in a typical urban road.

The accuracy is calculated as the difference between the measured intensity in a point of the grid and the corresponding intensity of the fitting polynomial function of the model.

As it can be seen the conventional model shows a significant higher error compared to the models proposed in this section. The average RMSE of the



(a) Accuracy of the conventional Lambertian model.

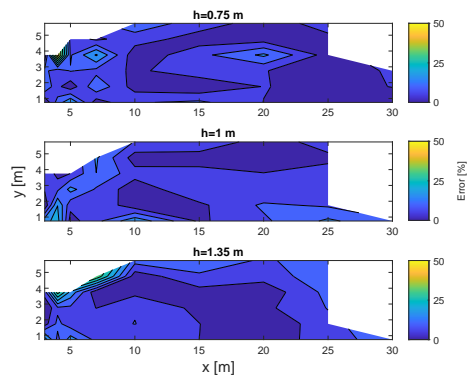
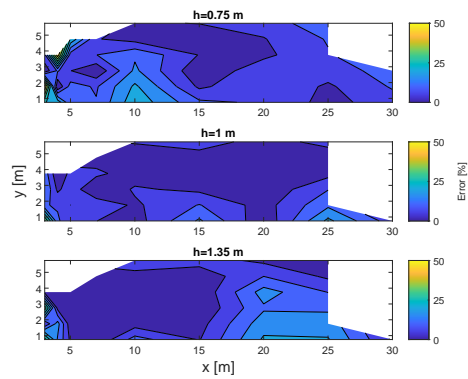
(b) Accuracy of the I_1 model.(c) Accuracy of the I_2 model.

Figure 3.11: Accuracy of proposed models.

conventional Lambertian is 0.097, while the one of the two proposed models (with, e.g., 12 parameters) is 0.030 and 0.029 (see Table 3.1 and 3.2).

Performance Analysis

To evaluate the performance in terms of probability of error and maximum achievable bit-rate, we first estimate the noise level in each point of the measurements grid. The error probability of digital signalling in wireless channels is given by

$$P_e \leq (S - 1)Q \left(\sqrt{\frac{a^2 \rho_{min}^2}{4N_0}} \right) \quad (3.27)$$

where S is the number of symbols in the digital constellation, a is the fading coefficient, ρ_{min} is the minimum distance between the symbols and N_0 is the noise spectrum density power, in this case the OOK Manchester modulation was considered as Binary Phase-Shift Keying (BPSK).

Supposing than an AWGN model holds, the relation between the probability of error and the noise level becomes

$$P_e = Q \left(\sqrt{\frac{\rho_{min}^2}{2N_0}} \right) \quad (3.28)$$

The distance ρ_{min} depends on the specific constellation that has been transmitted. In experiments, an antipodal (BPSK) constellation was used, thus the P_e can be written as

$$P_e = Q \left(\sqrt{\frac{P_R}{\sigma_N^2}} \right) = Q \left(\sqrt{SNR} \right) \quad (3.29)$$

where P_R is the received power and σ_N^2 is the noise variance. To estimate the noise variance the following procedure has been carried out. Let us first remind that the received signal vector at location i is

$$\vec{s}_i = [\vec{s}_{i1} \ \cdots \ \vec{s}_{iN_b}] \quad (3.30)$$

where \vec{s}_{ij} is the vector coming from the sampling of the waveform in (3.5). The received vector at the reference location ($i = \text{ref}$) is averaged over the repetition periods

$$\vec{s}_{\text{ref}} = \frac{1}{N_b} \sum_{j=1}^{N_b} \vec{s}_{\text{ref}j} \quad (3.31)$$

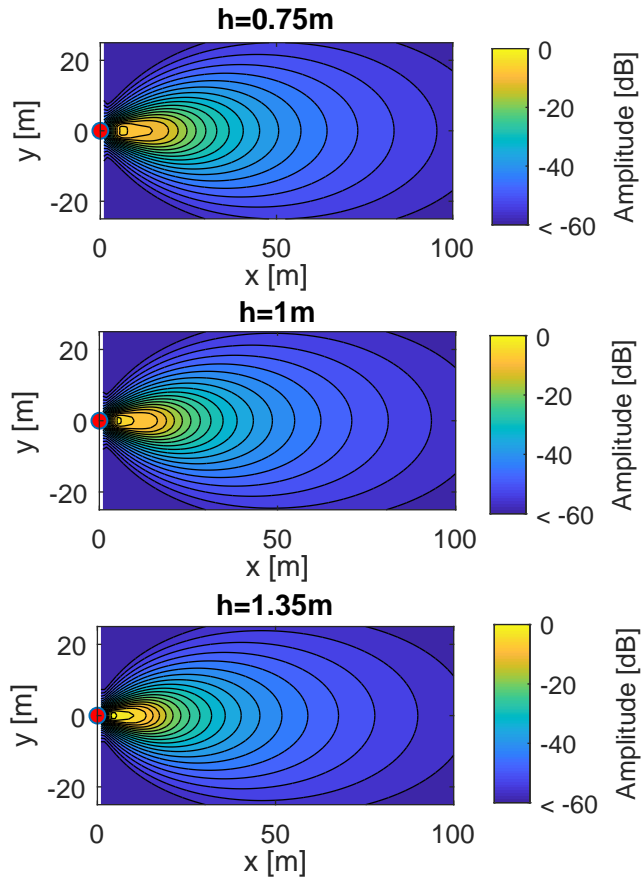


Figure 3.12: Intensity of the propagation model $I_1(\alpha, \beta, d)$ with Gamma distribution in an area 100×50 m. The photodetector heights are $\{0.75, 1, 1.35\}$ m. The polynomial order for α and β is 4.

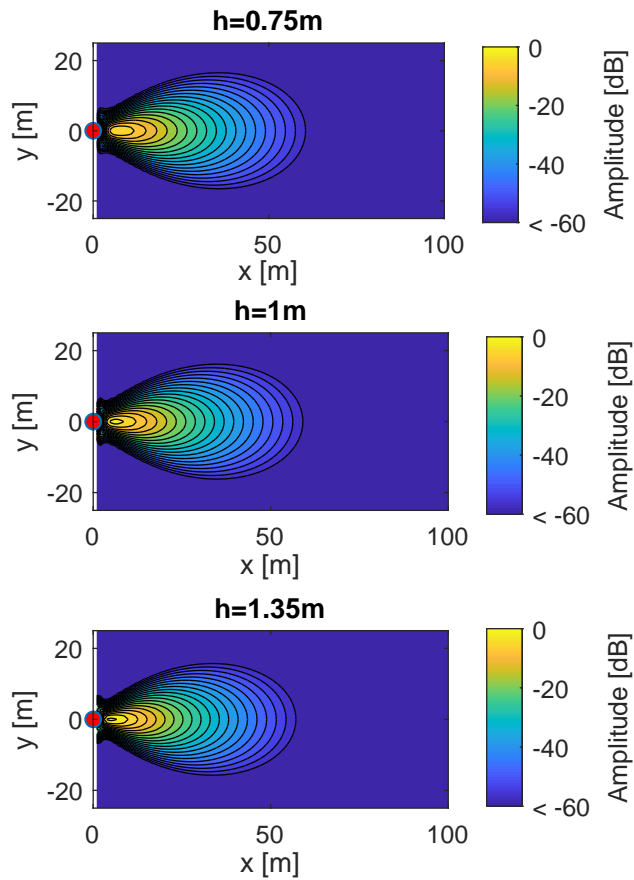


Figure 3.13: Intensity of the propagation model $I_2(\alpha, \beta, d)$ with Poisson distribution in an area 100×50 m. The photodetector heights are $\{0.75, 1, 1.35\}$ m. The polynomial order for α is 3, for β is 2 and for d is 1.

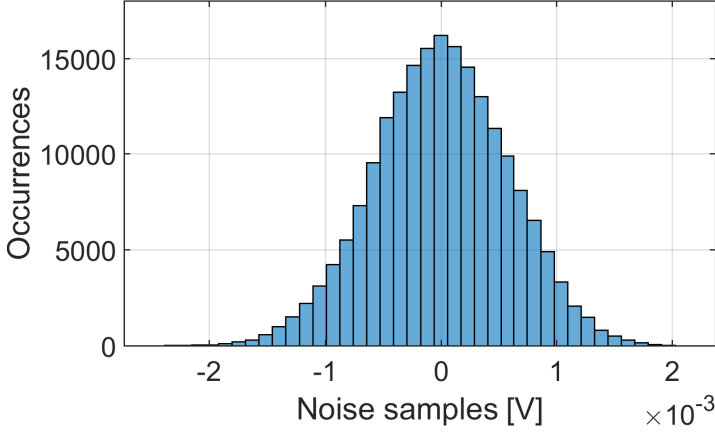


Figure 3.14: Histogram of the noise vector at the grid point i is ($x = 30, y = 1.75, z = 0.75$) m.

Now, the estimated noise vector at location i

$$\vec{w}_i = [\vec{w}_{i1} \ \cdots \ \vec{w}_{iN_b}] \quad (3.32)$$

is calculated as the difference between the received signal vector at location i and the averaged vector at reference location multiplied by ΔH_i (3.7)

$$\vec{w}_{ij} = \vec{s}_{ij} - (\vec{s}_{\text{ref}} \Delta H_i) \quad j = 1, \dots, N_b \quad (3.33)$$

The noise vector in (3.32) is then used to estimate the noise variance $\sigma_{w_i}^2$ at location i . An example of histogram of the noise vector \vec{w}_i is reported in Fig. 3.14, where the grid point i is ($x = 30, y = 1.75, z = 0.75$) m. Fig. 3.14 shows the occurrences (y-axis) of the noise samples (x-axis) as in (3.33).

The signal-to-noise ratio (SNR) can thus be calculated as

$$SNR_i = \frac{E[\vec{s}_{\text{ref}}^2] \Delta H_i^2}{\sigma_{w_i}^2} \quad (3.34)$$

This result can be used to calculate the error probability (3.29) in every point of the measurement grid. The map of the error probability is reported in Fig. 3.15 for the height 0.75 m. A probability of error of 10^{-3} (uncoded) can be provided even at 30 m away from the traffic light. The map shows the error

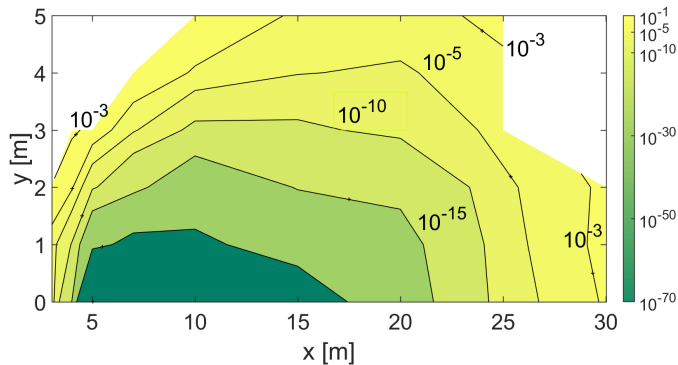


Figure 3.15: Map of the error probability over the measurements grid.

probability over the perimeter where the experimental measurements have been carried on. The intensity models proposed in this work can be anyway used to calculate the performance of a VLC system in different perimeters.

3.4 Receiver optical lens

After the characterization of transmission emission pattern and optical wireless channel, the study is focused on receiver optical lens. This work is very recent, the experiment campaign has been carried out in this summer and now we are writing a possible paper with results.

The characterization of this transfer function usually starts to hypothesis of point source, typically used for a study of VLC system. From this hypothesis, the image of source on photodiode is a point. If the image is inside a photodiode the TF is equal to a gain of lens, otherwise the TF is zero, i.e. a field of view (FoV) is the unique parameter considered.

$$h_{\text{RX}}^{\text{op}} = \begin{cases} G_{op} & \psi \in \text{FoV} \\ 0 & \psi \notin \text{FoV}. \end{cases} \quad (3.35)$$

with G_{op} is optical ratio, i.e. a ratio between photodiode and lens area, and ψ is angle of incidence, i.e. $\psi = 0$ if the image of source is in the middle of receiver surface.

The field of view for point source is equal to:

$$FoV = 2 \arctan \frac{d}{2f} \quad (3.36)$$

with d is diameter of photodiode and f is focal distance of lens. For the same photodiode, the lower the focal distance, the higher the field of view.

Without the hypothesis of point source, it is necessary to consider the magnification, i.e. the real dimension of source image on the photodiode surface. The magnification (M) can be define as:

$$M = \frac{q}{p} \quad (3.37)$$

with q is a distance between image and lens, while p is a distance between source and lens. For a thin lens formulation:

$$\frac{1}{p} + \frac{1}{q} = \frac{1}{f} \quad (3.38)$$

typically in VLC communication experiment (in particular for ITS application) $p \gg f$ the distance lens to source is in meters order, while focus lens is in millimetres order, and from the equation 3.38 it is possible $q = f$. The formula of magnification 3.37 can be rewritten as:

$$M = \frac{q}{p} = \frac{f}{p} \quad (3.39)$$

E.g. the distance between traffic light and vehicle can be in the range 3-50 meters and the lens focal distance, with a good FoV, is about 20 millimetres. For this parameter, the magnification is about 0.007 for 3 metres and 0.0004 for 50 metres. If the source diameter of traffic light lamps is 20 centimetres, then the image of the source is 1.4 mm at 3 m and 0.08 mm at 50 m. The active area of photodiode DET36 Thorlabs, used in a experiment campaign, is 3.6×3.6 mm. If a distance between traffic light and vehicle is 50 m, the hypothesis of point source is correct due to the image is smaller than active area of photodiode, but for 3 metres, the diameter of image is comparable to the photodiode side.

The first mathematical model developed takes account of magnification. With geometrical model (see figure 3.16) it can to define:

$$x = f \tan \psi \quad (3.40)$$

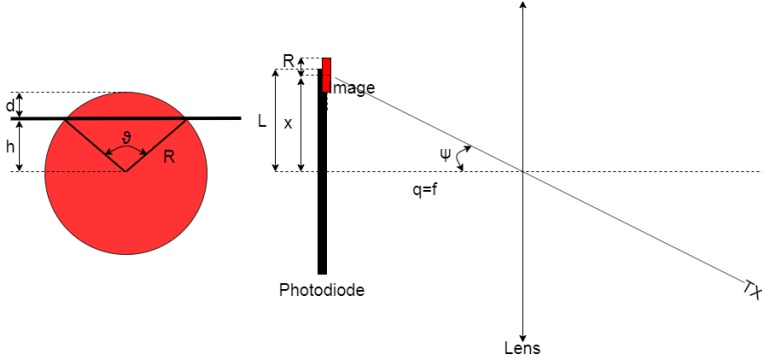


Figure 3.16: The image of source inside a photodiode surface.

with x is the distance between the centre image and optical axis, ψ is incidental angle and f is focal length.

Firstly, the model split the problem in three parts:

- All source image is on the receiver ($x + R < L$), i.e.:

$$\psi < \arctan\left(\frac{L - R}{f}\right) \quad (3.41)$$

- The image is all outside of photodiode surface ($x > L + R$), i.e.:

$$\psi > \arctan\left(\frac{L + R}{f}\right) \quad (3.42)$$

- Transition zone

with R is the radius of image and L is half length of photodiode (see figure 3.16)

In the transition zone, the image part outside to photodiode is define with a formula of circular segment.

$$A = \frac{1}{2}R^2(\theta - \sin \theta) \quad (3.43)$$

with geometrical proprieties, $\theta = 2 \arccos\left(\frac{h}{R}\right)$ and $h = x - L$. Replacing x with equation 3.40, θ results:

$$\theta = 2 \arccos\left(\frac{f \tan \psi - L}{R}\right) \quad (3.44)$$

The mathematical model of receiver lens results:

$$I = \begin{cases} I_0 \cos \psi & \psi < \arctan\left(\frac{L-R}{f}\right) \\ 0 & \psi > \arctan\left(\frac{L+R}{f}\right) \\ I_0 \cos \psi \left(1 - \frac{\theta - \sin \theta}{2\pi}\right) & \arctan\left(\frac{L-R}{f}\right) < \psi < \arctan\left(\frac{L+R}{f}\right) \end{cases} \quad (3.45)$$

The aberration effect is not considered in this model, the error between the mathematical model and the experimental results is attributable to this property of optical system. The mathematical characterization of aberration is very difficult to define, because the term aberration includes some effects as:

- Defocus
- Coma
- Spherical aberration
- Astigmatism
- Field Curvature
- Image distortion

3.4.1 Comparison between model and experimental data

The measurements campaign have been carried out in the corridor of department of physics in Sesto Fiorentino (see figure 3.17). Four lenses are used in this test:

- 1 inch aspherical lens with focal length 16 mm
- 2 inch aspherical lens with focal length 32 mm
- 1 inch fresnel lens with focal length 25 mm
- 2 inch fresnel lens with focal length 32 mm

The receiver has been positioned in front of traffic light to variable distance (6, 12, 18, 24, 30, 36, 42 and 50 m). For each position, firstly we aligned the optical axis of receiver towards the centre of transmission source ($\psi = 0$).

After, we changed the incidental angle with 1 degree step in vertical and horizontal directions.

The measurement data has been analysed (see an example in figure 3.18), the reflection has been removed with a gaussian fit. The field of view has been estimated with a performance analysis of system (see a next section 3.5) in function of the signal amplitude. The threshold has been defined at signal amplitude of 20 mV (light on) and 8 mV (light off), these values correspond to a transmission data with packet error rate of 10^{-3} .

In the figure 3.19, it is possible to observe how the mathematical model estimation of FoV is always under the curve of fitting data. The difference between model and data is a contribution of aberration effect.

For evaluate the aberration effect, the receiver has been substituted with a Thorlabs camera. In the left pictures of figure 3.20, the camera has been aligned to traffic light. The light image is in the middle of camera sensor and its radius is 0.796 mm. In the right picture, the camera has been rotate so that the light image is inside the camera field of view near the border of sensor, the rotation is about 10 degree. In this case, the image is not a circle as a left image but it is a oval with a width equal to 0.910 mm. A width increase in 10 degree is about 15%.



Figure 3.17: Experimental setup.

3.5 Implementation and experimental test of a relay-based VLC: I2V2V

A typical VLC application based ITS is depicted in Fig. 3.2. The VLC systems are categorized in two types, namely, camera-based and photodiode-based systems. The new generation vehicles are usually equipped with cameras for pedestrian and lane detection. It is cost effective to use this existing cameras in VLC receiver modules, however, the noise performances of such elements are very low as compared to dedicated photo element. Moreover, such systems can cover distances of 1-2 m with very low data rates making it impossible to use in real traffic environments [58, 80]. The performances of system are greatly improved when high speed cameras are used and communication distances can go up to 100 m [47, 95, 96, 102]. However, the high speed cameras are still expensive to be used in automotive industry. On

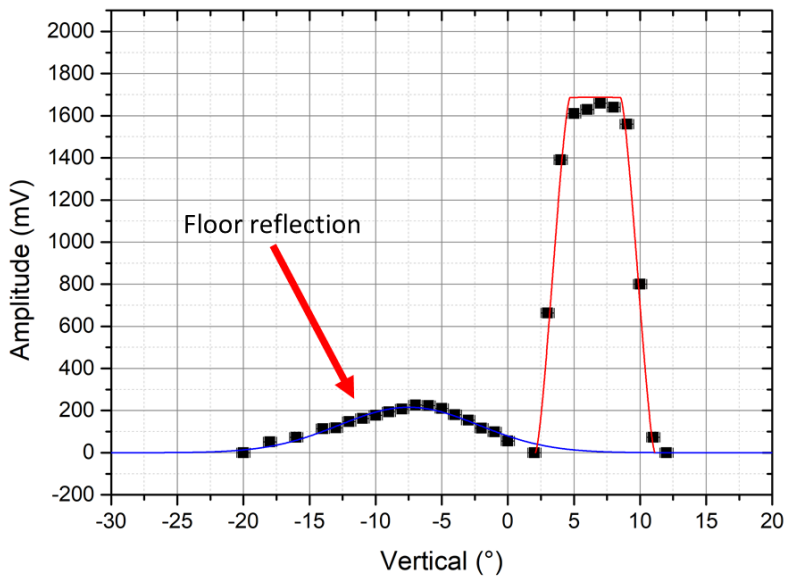


Figure 3.18: Example of measurement data for each receiver position (Vertical rotation, distance = 18 m, 2 inch aspherical lens). The blue line is a reflection of corridor wall (estimate with lambertian reflection model) and the red line is a fit curve without a reflection.

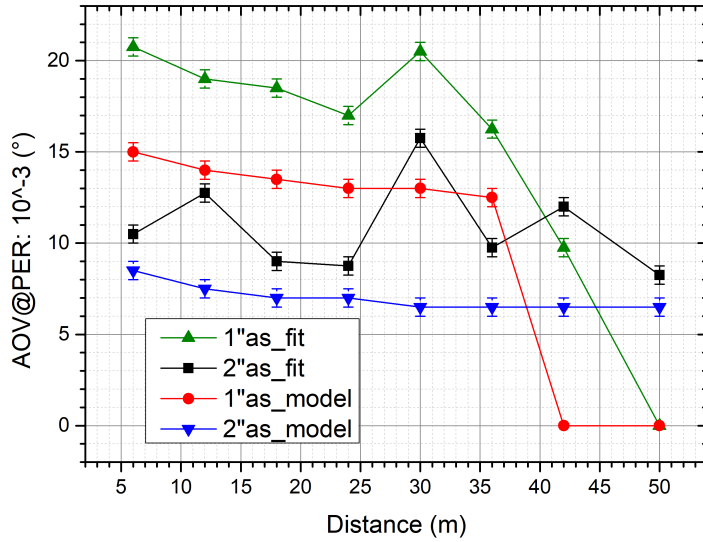


Figure 3.19: Field of view estimated with experimental data values and mathematical model for aspherical lens.

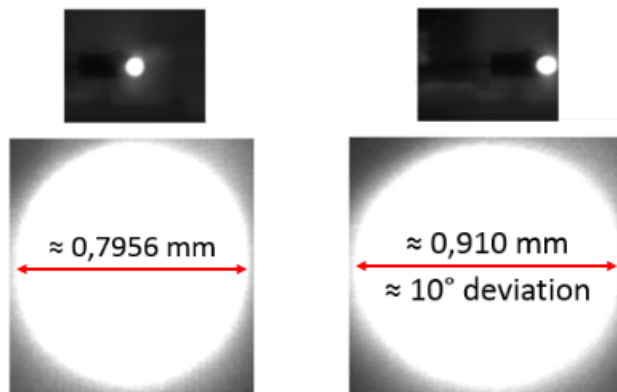


Figure 3.20: Image of source after lens with a Thorlabs camera.

the other hand low cost photodetectors are quite efficient regarding noise performances and can be used for long distances. [25, 26, 33, 65, 71, 97]. However, the existing photodetector based VLC systems achieve low data rates and communication distances that can be up to 30m. The previous work also lack in the performing analysis of the system for automotive domain applications.

In the perspective of introducing VLC as a robust and reliable technology in real ITS scenario, validating the low-latency and high-accuracy character of a IEEE 802.15.7-compliant VLC communication chain involving both I2V and V2V endpoints with real road signalling sources would be of high relevance for boosting the introduction of VLC in ITS applications, aimed, e.g., at minimizing road accidents and enable smart traffic management protocols in large cities.

IEEE 802.15.7-compliant [91] prototype system is aimed at providing a cost effective solution for a short to medium range VLC to be employed in ITS outdoor safety-critical applications, and is based on a low-cost, open-source microcontroller platform (Arduino DUE) and attains for the first time ultra-low, sub-ms total latencies in the total TX-RX-ADR path through VLC.

The experimental validation of this architecture, attaining baud rates as high as 230k with a Manchester encoding scheme, is performed using a regulated signalling infrastructure (a standard traffic light) for distances up to 50 m, featuring PERs approaching than 10^{-5} . The PER performances of prototype system are statistically analysed in order to retrieve average values for latency and packet delivery rate which can be used to reliably estimate automated reaction times to sudden events in ITS scenarios, paving the way towards a new generation of ITS and cooperative ITS implementations. In addition, a mathematical model of the latency is derived. The model is suitable to simulate the latency in real scenarios and design proper communication protocols and procedures for road safety in ITS applications.

The PER is a well established parameter used to evaluate performances of a communication system. However, as pointed out in [92], for active road safety application, PER alone could generally be insufficient to assess the awareness level of receiving units in case of sudden events, whilst a statistically-averaged latency value (SAL) (generalizing the Packet Inter-Reception time (PIR) parameter in [92] to the case of ADR systems), taking into account the distribution of errors in the transmission chain as a func-

tion of relevant experimental parameters, could provide a much more reliable performance indicator. In ADR systems, the bare latency can be defined as the time interval elapsed between the first bit of transmitted message and the last bit of the relayed message after a correct reception and decoding process. To understand the importance of retrieving a SAL parameter, let us consider an example where a TX unit X transmits 100 packets to a unit Y in 1 s, with a PER of 0.5 corresponding to an arithmetically-averaged latency value of 20 ms. Let's now imagine two different error distribution scenarios: in the first case, in the transmission a good packet and a bad one are evenly alternating. In second scenario, the packets received at Y form clusters: 20 packets are received in 0.2 s, then there is no reception of the packets for next 0.5 s, and the remaining 30 packets are received in last 0.3 s. From this example, it is evident that two scenarios differ enormously from road safety point of view, as in the former case Y has constant knowledge of X's status every 20 ms, in contrast to the second case where the Y's knowledge about X's status can be outdated for as much as 0.5 s, with evident consequences for any automated response in case of sudden critical event. Neither PER nor a simple average of latencies keep into account clustering of errors, while the SAL is calculated from the observed statistical distribution of error clusters size and hence represents a much more reliable metric to determine a statistical response time and success rate for automated actions in intelligent vehicular networks.

In this work we have constructed and tested a combined VLC Infrastructure-to-Vehicle-to-Vehicle architecture using as a transmitter an LED based regulatory traffic light received on a conventional photodiode driving an ultra-fast active decode-and-relay V2V stage. Our system is based on a low-cost, open-source microcontroller platform (Arduino DUE) and is fully compliant with the IEEE 802.15.7 specification. Our architecture has been tested to a rate of 230 kBd with a Manchester encoding scheme.

We evaluated the performance of our system by a direct measurement of the PER for distances up to 50 m, approaching a value of 10^{-5} in optimal conditions at our highest rate of 230 kBd. We performed a statistical analysis taking into account the distribution of errors in the transmission chain as a function of relevant experimental parameters, to obtain a model predicting statistically-averaged latency values (SAL) below 1 ms with 99.9% probability for $\text{PER} \lesssim 5 \times 10^{-3}$. This makes prototype system already integrable in the new 5G standard protocols.

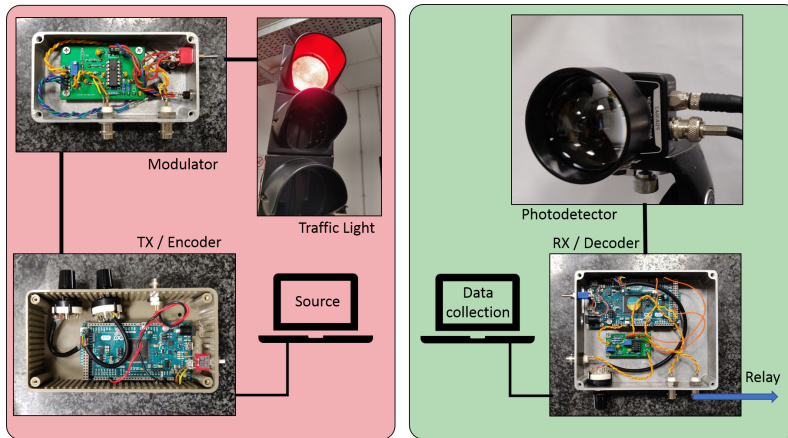


Figure 3.21: VLC hardware blocks for VLC active I2V2V decode and relay chain prototype. Left (red): TX-modulator block, and regulatory traffic light source provided by ILES srl, Prato; right (green): RX-ADR block. Both blocks feature an Arduino DUE-based architecture as digital encoding and decoding engine.

This work demonstrates, for the first time, the possibility to attain sub-ms active decode and relay I2V2V communication by integration of VLC technology in real road signaling infrastructures, and the measured performances can redefine new safety standards for a new generation of ITS and cooperative ITS implementations, such as automatic braking, collision avoidance, car platooning, as well as continuous information exchange in VANETs applications [98]. For example our VLC signalling system in a realistic road scenario can yield decisive advantages over conventional RF-based technologies in terms of total braking distance, especially in case of short distances or high speeds, where the car can stop *before* the crossing instead of getting *into the middle* of it.

3.5.1 I2V2V ADR system

VLC I2V2V ADR prototype system (Fig. 3.21) is composed by a digital encoder/modulator, a regular traffic light, provided by ILES s.r.l, acting as TX light source, a fast, high-gain RX unit, a digitizer/decoder and an embedded ADR digital stage providing the possibility to modulate a further

LED source (e.g. a rear lamp of a car) to relay received information to following units. A 1 Gs/s digital oscilloscope is used for signal recording and analysis. Details on the whole electrooptical TX-RX-ADR system will be given in a future work, as they are unnecessary to the scope of the present paper.

The TX stage is realized by adding current modulation to the LED lamp supply current. The modulation signal is provided by a digital encoder, realized through a microcontroller-based digital board (Arduino DUE). The TX stage transmits digital data up to 230 kBd by inserting digital information into the optical carrier emitted by the traffic light lamp. The On-Off Keying (OOK) is used for digital modulation, and Manchester encoding, obtained through a low-level, interrupt-based control of in-out ports of the board, is considered with OOK for data coding as it is recommended by IEEE 802.15.7 PHY 1 for outdoor VLC. The Manchester encoding guarantees a constant average signal allowing at the same time for a constant illumination by the traffic light, at the expenses of halving the effective bit rate of the communication chain. As the duty cycle of current driven into the LED source is 50%, in order to maximize the modulation intensity whilst preserving the overall regulatory intensity of 100%, we opted to perform a 0-200% modulation. This configuration did not lead to any derating in the LED source characteristics in several months of continuous operation.

The RX unit collects the light from TX on a 36 mm² transimpedance photodiode, with variable secondary-stage gain. The collecting optics is an aspherical 2" uncoated lens, allowing for high optical gain, fundamental to have an efficient communication for high TX-RX distances. The photodiode is physically AC-coupled before the first transimpedance stage in order to reject spurious DC stray light components (such as sunlight or 100 Hz from artificial lights). As only the modulation component is retained, the gain value could be increased to high values (up to +50 dB for low baud rates) without risks of first-stage saturation. This amplification stage ensures a magnitude level of input signal higher than 20-40 mV even at 50 mt distances, which is considered as our limit for successful communication.

The amplified analog signal is then digitized by a variable-threshold comparator stage, and then analyzed and decoded by a digital RX board (based on Arduino DUE platform as well). Thanks to the relatively high computational power and speed of such platform, the decoded signal can be processed, re-encoded and delivered to a further modulation TX stage, eventually acting

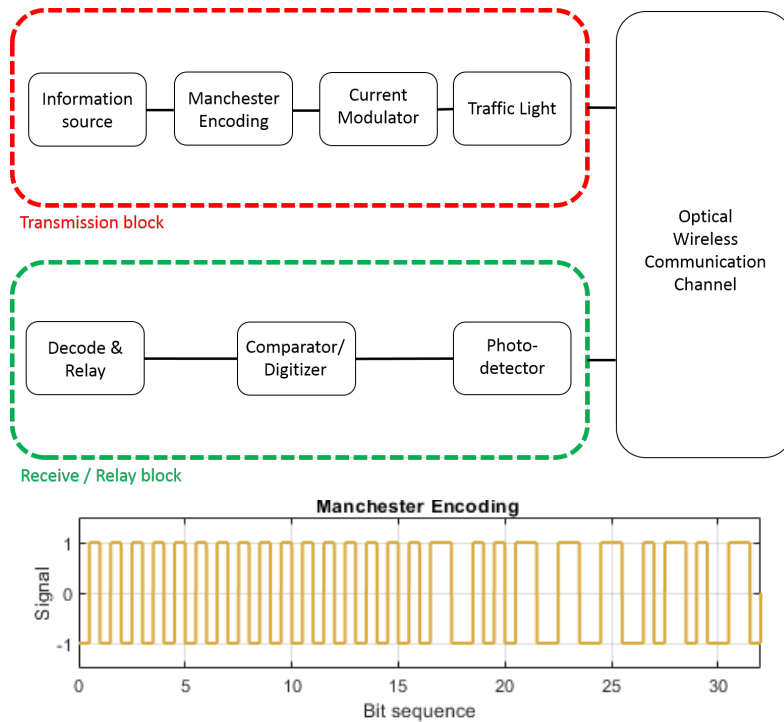


Figure 3.22: Functional block diagram of our VLC Active Decode and Relay (ADR) chain. Lower panel reports the used Manchester bistream, composed by a 2-bytes pre-equalization and a 2-bytes data streams.

on rear lamps/brake lamps for message relaying to following vehicles.

The functional block diagram of the system is shown in Fig. 3.22. The TX digital board produces the bit sequence (see lower panel of Figure) and packages it into a packet of 4 bytes (32 bits), 2 bytes preambles and 2 bytes of data (i.e. AL). Preamble follows a unique pattern (all 1's or 0's) that could be used for pre-synchronization between transmitter and receiver and also provide for useful signal equalization after transients. Then this data is fed into Manchester encoding block, providing the source signal for modulator, where data is inserted into the optical carrier using OOK current modulation, i.e. modulating the intensity of the traffic light, which represents the TX source. The signal is passed through the optical transmission channel and received at photodetector, and then decoded and interpreted. The RX block presented in our prototype embeds an active relaying node: the Arduino DUE board decodes and bit-wise compares the received message with a stored reference message in less than 10 μ s. If no errors are detected, the message is re-encoded and passed to a modulator for further clean relaying towards incoming units. We choose not to embed error correction algorithms as they are not inserted in the IEEE paradigms for outdoor VLC communications through 200 kHz carriers. Due to hardware limitations arising from interrupt conflicts, our ADR stage cannot receive bits while an active relaying of a previous data stream is occurring (see Fig. 3.25). We choose anyhow to keep the broadcast signal interpacket delay as short as possible (continuous broadcast) in order to limit signal level fluctuations due to long interpacket phase where no modulation is present. In this continuous broadcast configuration, the number of relayed messages if no errors are detected cannot exceed 1/2 the number of transmitted messages even in the ideal transmission case, so we set $PER = 1$ when the number of relayed messages equals 0.5 the number of transmitted ones. In the beaconing case, where the interpacket delay is by construction much longer than the packet length, this correction factor is not needed (Fig. 3.26). In both cases, the minimum attainable latency in the whole TX-RX-ADR process is highlighted in Figs. (3.25-3.26), and attains 595 μ s in both broadcast and beaconing configurations (see Sec. 3.5.4).

Performance Metrics

Prototype performance are evaluated according to the following metrics:

PER is defined as ratio between lost VS total transmitted packets. A



Figure 3.23: Experimental campaign: a standard traffic transmits VLC signal to a photo-receiver stage equipped with digital Active Decode and Relay block. The data collection unit consists of a PC and an oscilloscope. The distance between transmitter and receiver is up to 50 m limited by available line of sight length in the building.

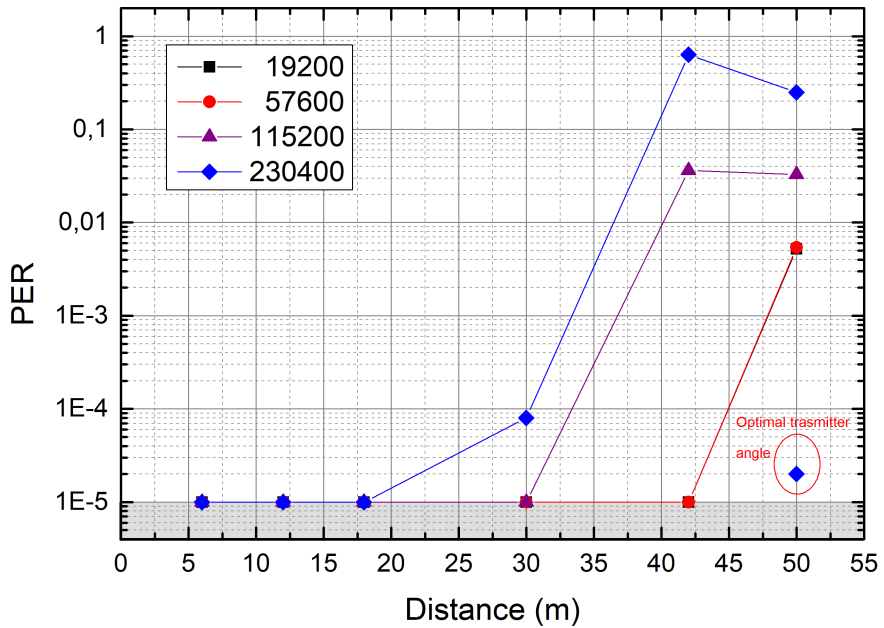


Figure 3.24: PER performance of designed VLC I2V2V ADR system. PER is shown as a function of distance for various baud rates 230 kBd, 115 kBd, 57 kBd and 19 kBd. Shaded area in figure represents our upper limit in the observable PER (10^{-5}) due to transmitted number of packets. The encircled point at 50 m represents the absolute best performance obtained at our highest baud rate, if the traffic light vertical angle is optimized by few degrees.

packet is considered to be lost if a single bit is altered during transmission. The lower observable PER ($< 10^{-5}$) is limited by the maximum number of transmitted packets (2×10^5), chosen to limit the duration of the whole campaign to reasonable values. An estimation of BER is also possible in the hypothesis that a single bit is lost when an error is detected, which is very reasonable for low PER values. As our packets are composed with 32 bits, this leads to an upper value of BER of 3×10^{-7} .

With reference to Figs. (3.25-3.26), latency is defined as the time elapsed between the first bit of a TX message and the last bit of an actively-relayed message after the ADR block.

3.5.2 Measurement Campaign

The measurement campaign is carried out in collaboration with ILES srl, a company producing and installing intelligent signaling elements, in the city of Prato - Italy. The measurements are performed in a long corridor (55 m) inside the Physics and Astronomy Dept. of the University of Florence (see Fig. 3.23). In experimental set up, the relative vertical height among photodetector and red lamp is set to implement a configuration where the collection lens is placed on the car dashboard (~ 105 cm from ground [27]). In this configuration, interference due to artificial and ambient light sources such as multipath reflections are always present, and require an equal or higher robustness in noise rejection schemes when compared to outdoor scenario implementations, where, e.g., the 100 Hz component is definitely less critical.

The received signal is proportional to the optical flux collected by the condenser lens, hence decreases with increasing distance and incidence angle between optical axes of the transmitter and receiver optical elements. In this measurement campaign, the photodetector optical axis is aligned towards the traffic light lamp center in order to maximize the amplitude of the received signal. In order to evaluate the performances of the designed prototype in various possible distance/gain configurations, the distance between traffic light and photodetector is changed from 6 m to 50 m with step sizes of 6 to 12 m, whilst the gain value is spanned in steps of 10 dB for all useful values, ranging from PER = 1 for too low or too high gain (limiting the RX electronic bandwidth to unsuitable values for a specific baud rate), up to the lowest detectable PER of $< 10^{-5}$, limited by the number of transmitted packets.

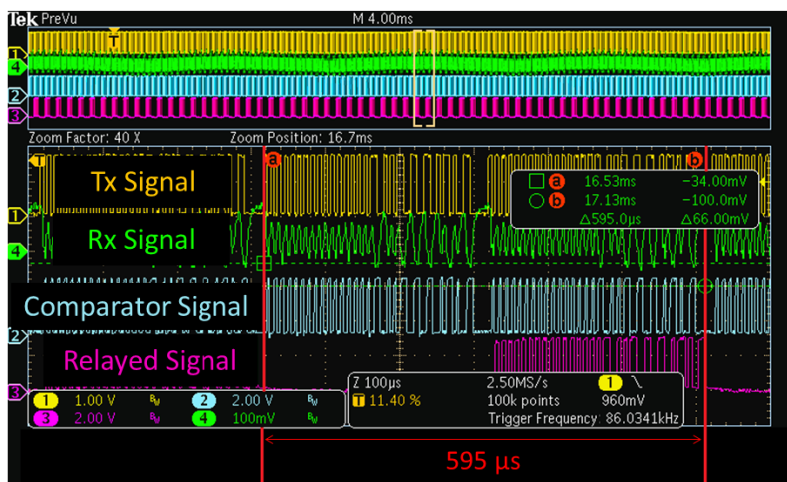


Figure 3.25: Continuous broadcast: oscilloscope screenshot (upper panel) with a zoom (lower panel) showing transmitted signal (yellow), received analog signal (green), digitized received signal (blue), and relayed signal after ADR block (purple). The red marker on the screenshot shows a minimum active packet relaying (Δ) of $595 \mu\text{s}$ obtained at a rate of 230kBd. Effects of artificial illuminations are visible in the analog green track as a 100 Hz residual oscillation.

3.5.3 PER Analysis

For these experiments a predefined message is sent continuously at 230, 115, 57, and 19 kBd rates. Fig. 3.24 shows the dependence of the PER performance on the distance between traffic light and photodetector for various baud rates. The PER performance of the system is decreased as the distance between the transmitter and receiver is increased due to reduction of the received modulation signal with respect to the residual stray ambient components and line noise, which are relatively independent on the RX-TX distance. Our measurements demonstrate that our VLC-based prototype is able to establish communications up to the maximum available distance of 50 m for all of the tested baud rates. A PER value $< 10^{-5}$, corresponding to a lossless transmission in our observation window, is obtained for distances up to 42 m for 19 and 57 kBd. Higher baud rates of 230 and 115 kBd achieve lossless transmission up to 18 and 30 m, respectively. The

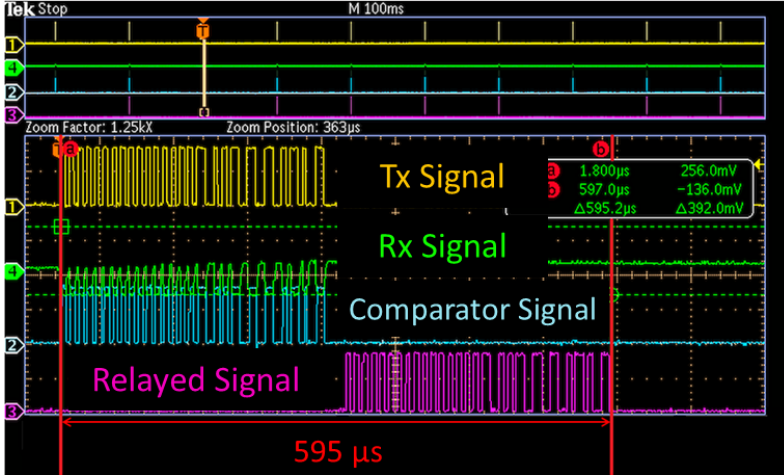


Figure 3.26: Beaconing configuration: oscilloscope screenshot (upper panel) with a zoom (lower panel) showing transmitted signal (yellow), received analog signal (green), digitized received signal (blue), and relayed signal after ADR block (purple). The red marker on the screenshot shows a minimum active packet relaying (Δ) of $595 \mu\text{s}$ obtained at a rate of 230kBd.

ultralow-latency configuration (230 kBd) features $\text{PER} < 10^{-4}$ at 30 m and still grants $\text{PER} < 0.3$ at 50 m. Noticeably, anyhow, near-lossless PER value of 2×10^{-5} is recovered at 50 m even for 230 kBd if the traffic light is slightly tilted backwards by few degrees. Indeed, as verified in a previous work of ours [27], roadside traffic lights are designed to maximize visibility (and so the VLC signal) in the range of 12-18 m. In case long distances should be privileged for casting long-range VLC signals, hence, it is beneficial either to recline the lamp optics of roadside traffic lights by few degrees in order to redirect the shaped beam towards higher distances, or to prefer the usage of over-road traffic-lights.

Without optimal lamp orientation, the PER performances at 50 m remain good (0.007) for both 19 and 57 kBd. In practice, a drop into the RX-ADR block capabilities to correctly receive packets is found around 20-40 mV in the signal level. This value is mainly arising from 100 Hz interfering signal at the receiver, resulting as a residual neon light component after the first AC filtering stage. We found not beneficial to further increase the AC decoupling

frequency, as this would start to cut the modulation signal as well. Fig. 3.25 is an oscilloscope screenshot of the data stream across various blocks, taken in real time during experiments. In this figure yellow colour shows the transmitted signal, the green colour presents the received analog signal after the photodetector, blue is for digitized received signal after comparator and the purple track shows relayed packets. The impact of the artificial lights on received signal shape can be observed as the residual modulation appearing in the green track of upper panel in Fig. 3.25. Incidentally, this could be the origin of the deviation of PER vs distance from monotonic behaviour at very low signals in Fig. 3.24 (i.e. distances > 40 m and high baud rates). Indeed, as the light coming from lamps on the ceiling can enter more or less the detector field of view depending on its position along the corridor, the consequences of this stray 100 Hz signal can start to have an effect on PER at very large distances, where the signal is much feebler.

We remark that the better experimental values obtained of $\text{PER} < 10^{-5}$ and estimated BER below 3×10^{-7} represent a worst-case limit due to limitations of number of transmitted packets. From Fig. 3.24 we have clear indications that, especially at distances up to 30 m, actual PER and BER limit values are much lower than our upper limits.

3.5.4 Ultra-low ADR latency performances

Besides the good PER and BER performances shown for distances up to 50 m, another remarkable feature of our VLC prototype is the demonstration of ultra-low, sub millisecond active decode and relaying latencies (see red markers in Figs. (3.25-3.26)): a data packet is transmitted, decoded, compared and relayed in $595 \mu\text{s}$ for IEEE-compliant modulation frequencies of ~ 200 kHz (230 kBd in our case). This achievement makes our low-cost, highly-integrable VLC architecture suitable for time-critical, road-safety ITS applications, Further, such low latency values indicate that this architecture would fulfill the latency standards of 5G technology in IoT applications. As a proof of principle, we also test the suitability of our system for beaconing of situational information in one example configuration (230 kBd). The beaconing interval is set to be much longer (100 ms) than the packet time ($\sim 280 \mu\text{s}$), and this constitutes a major difference with respect to the broadcast case, as the average amplitude of detected datastream is now much less constant due to signal transients driven by long interpacket delays. The beaconing performances are shown in the Fig. 3.26, and a sub-millisecond

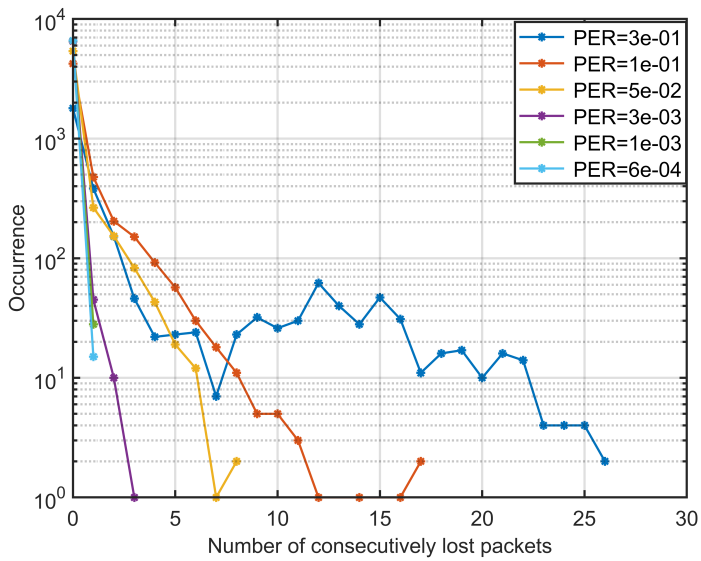


Figure 3.27: Occurrence vs number of consecutively lost packets (i.e. the cluster size), retrieved from data obtained during experiments for various PERs. Legend presents different PERs considered for latency analysis.

(595 μs) relaying is also achieved in this case, without appreciable loss of packets. Figs. (3.25-3.26) highlight that the prototype presented in this paper is suitable for both event-triggered message broadcast and continuous data transmission.

Statistical Latency Analysis

Neither bare minimum latency values corresponding to a certain baud rate, nor the PER alone can provide an effective metric to determine a most probable successful data delivery time in ITS applications. Since (especially for high PER values) clusters of consecutively lost packets can appear, a statistically-averaged latency (SAL) should be rather retrieved from a statistical analysis of the lost packets distribution. This section presents an analysis of such distributions, recorded for different PER values. Differently from PER measurements, in such measurements set we had to acquire whole tracks in order to perform an accurate post-processing analysis of errors distributions and latencies. The memory depth of the oscilloscope sets the acquisition length to a maximum amount of 10000 sent packets, and since we have to perform an analysis on statistically-relevant datasets, we restrict the analysis to PER values not lower than $\sim 10^{-3}$, in such a way that the total recorded number of lost packets in our observation window exceeds 10, considered as a limit value for a statistically-relevant error dataset. For lower PERs, indeed, errors distributions can be strongly affected by the finite-size nature of our ensemble, failing to provide for inferential capability to our statistical analysis.

The curves for number of occurrences vs. number of consecutively lost packets (cluster size) for different PERs are plotted in Fig. 3.27. It shows that the clustering in relaying messages is increased for higher values of PER. The maximum observed cluster size is 26 in case 3×10^{-1} , whereas it is 17 for 1×10^{-1} , 8 for 5×10^{-2} and 3 for 3×10^{-3} . For three PER cases (see Fig. 3.29) we extracted the corresponding probability mass function (PMF) and cumulative distribution function (CDF) [85], reporting the results in Fig. 3.29. The clustering of errors tends to increase as the PER is increased, still featuring a smooth trend as a function of the cluster size. In order to infer a best estimation for SAL, we tried to identify a most suitable model for clusters distribution testing three different fit models (binomial, negative binomial, and Poisson) against our data.

Fig. 3.29 shows the PMFs and the CDFs of the empirical data as well as

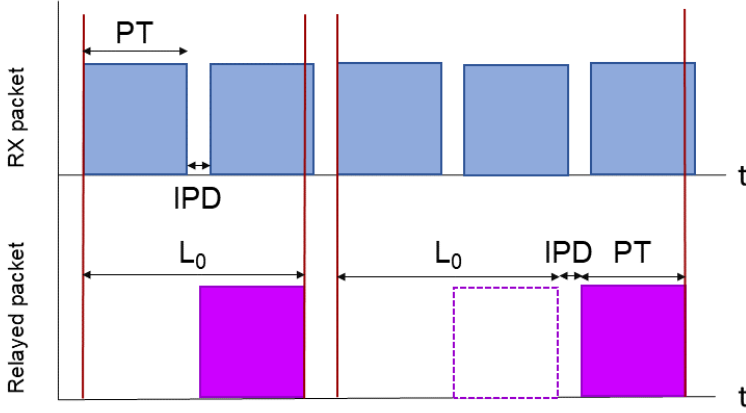


Figure 3.28: Latency reconstruction from packet structure: L_0 is the minimum time required to relay a packet, N_{Lost} is the number of consecutively lost packets, IPD is interpacket delay, and PT is the packet size in time.

three discrete distributions: binomial, negative binomial and Poisson. The same figure also reports the CDF error, i.e., the difference between the CDF of empirical data and the CDF of the above mentioned distributions.

As Fig. 3.29 shows, we obtain a very good agreement with negative binomial hypothesis for all of the analyzed PER values. The PMF of a negative binomial (or Pascal) distribution is

$$f(k, r, p) = \binom{r+k-1}{p} p^k (1-p)^r \quad (3.46)$$

where r is the number of failures, k is the number of successes, and p is the probability of success. This agreement enables us to use the negative binomial hypothesis in order to make predictions on system level performances of our implementation from the SAL point of view as a function of PER (Sec. 3.5.4).

In order to obtain a SAL it is first of all important to connect the CDF of error cluster size (central panels of Fig. 3.29) to its effect in terms of communication delay. With reference to Fig. 3.28, the latency can be inferred as a function of error cluster size (retrieved from raw data) using following equation:

$$L_n = L_0 + N_{Lost}(IPD + PT) \quad (3.47)$$

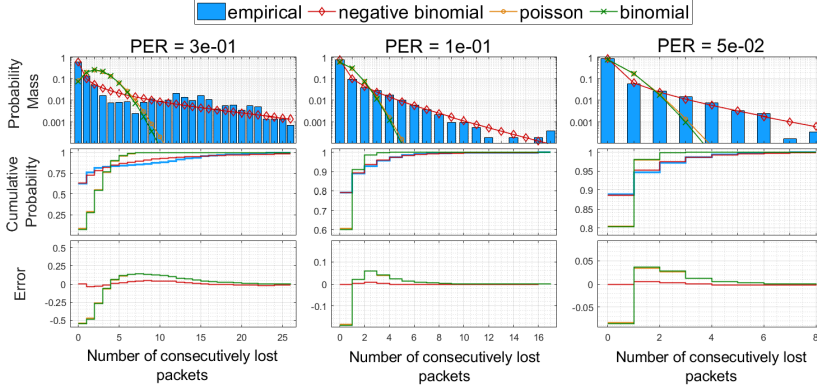


Figure 3.29: Latency PMF and CDF with curve fitting for different lost-packets distribution models (Negative binomial, Poisson, and binomial), along with fitting error (lowermost panel) for significant PERs (see text for details).

where L_n is the total latency, L_0 is the minimum time required to relay a packet, N_{Lost} is the number of consecutively lost packets (cluster size), IPD is interpacket delay, and PT is the packet duration. Parameters L_n , L_0 , IPD and PT appearing in Eq. 3.47 can be considered as constants, with observed deviations on the timescale of $10 \mu\text{s}$.

Importantly enough, the cluster size CFD analysis, performed for several PER configurations, delivers the required number of broadcast packet retransmissions granting a certain success probability in our TX-RX-ADR transmission chain (see solid lines of Fig. 3.30). In turn, through Eq. 3.47, we can link this packet number to the corresponding latency (right axis of Fig. 3.30, obtained inserting time parameters for 230 kBd).

The dashed vertical lines in the inset indicate three significant success probability levels (95%, 99% and 99.9%), whilst the horizontal line highlights the sub-ms latency regime. Most significantly, even in the worst PER case (3×10^{-1}), at 230 kBd, a successful transmission can be accomplished with 99.9% confidence level in only ~ 8 ms, whilst the sub-ms relaying regime (highlighted by the shaded area in the inset of Fig. 3.30) is granted already for PER values $\lesssim 10^{-3}$ (red line). When combined to results reported in Fig. 3.24, these result noticeably demonstrates, with a confidence level better than 0.999, that: a) our VLC system is able to perform successful

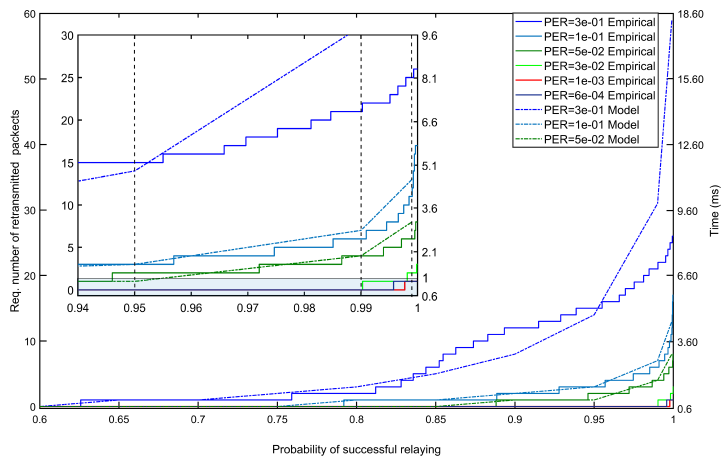


Figure 3.30: Performance of designed prototype for road safety critical applications. Right axis is calculated for 230 kBd, see Eq. 3.47. Inset image is a zoom in of the probability of successful relaying from 0.94 to 1. The vertical dash lines are used to represent the PSR of 0.95, 0.99 and 0.999. Dash-dot lines report the prediction of negative binomial model (see text).

communication up to 50 m at 230 kBd and perform ADR of information in less than 10 ms; b) successful communication with ultra-fast, sub-ms ADR performances is granted up to more than 30 m, where the measured PER @ 230 kBd attests well below 10^{-3} .

The best fitting model (negative binomial) for N_{Lost} (dash-dot lines) can analogously be used to infer L_n as a function of cluster size and to extract the SAL value from knowledge of cluster size distribution for different PER values.

As it can be seen, the latency values of the proposed model and the empirical data are close, and the discrepancy is always ≤ 5 packets for probability < 0.95 (see inset of Fig. 3.30 and Fig. 3.31). Only in case of higher probabilities and high PER (3×10^{-1}) the accuracy appears to get lower, as the predicted cluster size value is significantly higher than the measured value. Notwithstanding this model discrepancy, for which we did not find a trivial explanation addressing it to the finite-size nature of our experimental sample, the model proves to provide correct predictions for error distributions in a very wide set of transmission parameters.

Table 3.4: Parameters of best-fitting PMF model for latency.

PER	Parameters	Target probability			
		0.9	0.95	0.99	0.999
		Latency [no. of packets]			
3×10^{-1}	r=0.1691; p=0.0638	8	14	31	59
1×10^{-1}	r=0.1719; p=0.2555	2	3	7	13
5×10^{-2}	r=0.1089; p=0.3342	1	1	4	8
3×10^{-3}	r=0.028; p=0.7053	0	0	0	2
1×10^{-3}	$\lambda=0.0042$	0	0	0	1
6×10^{-4}	$\lambda=0.0023$	0	0	0	1

The latency model parameters corresponding to dash-dot lines of Fig. 3.30 are also reported in Table 3.5.4. It is worth to note that for the cases of very low PER (few errors in the measurements) the best fitting PMF is rather given by a Poisson distribution with λ parameter reported in Table 3.5.4. Similarly to the higher PER and higher success probability case, the discrep-

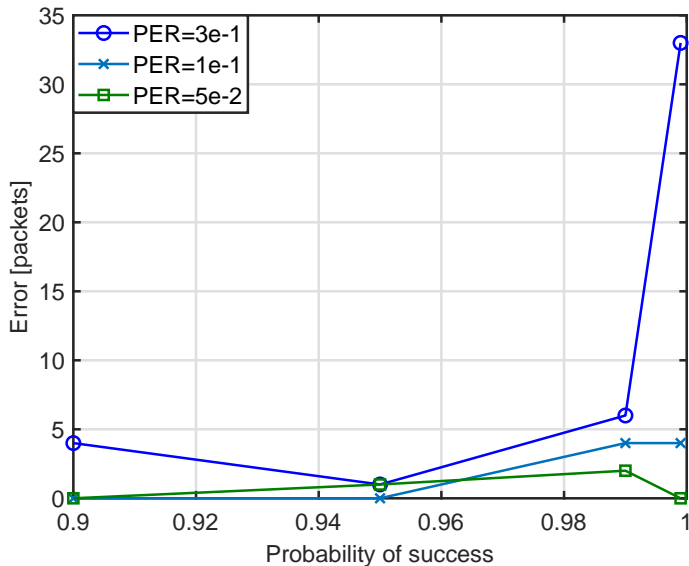


Figure 3.31: Difference between the predicted number of required packets and the measured values for three relevant PER values as a function of transmission success probability (see Fig. 3.30).

ancy can exceed 5 packets. The error of the model is depicted in Fig. 3.31.

Model estimation of SAL VS PER

By using the best fitting model, we can derive the expected latency (SAL) corresponding to a successful decode-and-relay transmission process with a target probability, in generic communication conditions corresponding to a certain PER. Fig. 3.32 shows the estimated SAL expressed as number of packets as a function of PER for different target probability of successful relaying. Right vertical axis shows the mapping on latency time obtained for 230 kBd by using Eq. 3.47. The latency grows monotonically with PER and target probability, but remarkably, even in the case of relatively high PER values (10^{-1}), which are far from suitable for internet links, the model predicts for our system ADR latencies below 10 ms even for target success probabilities of 99.9%, whilst the sub-ms regime is expected already for PER

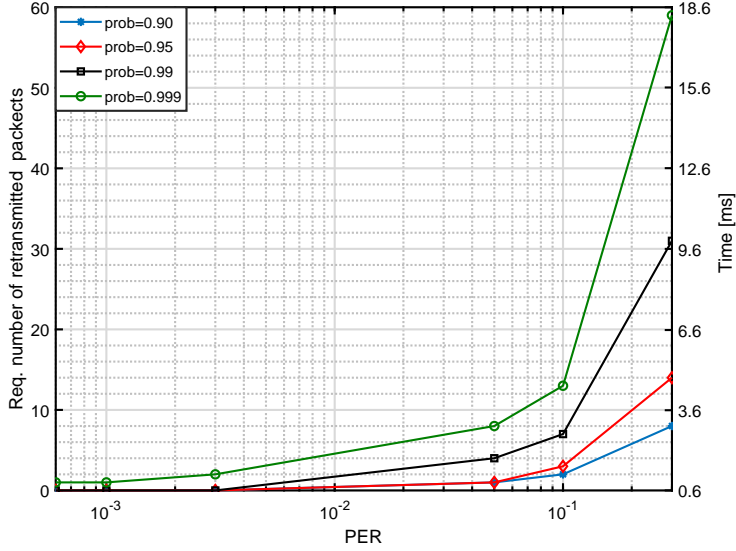


Figure 3.32: Model predictions for latency (SAL) as a function of the PER for different probability of successful relaying.

$\lesssim 5 \times 10^{-3}$.

3.5.5 Application to road safety

It is interesting to give a realistic estimation of the possible advantages in terms of road safety which could be obtained by introducing our low-latency architecture in realistic road scenarios. To this scope we give an estimation of the reduction in the stopping distance of standard vehicles in case of critical events (traffic light suddenly turns red) as compared to the human reaction case.

The total stopping distance is the sum of the perception-reaction distance D_{p-r} and the braking distance D_{brake} [100]

$$D_{stop} = D_{p-r} + D_{brake} = vt_{p-r} + \frac{v^2}{2\mu g} \quad (3.48)$$

where v is the vehicle speed, t_{p-r} is the reaction time, μ is the friction coefficient and g is the gravitational acceleration. A road in good condition

Table 3.5: Reaction and stop distance for an average family car with good tires over dry asphalt. VLC Vs IEEE802.11p Vs human latency.

v [km/h]	D [m]	PER @57kBd	Reaction latency @99% [ms]	Relay latency @99% [ms]	Brake distance [m] ($\mu = 0.7$)	Reaction distance [m]			Stop distance [m]		
						VLC	IEEE802.11p	Human	VLC	IEEE802.11p	Human
40	10	$\sim 10^{-5}$	~ 1.2	~ 2.4	9.00	0.01	1.11	15.22	9.01	10.11	24.22
60	20	$\sim 10^{-5}$	~ 1.2	~ 2.4	20.25	0.02	1.67	20.83	20.27	21.92	41.08
90	45	$\sim 10^{-4}$	~ 1.2	~ 2.4	45.55	0.03	2.50	34.25	45.58	48.05	79.80

usually shows a friction coefficient of 0.7.

As a general remark, since at large distances the PER value for the lowest examined baud rates (19 and 57 kBd) is orders of magnitudes better than for 230 kBd, we assume that in long-cast safety-critical message delivery applications ($\gtrsim 30$ m) it could be more effective to employ lower, more reliable baud rates, as such low PER values would correspond to a much lower SAL value even if the PT and IPD times are 4 times larger. Since long-distance performances of our system are equivalent at 57 and 19 kBd (see Fig. 3.24), in the following analysis we will use 57 kBd as transmission rate.

Table 3.5 shows a comparison between reaction and total stopping distances of an average family car in a dry road calculated for three relevant initial speed and distance-to-traffic-light situations. Different distances correspond to different PERs, and hence different latencies (see previous section). The reaction/stopping distances are evaluated by considering the reaction time equal to latency (delay) in the human-, IEEE802.p- and VLC-triggered braking case. Tests in real conditions found the fastest reaction time of car drivers to be $t_{p-r} = 1.37$ sec [106], whilst the latency requirements in outdoor road applications are given in [82]. In particular, IEEE802.11p standard provides a maximum latency of 100 ms for RF-based road safety applications. For the VLC case, the reaction Latency, i.e. the time interval occurring between the beginning of a transmitted packet and the first correct packet reception at the receiving unit (without relaying) can be obtained by simply subtracting to ADR latency the Packet Time (see Fig. 3.25 and Fig. 3.28). In case of low PERs, this nearly corresponds to half the ADR latency as the IPD time is very short.

As it can be seen, a VLC signalling system in a realistic road scenario can yield decisive advantages in terms of total braking distance, which can turn out to be paradigmatic in case of short distances or high speeds, where the car can stop *before* the crossing instead of getting *into the middle* of it (see Table 3.5). It is worth to note that this improvement in terms of stopping distance, could be not granted by RF-based communication technologies, for which the IEEE 802.11p standard for ITS envisions maximum average latencies of 100 ms, 10 times larger than the ones observed in our worst case scenario tests (0.999 probability, 50 m, 230 kBd, giving latencies below 10 ms, see Fig. 3.30). The latency depends on both the medium (RF or VLC) as well as on the protocol used to route the message. There are several protocols

specifically designed for ITS. Noticeably then, also total relay ADR latencies, reported in Table 3.5, still correspond to reaction distances well below 0.1 m even for speeds as high as 90 km/h. This important point suggests our architecture as a very promising candidate for implementation of low-latency cooperative ITS schemes such as short-distance vehicle platooning, where effective reaction distances well below the 1m range represent a challenging, key target.

3.6 Implementation and experimentation of VLC in 5G network

The fifth generation (5G) mobile networks [48] is the next generation cellular-based standard, and it aims at satisfying the International Telecommunication Union - Radio communication (ITU-R) recommendation M.2083-0 (hereafter referred simply as IMT-2020) [53]. In this document, ITU-R outlines the next generation cellular telecommunication standard goals, describing application trends (therefore potential users, traffic types and technological trends), and spectrum implications.

During the 5G standardization, the goal to fuel *new* communication scenarios is considered crucial. Toward this end, 5G aims at becoming a technology enabler for services that are foreseen to become more and more pervasive in the users' everyday life. Among the scenarios foreseen by ITU-R, the Smart Cities and Automotive applications are probably the ones that will have the most immediate 'visibility' by the user.

It is worth considering that the vehicular traffic management, mentioned in IMT-2020, is not 'only' about autonomous driving, and involves also the Smart City concept, including smart traffic lights, real-time information dissemination to drivers, etc. Related to this, it is also important to consider the adoption of the technology by the users (in this case, the automotive industry). With respect to this point, the adoption of direct-to-the-user 5G communication might be hindered by the adoption of 5G-enabled cars, and will pose a serious challenge to the network deployment.

In this work we will describe the challenges that we found during the Italian 5G testbed in Prato-L'Aquila, and where the ns-3 network simulator can be used to overcome them. We will also outline the major 5G features that, in our opinion, will draw attention from the academia and the industry in the near future. These points can (and should) be of interest for the net-

working simulators community, in order to build a reliable and reproducible simulation system.

The goal of 5G is to study and develop three scenarios:

In this context, three scenarios are considered:

- **Smart city management:** In a smart city, information flow from different area: environment, public and private mobility, social events, etc. The collected data coming from heterogeneous sensors provides an entire view of the city conditions, allowing fast alerts solutions thus limiting the negative effects on citizens coming from unexpected events (e.g., traffic jams, improvise storm, etc.). In this scenario, the main role is played by environmental and structural sensors/applications.
- **Public and private metering management:** In this context the objective is integrate smart metering services within a single transport network. In this way, the system development will be economically viable. Moreover, the citizen/company can remotely monitor the status of the metering, enabling the system to respond quickly. In this scenario a back-draw is the user privacy and data security: it is mandatory guarantee that the sensed data will not be used to violate the user's privacy or be used in a malicious way.
- **Industrial processes integrated management:** In these years we are witnessing the fourth industrial (Industry 4.0) revolution and the need for integrated industry management is a fundamental pillar for this innovation processes. The 5G network will provide a capillary infrastructure that will meet the severe requirements needed by industrial Cyber-Physical System (CPS), and is financially suitable.

These scenarios involve both mMTC and URLLC type communications, both indoor and outdoor.

Sensor networks will be connected together in 5G, allowing companies to implement low-cost custom and centralized management systems using easy and web-accessible tools. 5G technology will reduce the latency time allowing faster reaction in the system to early identify and solve critical conditions.

These scenario will also consider smart devices sub-networks (i.e. sensors, Ad-Hoc network), where the main challenge is related to devices security [23, 24, 41, 88].

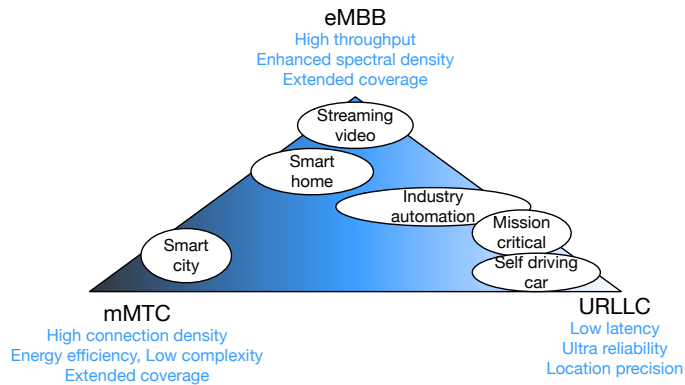


Figure 3.33: IMT-2020 Scenarios.

In particular, our testbed is related to the Smart city management. Fig 3.35 represent a use case where both VLC and sensors are used to inform citizen about city status. A VLC system for Infrastructure-to-Vehicle (I2V) communications allows to send broadcast messages to all vehicles that are in front of a single traffic light, slightly increasing the end-to-end latency. Furthermore the VLC system creates a discriminant based on the position of the vehicle, exploiting only the characteristics of the transport layer of the communication.

5G and VLC technologies

According to ITU-T [53], 5G will be an enabling technology for a number of scenarios, briefly summarized in Figure 3.33.

Two of the mentioned scenarios, i.e., *Smart cities*, and *Self driving cars* are particularly interesting for our system. These are respectively enabled by the Massive machine-type communications (mMTC) and Ultra-reliable and low-latency communications (URLLC) traffic types, and can be further enhanced by the use of VLC.

5G standardization status

The 5G standardization started in December 2013, under the umbrella of the 5G Public Private Partnership (5G-PPP), founded by the European Union (EU) in collaboration with the European Information and Communications

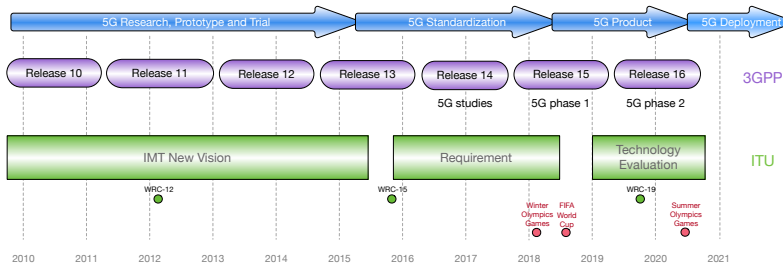


Figure 3.34: Ongoing 3GPP - ITU 5G Standardization.

Technology (ICT) industries and research centers. In 2015, 5G-PPP released the document *an overview of the 5G vision of the European ICT sector* [7], outlining the main goals of 5G.

5G standardization is still in progress and is being carried out by the major standardization bodies (3GPP, ITU-T, IETF, ETSI, IEEE). It is being carried out in *phases*: phase 1 was aimed at the pre-standardization of the entire 5G system (physical layer, network architecture and management). Phase 2, which is now ongoing, is aimed at field tests and further refinements of the standard (<https://5g-ppp.eu/projects/>). The standardization timeline is summarized in Figure 3.34

The networks deployment that will satisfy the requirements of IMT-2020 could be start in 2020. Currently a number of telecommunication operators around the world have announced 5G network testbeds. Among them, the Italian 5G testbed in Prato-L'Aquila is currently evaluating a number of application scenarios involving the 5G technology.

VLC technology in smart city

In the context of smart cities, the communication between infrastructure and vehicles is important. Traffic-lights are light sources always on, and spread around the city. VLC technology is beneficial since it can support a very low latency together with an energy saving. IEEE 802.15.7 is the standard for local and metropolitan area networks using optical wireless communications, including VLC [10].

5G network and VLC can be seen as a promising coupled technologies to provide an ultra-low latency information to the vehicles all around the urban territory.

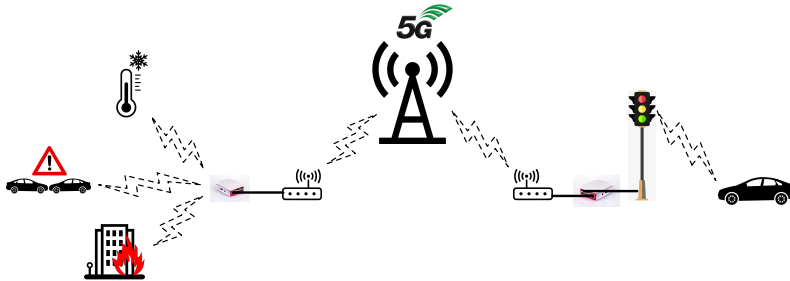


Figure 3.35: The Use Case 5 smart city management.

3.6.1 The 5G Prato project

The testbed was realized at the Polo Universitario Città di Prato (PIN) and it is schematized in Fig. 3.35.

In particular, it was composed by 2 Raspberry Pi 3 Model B+, 3 WeMos D1 mini, a compliant traffic light with the Italian regulation, a VLC transmitter, a VLC receiver, and some sensors:

- *flame*: used to simulate a fire;
- *gyroscope/accelerometer*: used to detect an incident between to (scale model) cars;
- *button*: used to simulate the presence of ice in a street.
- *temperature/humidity*.

The Raspberries role is to collect and forward, through the 5G network, data coming from the sensors. It is worth noticing that the temperature sensor sends periodically the sensed data, the other sensors send an *alarm* only if are triggered. The Raspberries are connected to the 5G Customer Premise Equipment (CPE), provided by the 5G network operator, though Ethernet Gigabit ports. In the traffic light a custom VLC transmitter is presented: the second Raspberry and the VLC block are connected by a serial cable (USB). The WeMos D1 mini peculiarity is the presence of a Wi-Fi module, in this way the connection between the sensors and the raspberry is through the air: the Raspberry provides a Wi-Fi Access Point and all the WeMos have an IP address. All the code in the Raspberries is written in Python 3 and all the code used to drive the sensor - WeMos is written in C/C++.

3.6.2 Latency of combined 5G and VLC Systems

These results are taken from an oscilloscope attached at the first Raspberry (yellow line), at the second Raspberry (pink line) and at the VLC receiver (green line). The yellow line, when high, represents an alarm trigger, in the pink line the rising edge represents the time necessary to forward the packet on the USB cable, the green line represents the arrived packet at the VLC receiver.

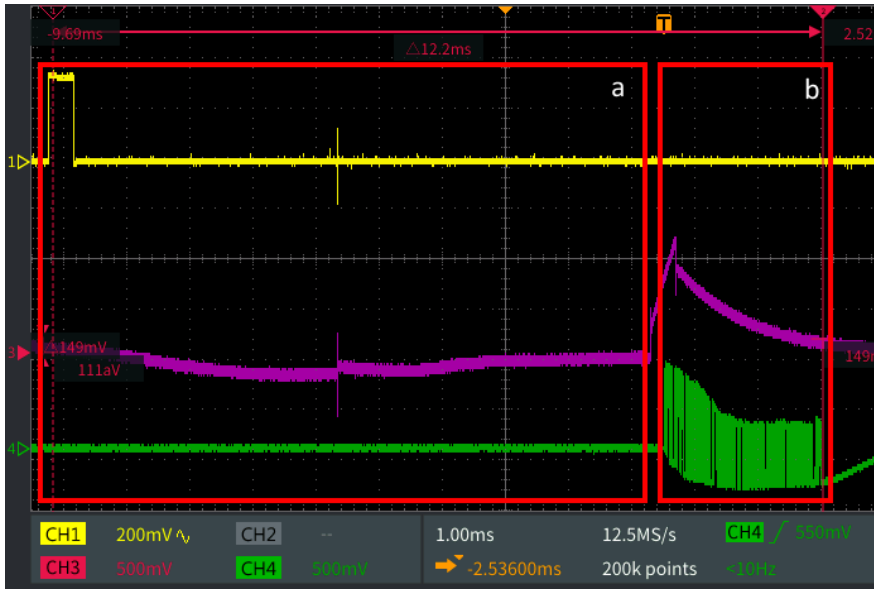
In particular, Fig. 3.36(a) and Fig. 3.36(b) represent the maximum and minimum measured end-to-end latency time. In the rectangle named *A* is shown the 5G latency time while in the rectangle named *B* is shown the VLC latency time. The portion between the two rectangles represents the processing time introduced by the second Raspberry Pi3.

As shown in both figures, the 5G latency time varies from 7.5 to 10 ms while the VLC latency time can be considered constant and equal to 2.5 ms and corresponds to the data transmission time through the optical channel at the rate of 100 Kbps, as defined in the IEEE 802.15.7 standard [10] for outdoor applications. Moreover, the processing time of the second Raspberry Pi 3 results highly stable and it is equal to a few hundred μ s.

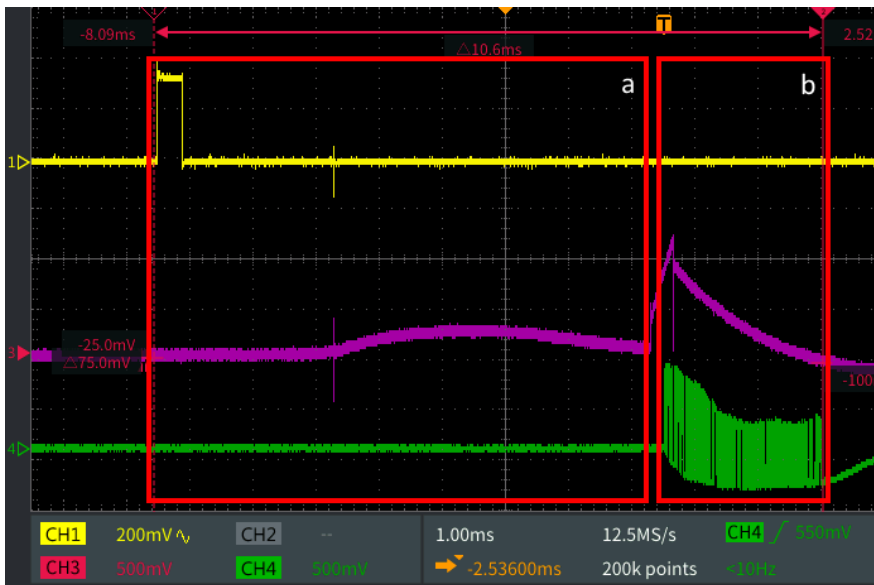
We can assert that the main part of the end-to-end latency is introduced by the 5G network due to the Packet Error Rate (PER) optimization: the network provider may have implemented techniques to reduce the PER to zero. It is also moreover possible to decrease the VLC latency by reducing the packet length (i.e. optimize the message to send).

Conclusion

In this section we outlined the 5G experimental activities in the city of Prato, and in particular, the use case of 5G network supporting VLC communications between traffic-lights and vehicles. The paper reports detailed description of the test-bed and experimental activities, as well as the application scenario. The results show that 5G and VLC can be successfully coupled to obtain very low latency from IoT sensors spread along city to the vehicles.



(a) Maximum end-to-end latency time.



(b) Minimum end-to-end latency time.

Figure 3.36: Measured latency time.

Chapter 4

Other research projects

In this chapter possible indoor applications have been analysed, in particular museum and office applications have been considered. These works start from collaborations with two different research groups belonging to research fields that could be interested in applying a visible light communication. The first work is focused on the effect of modulation light in human perceptivity of colour and read performance. The other work is an evaluation of VLC impact on light design regulations and the possibility of integrating illumination software for the sizing of a VLC network.^{1 2} The other work is focused on the respect of regulations in a VLC application and the possible use of software and techniques typical used in light design.^{3 4} For both cases, the technical contribution provided made it possible to analyse the problems that could arise from the diffusion of application based on VLC technology.

Possible indoor applications range from Internet connection at home/of-

¹Part of this work was conducted while the author was a correlator of students Valentina Orsi and Vittoria D'antoni, and working with Prof. Alessandro Farini and Prof. Elisabetta Baldanzi (Institute for Research and Studies in Optics and Optometry, IRSOO).

²The work presented in this chapter has been submitted as "Experimental reading and colour tests with information-modulated visible light in indoor environments" in *PLOS ONE*, 2019

³Part of this work was conducted while the author was a correlator of student Alessio Scacchi, and working with Prof. Carla Balocco (Department of Mechanical Engineering)

⁴The work presented in this chapter has been published as "Lighting Design and Visible Light Communication" in *LUCE*, 2018

fice to multimedia contents delivery in a museum. Despite the vast interest of researchers in both theoretical analysis and experimentation on VLC technology, no studies have been carried out on the human perceptions of objects illuminated by VLC-based lamps and how this technology will impact light design regulations.

It is important to define if a VLC lamp decreases the reading capability or modifies the colours perception in order to make VLC a technology for every-day life use. In this chapter there are a describe of the results of psychophysical tests on humans to define if the VLC lamp modifies the perception of colours or the reading speed.

Moreover, lighting engineering in terms of research and design is today a very broad and complex discipline. It often requires interdisciplinary approaches, interacting with other sciences and disciplines, and is constantly expanding and evolving. It is a sign of success, but also of acquired complexity. The use of visible light for communication is a new field for telecommunication research, but it is known topic for lighting engineering. It is important to analysed the tools and techniques used in light design for an integration of VLC with a correct project of museum or office illumination.

4.1 VLC lamp for indoor application

The scope of the first work (see a section 4.2) is an evaluation of modulated minimum frequency to avoid a VLC human perception. Moreover, in the second work, the scope is a measure of intensity of six lamps on the desk. For these reasons, a system created is not required a high data rate, and consequently the VLC lamps created for these experimental campaigns are a cheap solution comparison of the prototype presented in a previous chapter(see a figure 4.1).

The lamps used is a commonly marketed light bulb, typically used for desk lamps, with G4 socket and 12 V power supply. This light bulb, produced by Goobay, has a consumption of 2 Watt and a luminous flux of 170 lumen (similar to a 20 W traditional incandescent lamp). The lamp [52] is composed of 12 phosphor LEDs and a circuit regulating the current to keep the luminous intensity of the lamp as constant as possible. The characteristics of which are summarized in table 4.1.

With the analysis of regulation circuit components, it emerged that the integrated circuit (IC) used to obtain a constant light intensity has a analogue



Figure 4.1: Table lamp modified for VLC Light.

Table 4.1: Characteristics LED Lamp

Type	LED built-in Spotlight
Power	2 W
Luminous Flux	170 lumen
Diameter	30 mm
Lamp cap	G4
Efficiency	Equivalent to incandescent bulb: 20
Energy consumption	2 kWh/1000 h(class A)
Colour temperatures	2800 K
Colour rendering	80
Lifetime	30000 h
Mercury Content	0 mg

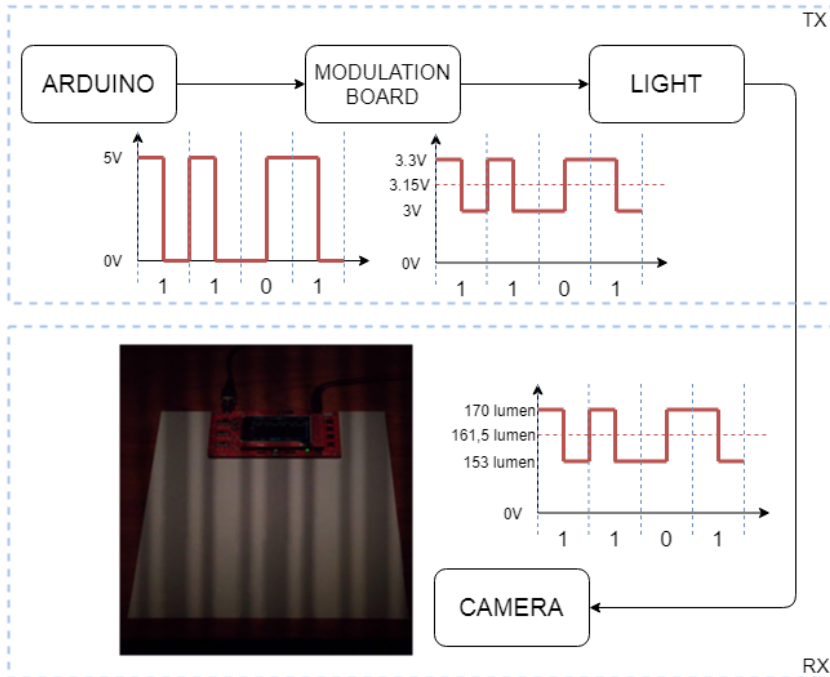


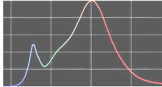
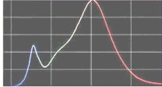
Figure 4.2: Block diagram of the transmission system used for experiments. The picture, in a bottom of figure, was obtained through a common smart-phone.

input for brightness adjustment, which are not used. Through two welded wires it was possible to insert the modulated signal into the emitted light. The IC required a range of voltage from 3 to 3,3 V. To connect a Arduino, it was necessary to insert a simple circuit to convert the output of board (0-5V) to a required voltage. The circuit was created with a simple operational amplifier.

The figure 4.2 represents a block diagram of a signal transformation from Arduino to Camera receiver, i.e. a typical diagram of optical camera communication (OCC).

The system model design were test also for a communication low data rate with a photodiode, an other arduino and pc, as it represents in figure

Table 4.2: Comparison between VLC On and Off

Characteristics	VLC Off	VLC On
Power	2 W	2 W
Luminous Flux	170 lumen	170 lumen
Emission Spectrum		
Colour temperatures	2912 K	2984 K
Lifetime	30000 h	≤ 30000 h

4.3.

After a prototype created, the technical characteristics of the lamp have been verified with a without modulation with a CS 1000 Konica Minolta spectrum radiometer to evaluate the present of variation with a modulation inserted. The test results are possible show in Table 4.1.

The VLC system connected to the LEDs has been tested and verified so that the lamps are able to transmit a simple datum to the receiving photodiode. The method followed is summarized as follows:

- the starting data is modulated, through the Arduino software platform using the "Manchester coding", ie a procedure that nullifies the signal average. The Manchester code assigns to each ignition value (1) a subsequent shutdown phase and, vice versa, at each shutdown value (0) an ignition phase, in order to maintain the average value of the luminous flux of the constant lamp;
- the regulation circuit has the function of transforming the classic digital signal (0V - 5V) into a value accepted by the lamp circuit (0.3V - 3V), through two variable resistances, which modify the average value and the depth of the modulation;
- the lamp circuit is supplied with an analogue port which was used to insert the modulation;
- the LED therefore transmits the signal at higher frequencies than the flickering regulation. The signal is transmitted to a photodiode, which

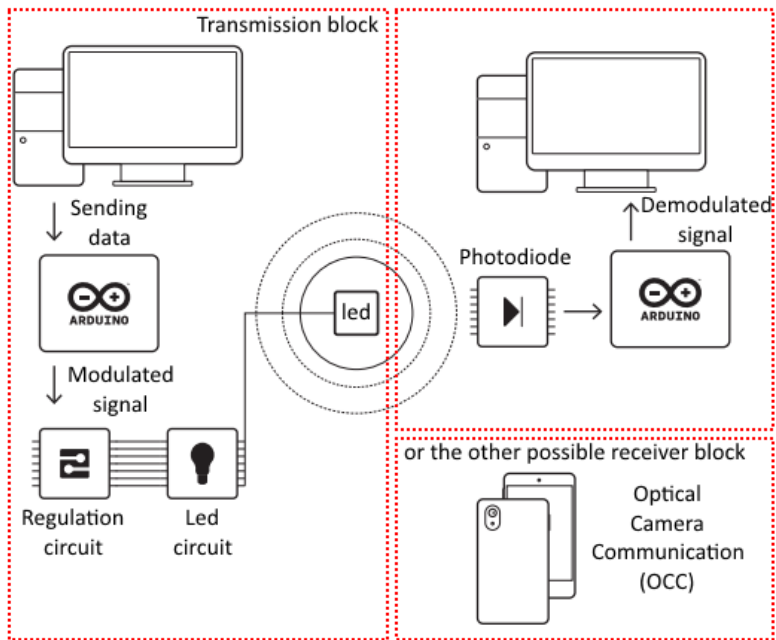


Figure 4.3: VLC transmission / localization scheme. In the case of data reception to the PC it will be necessary to implement a reception system, composed of a photodiode and microcontroller that acts as a peripheral device for connection between electronics and PCs. While with regard to localization, the system turned out to be simpler, because the camera will be the signal receiver and all signal processing will be entrusted to the smartphone's processor.

in turn is connected to a second Arduino software platform aimed at signal demodulation.

During the measurements, we have set the luminous intensity at 95% of the standard intensity of the lamp, the amplitude modulation at the 10%, to achieve a lamp emission oscillating between 90% and 100%.

4.2 Human perception of modulated light

Basically, any indoor lighting system, such as in shopping centre, office or home, can potentially become the transmitter of a data communications system. Optical communications with visible light are also particularly suitable for applications such as Indoor Position System (IPS), to trace and find the position of a target in environments where GPS tracking is not possible, such as inside buildings [15, 68, 104, 105].

A low cost solution for IPS is based on a LED light as source and a smartphone camera as receiver. This technology for the standard IEEE 802.15.7 [9] is called Optical Camera Communication (OCC), and it appears only in a first revision of the standard. The definition of the range of frequencies to be used for OCC is postponed to the next revision of the standard. The image sensor of a smartphone typically consists of a number of pixels, each pixel contains a photodiode, which can be used as a VLC receiver [38]. This sensor is not designed to receive VLC signal and thus the performance is better for modulation at low frequencies.

The Standard IEEE 1789-2015 [5] includes a definition of the concept of modulation frequencies for LEDs and it also describes the health risks for humans about flickering light. This standard is followed especially by companies that produce LED drivers. The driver for dimming of LED light usually is achieved by a pulse width modulation (PWM) signal [49]. The guidelines of standard are limited to periodic signals, typically of LED driver. The VLC modulation of LED light is not considered in this standard.

The approach of the standard IEEE 1789-2015 is basically a medical approach based on statistical occurrences of serious health symptoms, e.g., abnormal EEG response, seizures from light stimuli, epilepsy. In this document has been defined, in function of frequency and modulation depth, a critical, low-risk and no observable effect level (NOEL) area (Figure 4.4).

To enable the OCC technology to be used in every-day life, it is of much importance to study also the effects of information-modulated light sources

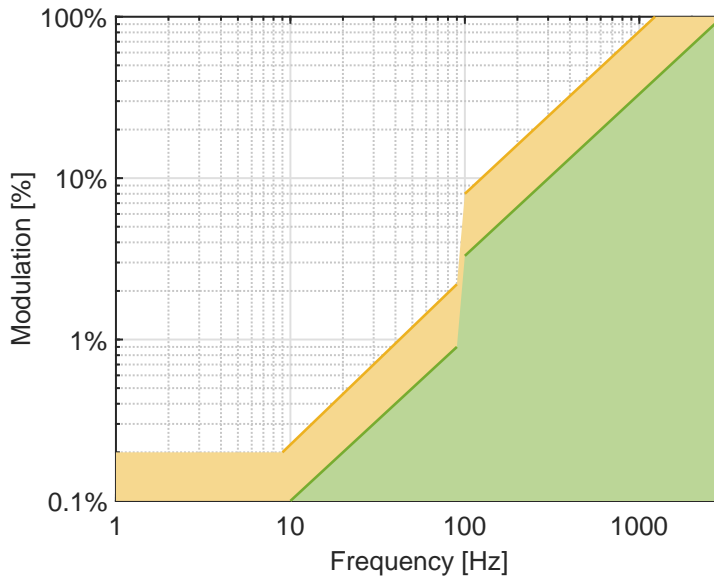


Figure 4.4: In yellow a low-risk area, in green a no observable effect level (NOEL) area, in according to standard IEEE 1789-2015 [5].

on the perception of human beings. In particular, it is important to investigate if the modulation of the light can affect the reading capability or the colour perception of an individual. To the best of authors' knowledge there are no studies on this topic published in the literature.

The main contribution of this section is the experimental evidence of a reasonable theoretical hypothesis: the use of a VLC technology do not modify perception of colours and reading speed. This hypothesis was verified using some psycho-physical tests. For every test, the subjects performed a test one time with a modulation lamp on and another time with a continuous light source. From the comparison of the results of the two tests it was possible to validate the hypothesis mentioned above.

4.2.1 Optometric Equipment

Optometric tests, used for this experiment campaign, are the typical tools used for the diagnosis of vision problems, they are classified as follow:

- Reading Test

R.E.X.

Radner

- Colour Vision Test

Ishihara

Farnsworth-Munsell 100 Hue

City University

For this experimentation, it is evaluated the difference between a test with modulated and constant light, i.e. VLC on and off.

R.E.X.

The REX test (Fig.4.5) is an eye chart which allows estimating the reading performance while changing the text/background contrast levels [46].

The REX test presents two sets, each one with four charts. Every page of the test has three different phrases arranged on three lines with aligned margins. Each phrase has 60 letters. The contrast of each phrase decreases with a logarithmic progression from top to bottom. The subject respects a reading distance of 40 cm. The letter size on each chart is equal to 1.0

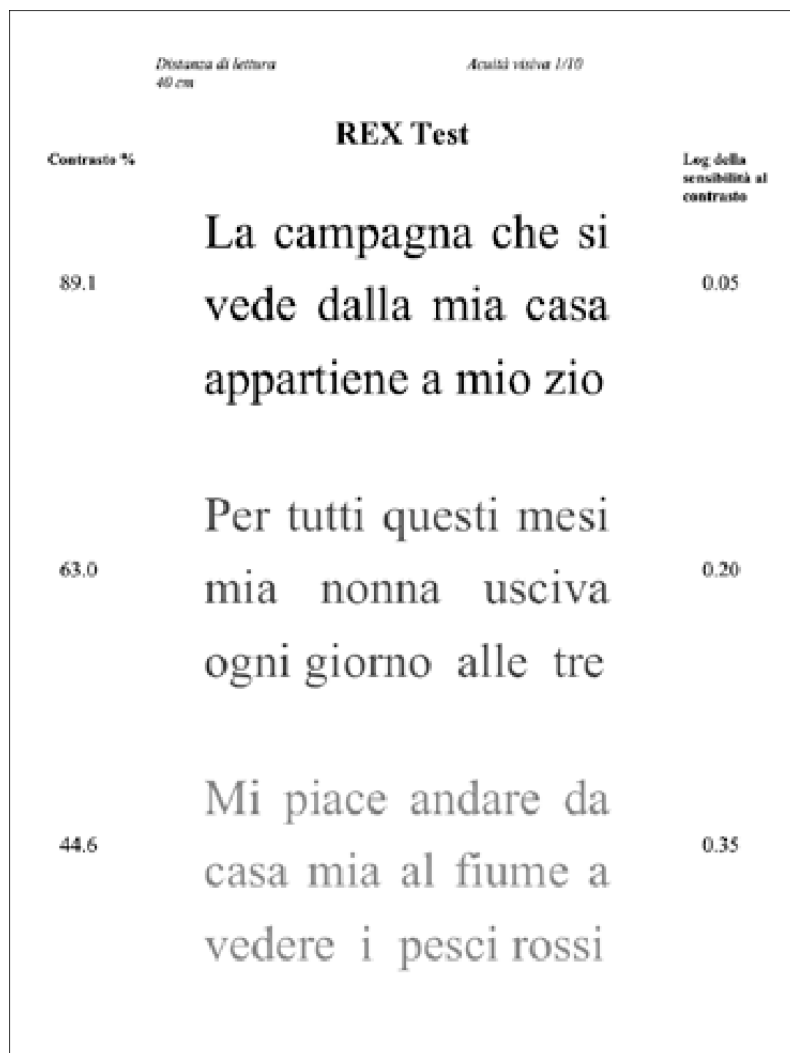


Figure 4.5: REX test.

logMAR. The text/background contrast in the first line phrase of the REX charts is equal to 89.13%. The reading of this contrast level requires a contrast sensitivity of at least 1.122%; that is, 0.05 in logarithmic units. Each following phrase corresponds to a logarithmic contrast sensitivity 0.15 units higher than the previous one, up to 1.7 units for the last (12th) phrase [46]. The subjects read aloud the phrases, starting from the one with the higher contrast. The following phrases are covered. The person who conducts the test annotates the non-read words or the one read incorrectly. The subject is invited to read as quickly yet precisely as possible. The reading time in seconds for each phrase t_{REX} (s) is measured to calculate the reading speed, v_{REX} .

$$v_{REX} = \frac{600}{t_{REX}} \quad (4.1)$$

We submitted the REX test to a total of 20 subjects (9 females, 11 males) with ages between 25 and 60 years. Every subject wore its optical correction if needed. The subjects had to read the 12 phrases of the REX test, one time with the VLC lamp on and another time with the lamp turned off without them knowing it. We measured the reading times (t_{ON} , t_{OFF}) for each phrases with a different contrast. Thus, we calculated the reading speeds (v_{ON} , v_{OFF}) using the equation 4.1.

Radner

The Radner Reading test (Fig.4.6) [90] is an eye chart which allows evaluating the near visual acuity.

The chart presents 24 phrases that present a standardised structure. From top to bottom the font size decreases by 0.1 logarithmic units. We measured the reading time t_{Radner} (s) and we calculated the reading speed v_{Radner} as follows:

$$v_{Radner} = \frac{14 \cdot 60}{t_{Radner}} \quad (4.2)$$

We asked the same subjects to take the Radner test. The same way we did for the REX test, we measured the reading times for each phrases corresponding to different visual acuities (VA). We proceeded to calculate the reading speeds (v_{ON} , v_{OFF}) with the equation 4.2.

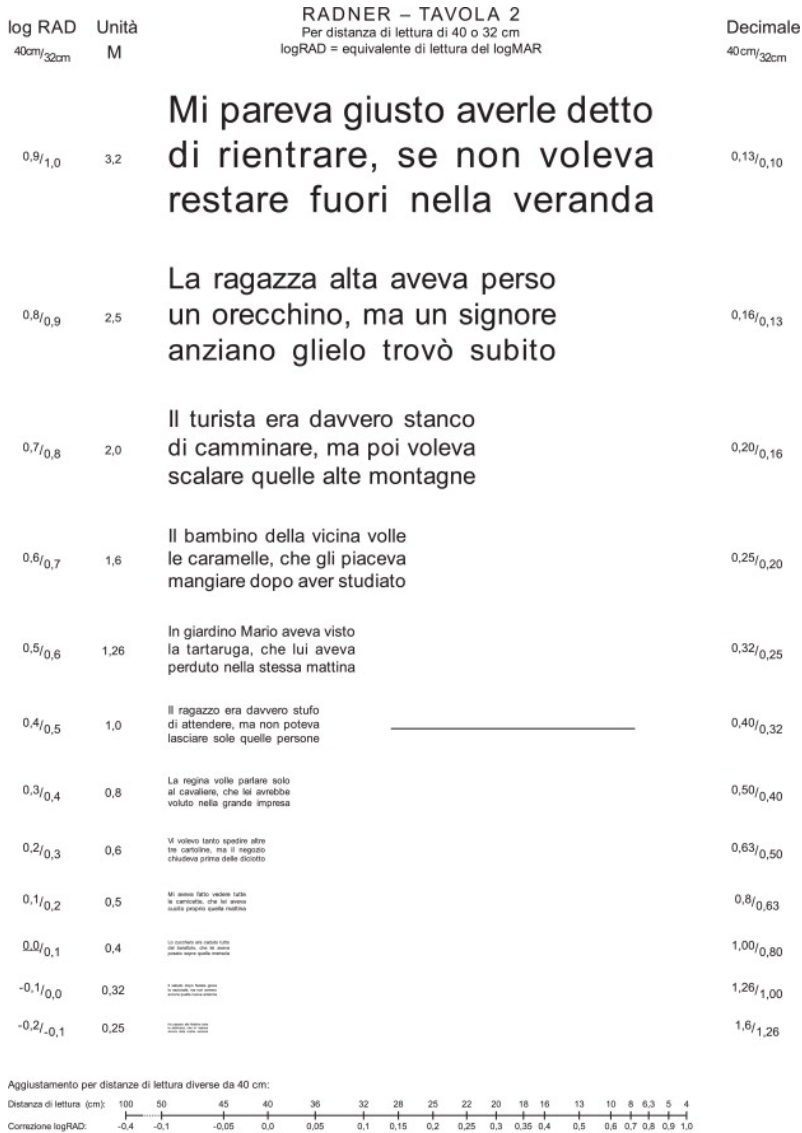


Figure 4.6: Radner test.

4.2.2 Ishihara

The Ishihara Colour Test (Fig.4.7) is a Pseudoisochromatic Plate test [54]. It consists of 38 plates; each of the plates presents dots with different sizes and colour but with the same luminosity. Some of these dots form a path or a number easily distinguishable from whom has a normal colour perception.

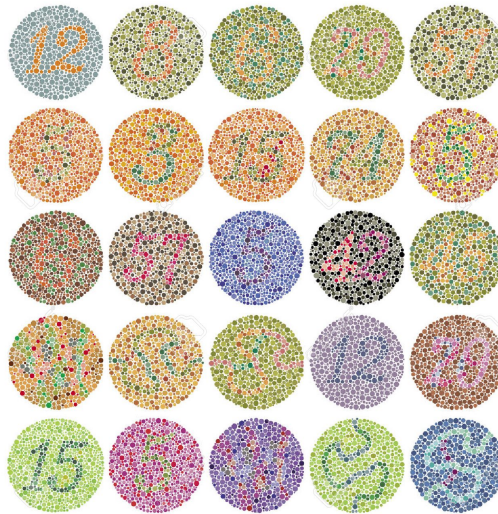


Figure 4.7: Ishihara Test.

If the examined subject finds difficult or impossible to determine the number or the path of the plates, we have individuated a subject with an anomalous colour sensitivity. The first plate (with number 12) is not a pseudoisochromatic image, thus the number is visible also for a subject with altered colour perception. Errors in the identification of the figure on plates from 2 to 17 represent anomalies in the perception on the R/G axis. Plates from 18 to 21 are visible only those who have an altered perception of the colours on the R/G axis. Plates from 22 to 25 allow distinguishing colour blindness (protanopia for red, deuteranopia for green) from partial colour blindness (protanomaly or deuteranomaly). Plates from 27 to 38 present path that the subject can indicate and allow to propose the test also to illiterate subjects. The subject needs to stay at a distance of 30-40 cm, using the right optical correction if needed.

Farnsworth-Munsell 100 Hue

The Farnsworth-Munsell 100 Hue Colour Vision Test (Fig.4.8) is an Arrangement test. The subject is asked to put in the right order the shown coloured plates [42]. If the subject finds the assigned task difficult to accomplish, it can indicate an anomaly in the colour vision [19]. The Farnsworth-Munsell 100 Hue Colour Vision Test consists in 85 coloured plates, numbered from 1 to 85, divided into 4 groups (the first set contains the colours from 85 to 21, the second from 22 to 42, the third from 43 to 63, and the fourth from 64 to 84). The examined subject is given each test one at a time and orders the plates of the set.



Figure 4.8: Farnsworth-Munsell 100 Hue Colour Vision Test.

The examiner checks the order of the number signed on the back of each coloured plates and writes down the results. Once all the four groups have been ordered, it is possible to calculate the error score of every single colour (Eq.4.3).

$$ErrorScore = |n - (n - 1)| + |n - (n + 1)| \quad (4.3)$$

where n is the number indicating a certain colour.

If the colours are put in the right order, then $Error\ Score = 2$, thus 170 is the best score a subject can obtain. The total error score (TES) is calculated by summing each single error score and then deducting 170. As the number of errors increases, also the total score increases, because when a plate is misplaced the $Error\ Score > 2$. Verriest et al [99] showed that the distribution of the total error score is not Gaussian and that the square root of the total error score has a Gaussian distribution. The Farnsworth-Munsell 100 Hue Colour Vision Test demands a good collaboration from the examined subject. It takes about 20 minutes doing the test. The results can

be affected by the age of the subject, by the visual acuity, and by the retinal illumination.

City University

The City University Colour Vision Test (CUT) [44] is a matching test. It consists of two parts: with the first one it is possible to detect the colour vision deficits; the second part of the test allows to evaluate the severity of the anomaly. Using the CUT it is possible to uncover subjects with tritanopia (colour-blindness towards the blue-wavelengths).



Figure 4.9: City University Colour Vision Test.

Initially, the tests present four columns of coloured dots, two in the upper part and two in the lower part of the page. The task of the patient is to identify the dots with a different colour from the other ones in the same column. The subject with a normal colour sensitivity should be able to identify correctly 9-10 of the dots. The second part of the test has 10 tables; each table presents a central dot with four other dots around it. The patient must indicate which out of the four peripheral dots has the most similar colour to the central one.

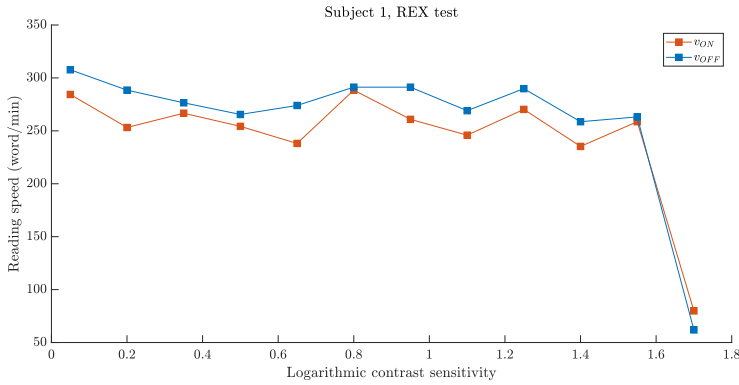


Figure 4.10: Reading speed depending on the logarithmic contrast sensitivity of subject 1 with the REX test. Observing the performances of subject 1, it is possible to notice that when the logarithmic contrast sensitivity is equal to 1.55, the reading speed values decrease abruptly. When this happens, we have reached the critical contrast sensitivity value, after which the subject is no more able to complete the asked task.

4.2.3 Reading performance

For each subject, we individuated the critical logarithmic contrast sensitivity, which corresponds to the minimum level of contrast that allows the subject to read the phrase with the same speed that the subject reach in the first black on white (maximum contrast) phrase. In figure 4.10 we can notice that after that critical value the reading speed decreases abruptly. Now, we proceeded by calculating the average reading speed for each subject, excluding the reading speed values after the critical point. We obtained the averages and the standard deviations \bar{v}_{ON} and σ_{ON} , \bar{v}_{OFF} and σ_{OFF} for every subject.

In figure 4.11 we collected the average reading speeds and the corresponding statistical errors for every subject. The axis of the ordinates reports the \bar{v}_{ON} and the horizontal bars represent σ_{ON} . The axis of the abscissas reports the \bar{v}_{OFF} and the horizontal bars represent σ_{OFF} . The graphic also displays the equation of the linear fit and the Pearson coefficient R . By observing the graphic 4.11, we can notice that there is a strong positive correlation between the reading speed measured when the device was on and when it was off.

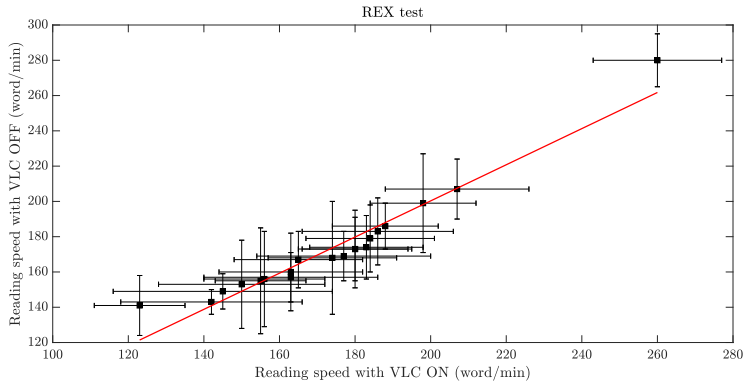


Figure 4.11: Scatter plot between $\bar{v}_{ON} \pm \sigma_{ON}$ and $\bar{v}_{OFF} \pm \sigma_{OFF}$ for each examined subject when taking the REX test. The figure also displays the linear regression fit, represented by the equation $y = 1.02x - 4.60$, and the Pearson correlation coefficient $R = 0.97$. We can notice that there is a positive correlation between \bar{v}_{ON} and \bar{v}_{OFF} .

Therefore it is possible to conclude that the presence of the VLC lamp does not influence the contrast sensitivity of the patients. This statistical analysis returned for the REX test a bias of 0.3500 and a standard deviation on the difference between the two measurements of 7.6590.

Similarly to the REX test, we detected the critical values of VA for each candidate, and we computed the average and the standard deviation of the reading speeds without taking into account the reading speed values after the critical point. In figure 4.13, we reported the values of $\bar{v}_{ON} \pm \sigma_{ON}$ and $\bar{v}_{OFF} \pm \sigma_{OFF}$ of the subjects with the Radner test. Comparably to the REX test, also with the Radner test we did not notice a significant change in the reading speed with VLC on and off ($R = 0.91$).

We also proceeded to execute the Bland-Altman Plot [20] for both the results of the REX and the Radner test (Fig. 4.12 and 4.14). This statistical analysis returned for the Radner test a bias equal to 0.3000 a standard deviation on the difference of 12.7325.

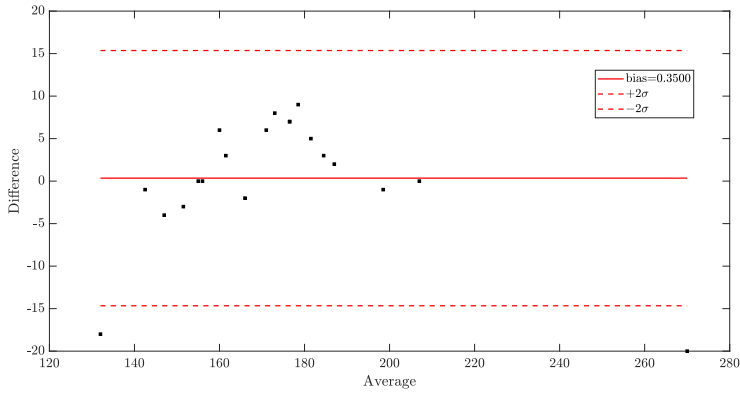


Figure 4.12: REX bias=0.3500, dev.sdt.diff=7.6590 [20].

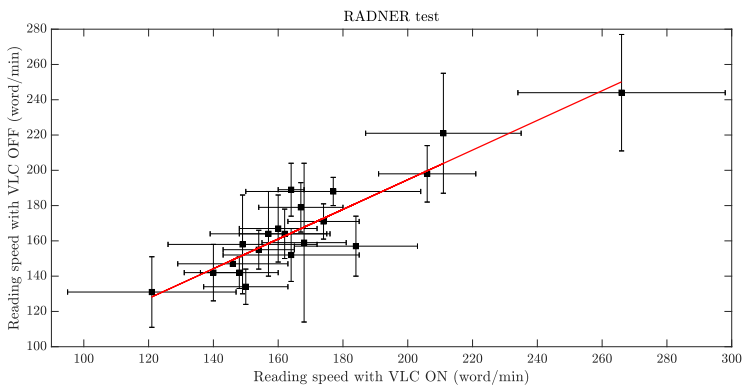


Figure 4.13: Scatter plot between $\bar{v}_{ON} \pm \sigma_{ON}$ and $\bar{v}_{OFF} \pm \sigma_{OFF}$ for each examined subject when taking the Radner test. The figure also display the linear regression fit, represented by the equation $y = 0.84x + 26.53$, and the Pearson correlation coefficient $R = 0.91$. We can notice that there is a positive correlation between \bar{v}_{ON} and \bar{v}_{OFF} .

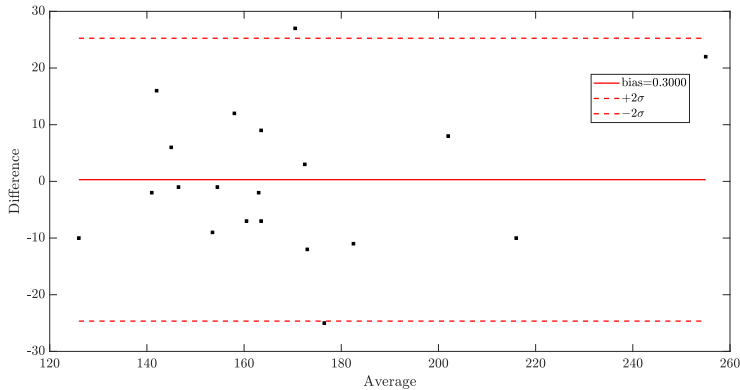


Figure 4.14: Radner bias=0.3000, dev.sdt.diff=12.7325 [20].

4.2.4 Variation of colour perception

For the colour vision test, we had a group of 20 subjects, 11 females and 9 males, with ages between 20 and 65 years. All of the subjects had their optical corrections on if needed.

For the Ishihara test and the CUT, we counted how many errors the subjects did when the VLC lamp was on and when it was off. The figure 4.15 reports the registered errors with the Ishihara test. To understand if the differences were statistically significant, we ran the *Fisher Exact test* [43]. The p-value results to be equal to 0.2351, much greater than 0.05, which lead us to state that the reading speed is not influenced by the presence of the VLC device. Instead, it was not necessary to run any statistical tests for the CUT, because we observed the same number of error with the VLC on or off.

In figure 4.16, we have compared the square roots of the total error scores made by the 20 subjects when the VLC lamp was on or off, with age-tabulated values of mean and statistical errors of \sqrt{TES} [99]. We can notice that all the subject have $\sqrt{TES_{OFF}}$ and $\sqrt{TES_{ON}}$ rather similar, for the exception of subject 11 and 14 they present the highest differences between those two number ($|\Delta_{max}| = 2.59$ for subject 11). Moreover, 15 patients over 20 were found to be within the age range [99], with the exceptions of subject 3, 5, 8, 12, and 14. Subject 3 has both $\sqrt{TES_{OFF}}$ and $\sqrt{TES_{ON}}$ a lot higher than the average of his peers; this might indicate that this patient has

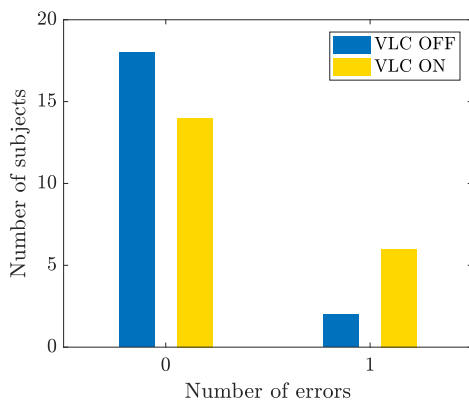


Figure 4.15: Bar plot representing the number of errors for the Ishihara test with VLC on (yellow bar) and off (blue bar).

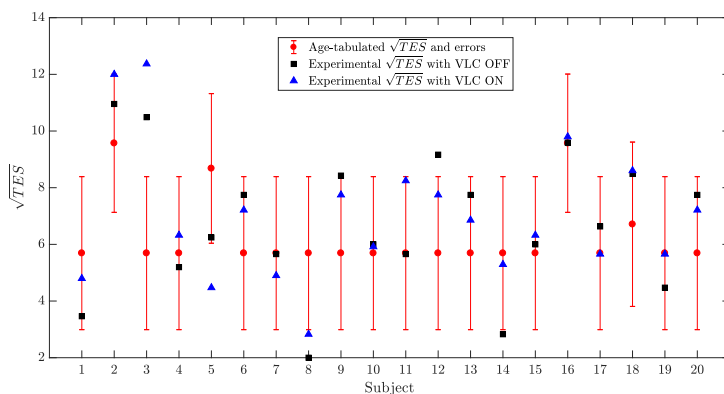


Figure 4.16: Representation of square roots of the total error score values for each subject. In red are reported the average values of \sqrt{TES} and their statistical error based on the age range of the patient [99], in black are reported the \sqrt{TES} measured with VLC off, and in blue the \sqrt{TES} measured with VLC on.

some difficulties in the colour discrimination, even if it was not detected from the other colour vision test (this could be an hint toward a tritan anomaly). Subject 5 has a better $\sqrt{TES_{OFF}}$ than its age range, and also $\sqrt{TES_{OFF}}$ is at the lower limit of this interval. Subject 8 has both $\sqrt{TES_{OFF}}$ and $\sqrt{TES_{OFF}}$ lower than the average of his peers, showing better capabilities in the colour discrimination task. Subject 12 presents an higher $\sqrt{TES_{OFF}}$, and subject 14 has a $\sqrt{TES_{OFF}}$ slightly below the average.

4.2.5 Conclusion

Our experiments showed that there are no differences in reading speed with or without data transmission. This fact can assure that VLC technology could be used in offices, schools or other locations where reading plays an important role. Our experiment were also promising about colour perception and colour discrimination because we did not find differences. VLC technology could be used also in environments where colour perception is important.

4.3 Light design and Visible Light Communication

Through this work of operational research we have evaluated the possibility of combining, in a single lamp, communication and lighting, LED and VLC, verifying the possibility of obtaining light scenes that are currently unthinkable, connected to indoor communications/localizations, to purpose of safety, intelligent lighting, quality of vision, but also energy saving and sustainability.

The results of the experimental measurements campaign made it possible to validate the lighting engineering simulations carried out to obtain the photometric and ergonomic parameters whose values were compared with the limit values suggested by the current workplace regulation. This is a first work with this approach, in a future it is possible to repeat this experimental campaign for museum or automotive application.

The VisiCoRe laboratory of the University Campus of the city of Prato is the case study considered. The results of the trial campaign showed the validity of the proposal in methodological and application terms, highlighting how the VLC system integrated with LED sources is a valid, effective

and safe support. Uniformity of illuminance, luminance balance and absence of glare are appreciable and important results, especially if combined with the consequent energy saving, as well as the total absence of effects of alterations and / or changes of an optical / photometric type on the LED-VLC modulated lamps.

This operational research is proposed as a pilot project for similar environments, even in particular buildings such as libraries, reading rooms also included in existing/historic buildings that are part of our Cultural Heritage, where the lighting project must focus on solutions of right balance between safeguarding, preventive protection, safety and safeguarding of objects/works with the protection of health, vision and the safety of people/operators.

The results of the simulations of the luminous climate produced by the proposed solution of VLC light, provide the necessary basis for future proposals that can lead to the realization of the pilot project as a guideline for all environments of similar purposes.

4.3.1 Techniques and tools for office light characterization

Each lighting project, especially if it is intended for workplaces, should be aimed at:

- guaranteeing quantitative light requirements to allow flexible management and regulation, reducing energy consumption and management and maintenance costs
- promoting visual well-being, health and safety of the user, guaranteeing the optimal condition for performing visual tasks, increasing productivity, ensuring ergonomics of vision, allowing all types of safe handling, facilitating orientation and communication.

The luminous climate present in a typical work environment for the office of the University of Prato was studied, with the aim of evaluating the quantitative and qualitative aspects of the light in the current state, to propose an innovative light project because it guarantees quality of vision and perception through the transmission of information and therefore of communication.

The use case is the VisiCoRe laboratory (4.17), located on the ground floor of the P.I.N. University Campus of the city of Prato, with a rectangular



Figure 4.17: Use Case.

plan of 43.46 m^2 and height 3.25 m (volume 141.24 m^3). On the north wall there are three windows (width 0.9 m and length 2.4 m), with steel gratings.

The environment is divided transversely into two rooms by a furniture, as long as the width of the office and with a dividing door to guarantee passage. The latter have been named area 1 and area 2 as they are characterized by different visual tasks and therefore by different lighting climates both in the current state and for the proposed design solution. Table 4.3.1 shows the characteristics of the two areas.

The following surveys were carried out: of geometric-architectural type (finalized to the construction of a 3D model useful for light simulations); to identify orientation and climatic location of the building and its transparent components; on the optical and photometric colorimetric characteristics of all the surfaces present in the environment (in particular glass). On the position and characteristics of the lighting fixtures present, using if necessary, the comparison with experimental evidences of literature on the subject. With reference to the current legislation [56], to the total number of points identified with the regulated grids placed on the floor and on the work sur-

Table 4.3: Characteristics of the two areas examined

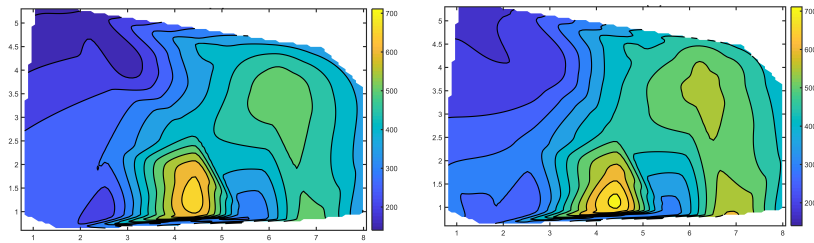
Zone 1		
Room Size:	Length	3 m
	Width	5.3 m
	Area	15.9 m ²
Field of view area	Desk	2
	Sizes	1.7 x 0.6 m, 1.8 x 0.8 m
	Height	0.8 m
Field of view	Movement Area	
	Laboratory	
	Data Processing	
Zone 2		
Room Size:	Length	4.7 m
	Width	5.3 m
	Area	24.91 m ²
Field of view area	Desk	5
	Sizes	1.5 x 1.8 m
	Height	0.8 m
Field of view	CAD	
	Informatics Laboratory	
	Electronics Laboratory	

faces, to sample measurement points on the vertical walls (useful for the subsequent calibration of the simulation model), to the profiles temporal use of the environment, in lighting conditions due only to natural light, only artificial and their admixture, the lighting measures necessary to calculate the average illuminance maintained on the worktops were carried out with Konica Minolta digital lux meters.

The lighting engineering campaign was limited to the period September-December 2017 due to accessibility problems. However it was necessary to define a measurement protocol so that the measures could be easily repeatable, carried out in the shortest possible time and in a sequential manner. The 10% average error on the measurement estimated with the standard deviation and the Chi-Quadro test allowed us to consider the experimental data as reliable and therefore able to use them to calibrate and calibrate the lighting simulation model, as an example of study in figure 4.18.

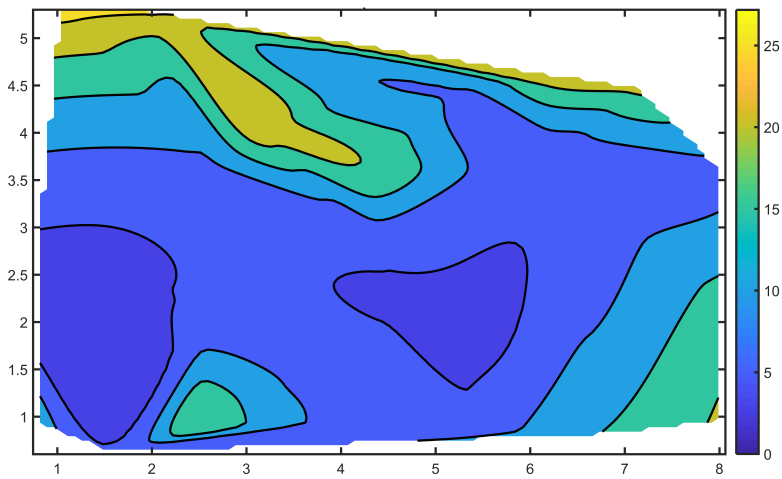
The extreme variability of the climatic parameters, with impulsive fluctuations even in very short times, particularly related to the variability of the sky, manifested during the campaign of measures, has led us to define and construct the "characteristic and representative day" of the autumn period (characterized by from intermediate sky conditions and the presence of direct solar radiation) based on the processing of all measurements. For this purpose, the average external illuminance values provided by the LAMMA Consortium, Environmental Monitoring and Modelling Laboratory for sustainable development were compared - Laboratory for Meteorology and Environmental Modelling. The artificial light sources present in both areas are linear fluorescent (Lumilux T8 Osram, model L58W / 840), arranged in pairs, in watertight ceiling lights and with transparent polycarbonate diffuser, on the ceiling at 2.90 m, in central position with respect to the width of the office and respectively at an intermediate distance of about one third of its length. The positioning of the partition between the two zones, placed after the creation of the office, limits the emission of one of the two lights. Table 4.3.1 shows their technical characteristics.

Once the solid architectural model of the environment was constructed, divided into the two zones, simulations were conducted in the different light conditions, for the typical autumn day, described above, and for the hours of occupation of the office with the use of the software commercial DIALUX-EVO. The models were calibrated and calibrated with the measured data. This made it possible to obtain the lighting engineering parameters necessary



(a) Experimental Data.

(b) Simulated Data.



(c) Error (%) between simulated and the experimental data.

Figure 4.18: Experimental data VS Simulated data.

Table 4.4: Characteristics LUMILUX T8, L58W/840

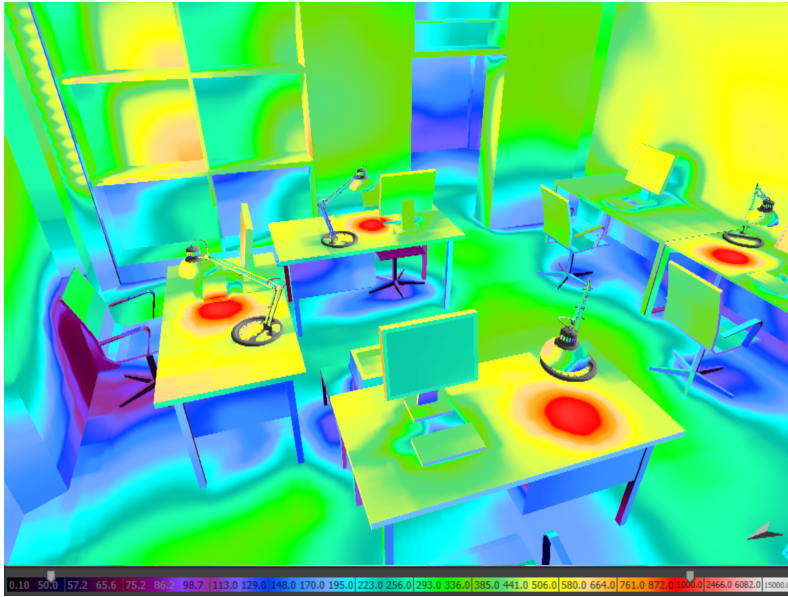
Type	Linear Fluorescent Lamp
Power	58 W
Luminous Flux	5200 lumen
Efficiency	90 lumen/Watt
Energy consumption	68 kWh/1000 h(classe A)
Colour temperatures	4000 K
Colour rendering	≥ 80
Lifetime	20000 h
Mercury Content	2.5 mg

for comparison with the requirements imposed by the legislation dedicated to offices [4, 56, 79]. The results obtained showed an uneven distribution of the illuminance and above all in all cases (ie in conditions of only natural light, only artificial light and a mixture of both) and for all the hours of use of the zones, the non-compliance with the limit values suggested by the legislation for the different visual tasks. Essentially both for the areas of visual tasks, and for the areas immediately surrounding (0.5 m around visual task), as well as for the background area (area of area of at least 3 m around the immediately surrounding area, which must present an average illuminance value equal to 1/3 of the average illumination foreseen for the immediately surrounding area), in all the analyzed situations the average illuminance value and the one obtained on the work surfaces is always much lower (on average around to 200 lx) of that suggested by the standards.

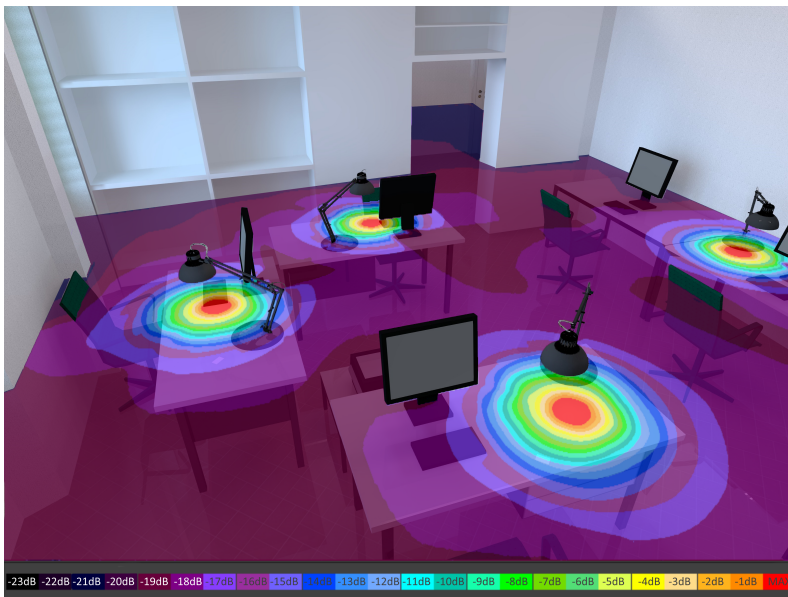
4.3.2 Compliance with lighting regulations

The proposed new light is based on an innovative approach to light design that integrates lighting with telecommunications. Experimental measurements were repeated in both areas, on workstations, for all the light conditions considered and for the hours of use of the environment. The relative lighting engineering simulations were then conducted on a modified and calibrated simulation model with the data of the new measurements.

The results obtained guarantee the levels of illumination required for the required visual tasks, uniformity and balance of luminance and illuminance and their respective limit ratios, respect for the value of the unified glare



(a) Light Design.



(b) VLC Path Loss.

Figure 4.19: Simulated data in current light configuration.

index UGR (Unified Glare Rating) and the yield index contrast on all work surfaces and in the immediate surrounding areas.

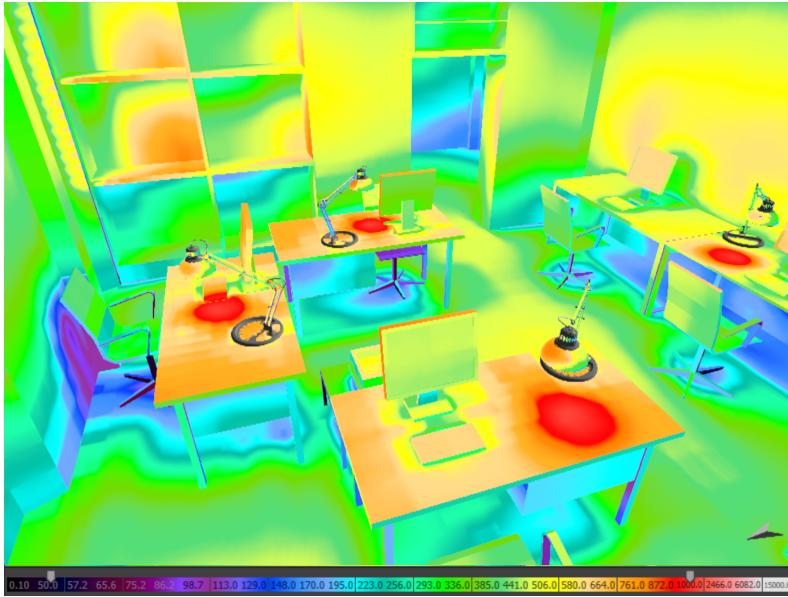
Figure 4.19 shows by way of example, in the form of a false colour map, obtained for a zone, the quality of the light both from a lighting point of view and from the point of view of telecommunications. In particular, from the analysis and comparison of the results it can be inferred that with the only natural light on the work surfaces, as expected, the value suggested by the standards is never reached (the highest value is 300 lx for the central hours of the day on a single location), with the combination of natural-artificial light, but also with artificial light alone (in both cases produced by linear fluorescents).

The suggested values are not respected reaching an average of 400 lx on almost all workstations, and finally with the structured light solution (addition of table light fixtures to LED sources with VLC) not only achieves the lux suggested by the standard, but since in most workstations values are also obtained which are appreciably higher at certain times of the day, it is possible solve the requests related to critical visual tasks, give maximum importance to accuracy or high productivity, provide a solution for the situations of subject's visual abilities lower than normal, improve the view of the details of the small visual task or with low luminance contrast and ensure the correct light for visual tasks to be performed over long periods of time.

Although the new project obtained with the proposed lighting solution involves a value of LENI (Lighting Numeric Indicator), calculated according to [2, 6] and in precautionary conditions, or at the maximum power of the sources and without regulation, of 20.04 kWh/m^2 per year, and therefore higher, but comparable with the LENI value of 19.34 kWh/m^2 per year obtained for the solution with linear fluorescent lights, energy savings would be appreciated thanks to the replacement of traditional Wi-Fi base stations and at the same time quality and sustainability for the integration of lighting and communication.

With the introduction of VLC light exclusively on table lamps, it is possible to observe in figure 4.19 below, how the signal coverage is confined within the desk and limited to the same floors. In order to extend the coverage of the signal to the entire office, a design intervention is required that includes the redesign of the main artificial lighting, replacing the LUMILUX T8 lamps, with LED lamps equipped with the VLC system.

Once the Dialux model was validated, it was also possible to evaluate



(a) Light Design.



(b) VLC Path Loss.

Figure 4.20: Simulated data in current light configuration.

the signal coverage trend by means of lighting simulation, in fact this new communication technology compared to radio frequency (RF) technologies is simpler from the design point of view, because the signal is proportional to the light received by the device.

For this reason, in the Dialux model, the fluorescent tube ceiling lamps have been replaced with six of the least powerful LED lamps, so as to have the same value of luminous flux emitted but greater uniformity in the distribution of light within the office, this last feature is fundamental for a correct design also from the telecommunications point of view. It is possible to observe in figure 4.20 the limits recommended by the lighting engineering regulations [2,4,6] for this type of environment, they are more respected and how the coverage of the VLC signal extends to the entire office in a uniform manner with better performance from the point of view of the signal.

4.3.3 Conclusion

The proposed design solution shows how a different approach to lighting design is possible. This approach has innovative aspects thanks to the introduction of typical features and solutions in the field of telecommunications. It is interesting to note that the solution obtained, by seeking signal optimization, is not critical, as regards the respect of the lighting regulations in the workplace, but generates an improvement in visual comfort.

We would like to point out that an approach based on the integration of lighting solutions using LED technologies, with Visible Light Communications systems, not only guarantees quantity and quality of light, but also transmission of information, which can in turn be addressed to communication (would be transferred information to individual users / users and at the same time also to all), to training (information could be transferred and information of a cognitive-cultural and educational nature), to safety (locations and distances between the users / users themselves and between them and the objects, but also transmitted information on the environment, its conditions and the building in which it is located) in the workplaces, but also in different environments destined for museums and / or exhibition spaces, for commerce and schools.

Furthermore, the use of LEDs allows to obtain projects of quality light, ever-increasing information content and the possibility of intelligently optimizing consumption thanks to the modulation and clean transmission of the signal.

Chapter 5

Conclusion

The Visible light communications were found to be a reliable technology with low latency. For these reasons, they are ideal for application in intelligent transportation system (ITS). This technology application is not a health-hazard in according to experiments conducted and it is easy to integrate with current regulations and techniques of light design.

5.1 Summary of contribution

During the PhD period, the VLC argument were treated starting from scratch. The experiments started with the analysis of the optical wireless channel through a single low power led and simple a photodiode (see a section 2.3.1). The next step was the transition form a controlled environment (laboratory test) to a real scenario. During this period the study is focused on development of electronics circuit for increase transmission power and range (see a section 3.2). Once the prototype was completed, experiments is focused on the characterization of typical VLC system model, with an analysis of emission pattern (see a section 3.3) and the optical receiver lens (see a section 3.4), and the analysis of communication characteristics as a Packet Error Rate and Latency (see a sector 3.5) with experiment campaigns as during Prato 5G experimentation (see a section 3.6).

At the same time, two important collaborations on VLCs have been carried out: A study of human perceptive of modulated light and possible risk of damage to sight (see a section 4.2); and a integration of VLCs in Light design with a respect of regulations (see a section 4.3).

5.2 Directions for future work

All works presented in this PhD dissertation need further development. In the ITT application, future work will concern:

- For development of electronic parts, it is necessary a step towards FPGA boards.
- Further experiments for a more in-depth characterization of transmitter optical lens
- A study of impact on the communication performance due to atmosphere conditions (rain, fog, ...), i.e. the effects on signal reflections and scattering.
- A development of forward error correction (FEC) in communication system and how this impacts on latency.

Moreover, this PhD dissemination is mainly focused on the outdoor application, but for a transition towards indoor applications, it is necessary to increase a data rate with a study of the now electronics circuit for led transmission and photodiode receiver. Finally, the other arguments to be explored is the Optical Camera Communication and the indoor localization system.

Publications

This research activity has led to several publications in international journals and conferences. These are summarized below.¹

International Journals

1. Carla Balocco, Francesco Saverio Cataliotti, Lorenzo Mucchi, Stefano Caputo, Alessio Scacchi: "Lighting Design and Visible Light Communication. Un esempio di luce strutturata e qualità della visione", *LUCE*, 106-111, Vol. n.324, 2018
2. Lorenzo Mucchi, Sara Jayousi, Alessio Martinelli, Stefano Caputo, Emanuele Intriери, Giovanni Gigli, Teresa Gracchi, Francesco Mugnai, Massimiliano Favalli, Alessandro Fornaciai, Luca Nannipieri: "A Flexible Wireless Sensor Network Based on Ultra-Wide Band Technology for Ground Instability Monitoring", *SENSORS*, 1-21 18(9), 2018
3. Lorenzo Mucchi, Alessio Martinelli, Sara Jayousi, Stefano Caputo, Massimiliano Pierobon: "Secrecy Capacity and secure distance for Diffusion-based Molecular Communication Systems", *IEEE Access*, 2019
4. Tassadaq Nawaz, Marco Seminara, Stefano Caputo, Lorenzo Mucchi, Francesco Saverio Cataliotti, Jacopo Catani: "IEEE 802.15.7-Compliant Ultra-low Latency Relaying VLC System for Safety-Critical ITS", *IEEE Transaction on Vehicular Technology*, 2019

Submitted

1. Stefano Caputo, Francesco Saverio Cataliotti, Lorenzo Mucchi, Regina Comparetto, Vittoria D'antoni, Alessandro Farini, Valentina Orsi, Jacopo Catani, Elisabetta Baldanzi: "Experimental reading and colour tests with information-modulated visible light in indoor environments", *PLOS ONE*, 2019

¹The author's bibliometric indices are the following: *H*-index = 2, total number of citations = 13 (source: Google Scholar on Month 2, 2020).

2. Stefano Caputo, Lorenzo Mucchi, Francesco Saverio Cataliotti, Marco Seminara, Tassadaq Nawaz: "Measurement-based VLC channel characterization for I2V communications in a real urban scenario", *IEEE Transaction on Vehicular Technology*, 2019

International Conferences and Workshops

1. Lorenzo Mucchi, Francesco Saverio Cataliotti, Luca Ronga, Stefano Caputo, Patrizio Marcocci: "Experimental-based propagation model for VLC", *Networks and Communications (EuCNC)*, 2017
2. Lorenzo Mucchi, Alessio Martinelli, Stefano Caputo, Sara Jayousi, Massimiliano Pierobon: "Secrecy Capacity of Diffusion-based Molecular Communication Systems", *Bodynets*, 2018
3. Lorenzo Mucchi, Sara Jayousi, Alessio Martinelli, Stefano Caputo, Patrizio Marcocci: "An Overview of Security Threats, Solutions and Challenges in WBANs for Healthcare", *ISMICT*, 2019
4. Alessio Martinelli, Sara Jayousi, Stefano Caputo, Lorenzo Mucchi: "UWB Positioning for Industrial Applications: the Galvanic Plating Case Study", *IPIN*, 2019
5. Francesca Nizzi, Tommaso Pecorella, Stefano Caputo, Lorenzo Mucchi, Romano Fantacci, Mattia Bastianini, Carlo Cerboni, Alessandra Buzzigoli, Andrea Fratini, Tassadaq Nawaz, Jacopo Catani, Marco Seminara: "Data dissemination to vehicles using 5G and VLC for Smart Cities", *AEIT*, 2019

Bibliography

- [1] U. 11248, “Illuminazione stradale, selezione delle categorie illuminotecniche,” Ente nazionale italiano di unificazione, Standard, 2016.
- [2] U. E. 12464-1:2011, “Luce e illuminazione, illuminazione dei posti di lavoro - parte 1: Posti di lavoro in interni,” UNI, Tech. Rep., 2011.
- [3] U. 13201-2, “Illuminazione stradale, requisiti prestazionali,” Ente nazionale italiano di unificazione, Standard, 2016.
- [4] U. E. 15193-1:2017, “Prestazione energetica degli edifici - requisiti energetici per illuminazione,” UNI, Tech. Rep., 2017.
- [5] I. S. 1789-2015, “Ieee recommended practices for modulating current in high-brightness leds for mitigating health risks to viewers,” IEEE, Tech. Rep., June 2015.
- [6] U. E. 1838-2013, “Illuminazione di emergenza,” UNI, Tech. Rep., 2013.
- [7] 5G-PPP, “5G vision,” 2015. [Online]. Available: <https://5g-ppp.eu/wp-content/uploads/2015/02/5G-Vision-Brochure-v1.pdf>
- [8] I. S. 802.15.7, *Visible Light Communication*, WPAN Task Group 7 (TG7), <http://www.ieee802.org/15/pub/TG7.html>.
- [9] —, “Ieee standard for local and metropolitan area networks—part 15.7: Short-range wireless optical communication using visible light,” *IEEE Std 802.15.7-2011*, pp. 1–309, Sep. 2011.
- [10] I. S. 802.15.7-2018, “Ieee standard for local and metropolitan area networks—part 15.7: Short-range optical wireless communications - redline,” *Revision of IEEE Std 802.15.7-2011 - Redline*, pp. 1–670, April 2019.
- [11] V. Aa, “Ieee std 802.11 p-2010, amendment 6: Wireless access in vehicular environments,” *IEEE Computer Society*, 2010.
- [12] F. Ahmed-Zaid, F. Bai, S. Bai, C. Basnayake, B. Bellur, S. Brovold, G. Brown, L. Caminiti, D. Cunningham, H. Elzein *et al.*, “Vehicle safety communications—applications vsc-a second annual report january 1, 2008

- through december 31, 2008,” Vehicle Safety Communications, Tech. Rep., 2011.
- [13] M. Akanegawa, Y. Tanaka, and M. Nakagawa, “Basic study on traffic information system using LED traffic lights,” *IEEE Intelligent Transportation Systems*, vol. 2, no. 4, pp. 197–203, 2001.
- [14] S. Alfattani, “Review of LiFi technology and its future applications,” *Journal of Optical Communications*, 2018.
- [15] T. Asai, T. Yendo, S. Arai, T. Yamazato, H. Okada, T. Fujii, and K. Kamakura, “Position estimation of led matrix in image sensor communication,” in *2016 Asia-Pacific Signal and Information Processing Association Annual Summit and Conference (APSIPA)*, Dec 2016, pp. 1–5.
- [16] S. Ayub, S. Kariyawasam, M. Honary, and B. Honary, “A practical approach of vlc architecture for smart city,” in *Loughborough Antennas and Propagation Conference (LAPC)*, Loughborough, 2013, pp. 106–111.
- [17] J. R. Barry, J. M. Kahn, W. J. Krause, E. A. Lee, and D. G. Messerschmitt, “Simulation of multipath impulse response for indoor wireless optical channels,” *IEEE Journal on Selected Areas in Communications*, vol. 11, no. 3, pp. 367–379, 1993.
- [18] A. G. Bell, “The photophone,” *Science*, vol. 1, no. 11, pp. 130–134, 1880. [Online]. Available: <http://www.jstor.org/stable/2900889>
- [19] J. Birch, “Use of the farnsworth-munsell 100-hue test in the examination of congenital colour vision defects,” *Ophthalmic and Physiological Optics*, vol. 9, no. 2, pp. 156–162, 1989.
- [20] J. M. Bland and D. Altman, “Statistical methods for assessing agreement between two methods of clinical measurement,” *The lancet*, vol. 327, no. 8476, pp. 307–310, 1986.
- [21] M. Boban, A. Kousaridas, K. Manolakis, J. Eichinger, and W. Xu, “Connected roads of the future: Use cases, requirements, and design considerations for vehicle-to-everything communications,” *IEEE Vehicular Technology Magazine*, vol. 13, no. 3, pp. 110–123, 2018.
- [22] M. Boban, K. Manolakis, M. Ibrahim, S. Bazzi, and W. Xu, “Design aspects for 5G V2X physical layer,” in *IEEE Conference on Standards for Communications and Networking (CSCN)*, 2016, pp. 1–7.
- [23] L. Brilli, T. Pecorella, and L. Mucchi, “Physical layer security for IoT devices configuration and key management - a proof of concept,” in *Proceedings of the AEIT Annual Conference*, Oct. 2016.
- [24] L. Brilli, T. Pecorella, L. Pierucci, and R. Fantacci, “A novel 6LoWPAN-ND extension to enhance privacy in IEEE 802.15.4 networks,” in *Globecom 2016*. IEEE, 345 E 47TH ST, NEW YORK, NY 10017 USA, Dec. 2016, pp. 1–5.

- [25] A. Cailean, B. Cagneau, L. Chassagne, S. Topsu, Y. Alayli, and J.-M. Blosseville, "Visible light communications: Application to cooperation between vehicles and road infrastructures," in *Intelligent Vehicles Symposium (IV), 2012 IEEE*. IEEE, 2012, pp. 1055–1059.
- [26] A.-M. Cailean, B. Cagneau, L. Chassagne, S. Topsu, Y. Alayli, and M. Dimian, "Visible light communications cooperative architecture for the intelligent transportation system," in *Communications and Vehicular Technology in the Benelux (SCVT), 2013 IEEE 20th Symposium on*. IEEE, 2013, pp. 1–5.
- [27] S. Caputo, L. Mucchi, F. S. Cataliotti, and J. Catani, "Measurement-based VLC channel characterization for I2V communications in a real urban scenario," *arXiv e-prints*, p. arXiv:1905.05019, May 2019.
- [28] N. Chi, *Led-based Visible Light Communications*. Springer-verlag, Berlin AN, 2018.
- [29] N. Chi, H. Haas, M. Kavehrad, T. D. C. Little, and X. Huang, "Visible light communications: demand factors, benefits and opportunities," *IEEE Wireless Communications*, vol. 22, no. 2, pp. 5–7, 2015.
- [30] H. Chun, C.-J. Chiang, and D. C. O'Brien, "Visible light communication using oleds: Illumination and channel modeling," in *2012 International Workshop on Optical Wireless Communications (IWOW)*. IEEE, 2012, pp. 1–3.
- [31] D. Collett, *Modeling Binary Data*. New York: Chapman and Hall, 2002.
- [32] A. Correa, A. Hamid, and E. Sparks, "Li-fi based smart traffic network," in *IEEE Transportation Electrification Conference and Expo (ITEC)*, Long Beach, CA, USA, 2018, pp. 217–219.
- [33] R. Corsini, R. Pelliccia, G. Cossu, A. M. Khalid, M. Ghibaudi, M. Petracca, P. Pagano, and E. Ciaramella, "Free space optical communication in the visible bandwidth for v2v safety critical protocols," in *Wireless Communications and Mobile Computing Conference (IWCMC), 2012 8th International*. IEEE, 2012, pp. 1097–1102.
- [34] K. Cui, G. Chen, Z. Xu, and R. D. Roberts, "Experimental characterization of traffic light to vehicle VLC link performance," in *2011 IEEE GLOBECOM Workshops (GC Wkshps)*, 2011, pp. 808–812.
- [35] K. Cui, G. Chen, Q. He, and Z. Xu, "Indoor optical wireless communication by ultraviolet and visible light," in *Free-Space Laser Communications IX*, vol. 7464. International Society for Optics and Photonics, 2009, p. 74640D.
- [36] F. A. Dahri, S. Ali, and M. M. Jawaid, "A review of modulation schemes for visible light communication," *IJCSNS International Journal of Computer Science and Network Security*, vol. 18, no. 2, pp. 117–125, 2018.

- [37] P. A. Devijver and J. Kittler, *Pattern Recognition: A Statistical Approach*. London, GB: Prentice-Hall, 1982.
- [38] T.-H. Do and M. Yoo, “Performance analysis of visible light communication using cmos sensors,” *Sensors*, vol. 16, p. 309, 02 2016.
- [39] A. J. Dobson, *An Introduction to Generalized Linear Models*. New York: Chapman and Hall, 1990.
- [40] S. Eichler, “Performance evaluation of the ieee 802.11p wave communication standard,” in *2007 IEEE 66th Vehicular Technology Conference*, Sep. 2007, pp. 2199–2203.
- [41] R. Fantacci, T. Pecorella, R. Viti, and C. Carlini, “A network architecture solution for efficient IoT WSN backhauling: challenges and opportunities,” *Wireless Communications, IEEE*, vol. 21, no. 4, pp. 113–119, August 2014.
- [42] D. Farnsworth, “The farnsworth-munsell 100-hue and dichotomous tests for color vision,” *JOSA*, vol. 33, no. 10, pp. 568–578, 1943.
- [43] D. J. Finney, “The fisher-yates test of significance in 2×2 contingency tables,” *Biometrika*, vol. 35, no. 1/2, pp. 145–156, 1948.
- [44] R. Fletcher, *The City University colour vision test*. Keeler, 1980.
- [45] F. R. Gfeller and U. Bapst, “Wireless in-house data communication via diffuse infrared radiation,” *Proceedings of the IEEE*, vol. 67, no. 11, pp. 1474–1486, 1979.
- [46] G. Giacomelli, R. Volpe, G. Virgili, A. Farini, R. Arrighi, C. Tarli-Barbieri, R. Mencucci, and U. Menchini, “Contrast reduction and reading: assessment and reliability with the reading explorer test,” *European journal of ophthalmology*, vol. 20, no. 2, pp. 389–396, 2010.
- [47] Y. Goto, I. Takai, T. Yamazato, H. Okada, T. Fujii, S. Kawahito, S. Arai, T. Yendo, and K. Kamakura, “A new automotive vlc system using optical communication image sensor,” *IEEE photonics journal*, vol. 8, no. 3, pp. 1–17, 2016.
- [48] G.-P. A. W. Group, “View on 5G architecture, version 2.0,” 2017. [Online]. Available: <https://5g-ppp.eu/wp-content/uploads/2018/01/5G-PPP-5G-Architecture-White-Paper-Jan-2018-v2.0.pdf>
- [49] Y. Gu, N. Narendran, T. Dong, and H. Wu, “Spectral and luminous efficacy change of high-power leds under different dimming methods,” in *Sixth International Conference on Solid State Lighting*, vol. 6337, 2006. [Online]. Available: <https://doi.org/10.1117/12.680531>
- [50] F. Hu, *Vehicle-to-vehicle and Vehicle-to-infrastructure Communications: A Technical Approach*. CRC Press, 2018.

- [51] S. Y. Hui, S. N. Li, X. H. Tao, W. Chen, and W. M. Ng, "A novel passive of-line led driver with long lifetime," *IEEE Transactions on Power Electronics*, vol. 25, no. 10, pp. 2665–2672, Oct 2010.
- [52] industry electronics, Goobay, [Online; accessed 10-February-2019]. [Online]. Available: <https://industry-electronics.de/pdf/659709.pdf>
- [53] International Telecommunication Union, "IMT Vision – Framework and Overall Objectives of the Future Development of IMT for 2020 and Beyond," 2015. [Online]. Available: https://www.itu.int/dms_pubrec/itu-r/rec/m/R-REC-M.2083-0-201509-1!!PDF-E.pdf
- [54] S. Ishihara, *Ishihara's tests for colour deficiency: 24 plates*. Kanehara Shuppan, 1969.
- [55] M. S. Islim, S. Videv, M. Safari, E. Xie, J. J. D. McKendry, E. Gu, M. Dawson, and H. Haas, "The impact of solar irradiance on visible light communications," *Journal of Lightwave Technology*, pp. 1–1, 2018.
- [56] G. Italiano, "Decreto legislativo 09-04-2008 n°81, attuazione dell'art. 1 della legge 3 agosto 2007 n°123, in materia di tutela della salute e della sicurezza nei luoghi di lavoro," Governo Italiano, Tech. Rep., 2008.
- [57] G. James, D. Witten, T. Hastie, and R. Tibshirani, *An Introduction to Statistical Learning*. Springer, 2013.
- [58] P. Ji, H.-M. Tsai, C. Wang, and F. Liu, "Vehicular visible light communications with led taillight and rolling shutter camera," in *Vehicular Technology Conference (VTC Spring), 2014 IEEE 79th*. IEEE, 2014, pp. 1–6.
- [59] D. Jiang and L. Delgrossi, "Ieee 802.11p: Towards an international standard for wireless access in vehicular environments," in *VTC Spring 2008 - IEEE Vehicular Technology Conference*, May 2008, pp. 2036–2040.
- [60] J. M. Kahn, W. J. Krause, and J. B. Carruthers, "Experimental characterization of non-directed indoor infrared channels," *IEEE Transactions on Communications*, vol. 43, no. 2/3/4, pp. 1613–1623, 1995.
- [61] G. Karagiannis, O. Altintas, E. Ekici, G. Heijenk, B. Jarupan, K. Lin, and T. Weil, "Vehicular networking: A survey and tutorial on requirements, architectures, challenges, standards and solutions," *IEEE communications surveys and tutorials*, vol. accepted f, no. 4, pp. 584–616, 2011.
- [62] T. Komine and M. Nakagawa, "Fundamental analysis for visible-light communication system using lights," *IEEE Transactions on Consumer Electronics*, vol. 50, no. 1, pp. 100–107, 2004.
- [63] —, "Integrated system of white led visible-light communication and power-line communication," *IEEE Transactions on Consumer Electronics*, vol. 49, no. 1, pp. 71–79, 2003.

- [64] —, “Performance evaluation of visible-light wireless communication system using white led lightings,” in *Proceedings. ISCC 2004. Ninth International Symposium on Computers And Communications (IEEE Cat. No. 04TH8769)*, vol. 1. IEEE, 2004, pp. 258–263.
- [65] N. Kumar, N. Lourenço, D. Terra, L. N. Alves, and R. L. Aguiar, “Visible light communications in intelligent transportation systems.” in *Intelligent Vehicles Symposium*, 2012, pp. 748–753.
- [66] N. Kumar, N. Lourenco, M. Spiez, and R. L. Aguiar, “Visible light communication systems conception and vidas,” *IETE Technical Review*, vol. 25, no. 6, pp. 359–367, 2008.
- [67] P. A. Lachenbruch and M. R. Mickey, “Estimation of error rates in discriminant analysis,” *Technometrics*, vol. 10, no. 1, pp. 1–12, 1968.
- [68] C. Lartigue, J. Green, H. P. Rez-Olivas, J. García-Márquez, and S. Topsu, “High-efficient manchester coding for beacon-to-cmos camera in visible light communications,” in *2018 Global LIFI Congress (GLC)*, Feb 2018, pp. 1–4.
- [69] K. Lee, H. Park, and J. R. Barry, “Indoor channel characteristics for visible light communications,” *IEEE communications letters*, vol. 15, no. 2, pp. 217–219, 2011.
- [70] S. J. Lee, S. Y. Kwon, S. Y. Jung, and Y. H. Kwon, “Simulation modeling of visible light communication channel for automotive applications,” in *15th International IEEE Conference on Intelligent Transportation Systems*, Anchorage, Alaska, USA, 2012, pp. 1–7.
- [71] N. Lourenço, D. Terra, N. Kumar, L. N. Alves, and R. L. Aguiar, “Visible light communication system for outdoor applications,” in *Communication Systems, Networks & Digital Signal Processing (CSNDSP), 2012 8th International Symposium on*. IEEE, 2012, pp. 1–6.
- [72] J. M. Lozano Domínguez and T. J. Mateo Sanguino, “Review on v2x, i2x, and p2x communications and their applications: A comprehensive analysis over time,” *Sensors*, vol. 19, no. 12, p. 2756, 2019.
- [73] F. Martinez, C. Toh, J. C. Cano, C. Calafate, and P. Manzoni, “Emergency services in future intelligent transportation systems based on vehicular communication networks,” *IEEE Intelligent Transportation Systems Magazine*, vol. 2, pp. 6–20, 2010.
- [74] P. McCullagh and J. A. Nelder, *Generalized Linear Models*. New York: Chapman and Hall, 1990.
- [75] P. McCullagh and J. Nelder, *Generalized Linear Models, Second Edition*, ser. Chapman and Hall/CRC Monographs on Statistics and

- Applied Probability Series. Chapman & Hall, 1989. [Online]. Available: http://books.google.com/books?id=h9kFH2_FfBkC
- [76] F. Miramirkhani and M. Uysal, "Channel modeling and characterization for visible light communications," *IEEE Photonics Journal*, vol. 7, no. 6, pp. 1–16, 2015.
- [77] F. Miramirkhani, M. Uysal, and E. Panayirci, "Novel channel models for visible light communications," in *Broadband Access Communication Technologies IX*, vol. 9387. International Society for Optics and Photonics, 2015, p. 93870Q.
- [78] A. J. Moreira, R. T. Valadas, and A. Duarte, "Optical interference produced by artificial light," *Wireless Networks*, vol. 3, pp. 131–140, 1997.
- [79] L. Mucchi, F. S. Cataliotti, L. Ronga, S. Caputo, and P. Marcocci, "Experimental-based propagation model for vlc," in *European Conference on Networks and Communications (EuCNC)*, 2017.
- [80] T. Nagura, T. Yamazato, M. Katayama, T. Yendo, T. Fujii, and H. Okada, "Improved decoding methods of visible light communication system for its using led array and high-speed camera," in *Vehicular Technology Conference (VTC 2010-Spring), 2010 IEEE 71st*. IEEE, 2010, pp. 1–5.
- [81] H. Nguyen, J.-H. Choi, M. Kang, Z. Ghassemlooy, D. Kim, S.-K. Lim, T.-G. Kang, and C. G. Lee, "A matlab-based simulation program for indoor visible light communication system," in *2010 7th International Symposium on Communication Systems, Networks & Digital Signal Processing (CSNDSP 2010)*. IEEE, 2010, pp. 537–541.
- [82] M. Noor-A-Rahim, G. G. M. N. Ali, H. Nguyen, and Y. L. Guan, "Performance analysis of ieee 802.11p safety message broadcast with and without relaying at road intersection," *IEEE Access*, vol. 6, pp. 23 786–23 799, 2018.
- [83] W. H. Organization, "fact-sheets/detail/the-top-10-causes-of-death.available: <https://www.who.int/news-room/fact-sheets/detail/the-top-10-causes-of-death>," W. H. Organization, Tech. Rep., May 2018.
- [84] —, "Road traffic injuries. available: <https://www.who.int/en/news-room/fact-sheets/detail/road-traffic-injuries>," W. H. Organization, Tech. Rep., Dec 2018.
- [85] A. Papoulis, *Probability, Random Variables and Stochastic Processes*, 4th ed. McGraw-Hill, 2001.
- [86] H. Park and J. R. Barry, "Modulation analysis for wireless infrared communications," in *Proceedings IEEE International Conference on Communications ICC'95*, vol. 2. IEEE, 1995, pp. 1182–1186.

- [87] P. H. Pathak, X. Feng, P. Hu, and P. Mohapatra, "Visible light communication, networking, and sensing: A survey, potential and challenges," *IEEE Communications Surveys Tutorials*, vol. 17, no. 4, pp. 2047–2077, Fourthquarter 2015.
- [88] T. Pecorella, L. Brilli, and L. Mucchi, "The Role of Physical Layer Security in IoT: A Novel Perspective," *Information*, vol. 7, no. 3, p. 49, Aug. 2016. [Online]. Available: <http://www.mdpi.com/2078-2489/7/3/49>
- [89] Y. Qiu, H.-H. Chen, and W.-X. Meng, "Channel modeling for visible light communications. a survey," *Wireless Communications and Mobile Computing*, vol. 16, no. 14, pp. 2016–2034, 2016.
- [90] W. Radner, U. Willinger, W. Obermayer, C. Mudrich, M. Velikay-Parel, and B. Eisenwort, "A new reading chart for simultaneous determination of reading vision and reading speed," *Klinische Monatsblätter Fur Augenheilkunde*, vol. 213, no. 3, pp. 174–181, 1998.
- [91] S. Rajagopal, R. D. Roberts, and S. Lim, "Ieee 802.15.7 visible light communication: modulation schemes and dimming support," *IEEE Communications Magazine*, vol. 50, no. 3, pp. 72–82, March 2012.
- [92] M. E. Renda, G. Resta, P. Santi, F. Martelli, and A. Franchini, "Ieee 802.11p vanets: Experimental evaluation of packet inter-reception time," *Computer Communications*, vol. 75, pp. 26 – 38, 2016. [Online]. Available: <http://www.sciencedirect.com/science/article/pii/S0140366415002182>
- [93] G. Ruchi, "Li-fi: Data onlight instead of online," *Anveshanam, a national journal of computer science and applications*, vol. 1, no. 1, 2012-2013.
- [94] S. Series, "Visible light for broadband communications," Series, SM, Tech. Rep., 2018.
- [95] I. Takai, T. Harada, M. Andoh, K. Yasutomi, K. Kagawa, and S. Kawahito, "Optical vehicle-to-vehicle communication system using led transmitter and camera receiver," *IEEE photonics journal*, vol. 6, no. 5, pp. 1–14, 2014.
- [96] I. Takai, S. Ito, K. Yasutomi, K. Kagawa, M. Andoh, and S. Kawahito, "Led and cmos image sensor based optical wireless communication system for automotive applications," *IEEE Photonics Journal*, vol. 5, no. 5, pp. 6 801 418–6 801 418, 2013.
- [97] D. Terra, N. Kumar, N. Lourenço, L. N. Alves, and R. L. Aguiar, "Design, development and performance analysis of dsss-based transceiver for vlc," in *EUROCON-International Conference on Computer as a Tool (EUROCON), 2011 IEEE*. IEEE, 2011, pp. 1–4.
- [98] A. M. Vegni, M. Biagi, and R. Cusani, "Smart vehicles, technologies and main applications in vehicular ad hoc networks," in *Vehicular Technologies*, L. G. Giordano and L. Reggiani, Eds. Rijeka: IntechOpen, 2013, ch. 1.

- [99] G. Verriest, J. Van Laethem, and A. Uvijls, "A new assessment of the normal ranges of the farnsworth-munsell 100-hue test scores," *American Journal of Ophthalmology*, vol. 93, no. 5, pp. 635–642, 1982.
- [100] J. Wong, *Theory of Ground Vehicles. Second Edition*. Wiley, John and Sons, Incorporated, New York, N.Y., 1993. [Online]. Available: <https://books.google.it/books?id=99O7MAAACAAJ>
- [101] S. Wu, H. Wang, and C. Youn, "Visible light communications for 5G wireless networking systems: from fixed to mobile communications," *IEEE Network*, vol. 28, no. 6, pp. 41–45, 2014.
- [102] T. Yamazato, I. Takai, H. Okada, T. Fujii, T. Yendo, S. Arai, M. Andoh, T. Harada, K. Yasutomi, K. Kagawa *et al.*, "Image-sensor-based visible light communication for automotive applications," *IEEE Communications Magazine*, vol. 52, no. 7, pp. 88–97, 2014.
- [103] I. Yaqoob, I. A. T. Hashem, Y. Mehmood, A. Gani, S. Mokhtar, and S. Guizani, "Enabling communication technologies for smart cities," *IEEE Communications Magazine*, vol. 55, no. 1, pp. 112–120, 2017.
- [104] S. Yoshizawa, S. Handa, F. Sasamori, and O. Takyu, "A simple but effective approach for visible light beacon-based positioning systems with smartphone," in *IEEE 12th International Colloquium on Signal Processing and its application (CSPA)*, 03 2016, pp. 32–35.
- [105] F. Zhang, K. Qiu, and M. Liu, "Asynchronous blind signal decomposition using tiny-length code for visible light communication-based indoor localization," in *Robotics and Automation (ICRA), 2015 IEEE International Conference on*, May 2015, pp. 2800–2805.
- [106] M. Zhuk, V. Kovalyshyn, Y. Royko, and K. Barvinska, "Research on drivers' reaction time in different conditions," *Eastern European Journal of Enterprise Technologies*, vol. 2, pp. 24–31, 04 2017.